

**Revista Română de Inginerie Civilă**  
**Indexată în bazele de date internaționale (BDI)**  
**ProQuest, INSPEC, EBSCO**  
**INDEX COPERNICUS, ULRICH'S și JOURNALSEEK**  
**Volumul 12 (2021), Numărul 4**

Influence of illumination and tracers on Particle Image Velocimetry measurements on open flow channels Influența iluminării și a traseoarelor asupra măsurătorilor de velocimetrie a imaginii particulelor pe canalele de curgere deschise	365-370
<i>Ilinca NASTASE, Mihnea SANDU, Marius ILIESCU, Amjed ALBAIYATI</i>	
Steady heat transfer by natural (free) convection and radiation, for a horizontal circular pipe surrounded by air, using the Mathcad® software Transfer constant de căldură prin convecție naturală (liberă) și radiație, pentru o țevă circulară orizontală înconjurată de aer, folosind software-ul Mathcad®	371-390
<i>Gelu-Adrian CHISĂLIȚĂ, Raluca MOLDOVAN</i>	
Theoretical aspects regarding energy efficiency in foods refrigeration and freezing Aspecte teoretice privind eficiența energetică în refrigerarea și congelarea alimentelor	391-401
<i>Alina GIRIP, Răzvan CALOTĂ, Mădălina NICHITA, Anica ILIE</i>	
In-situ and Laboratory Analysis of Treated Marine Soil by Consolidation Methods Analiza in situ și de laborator a solului marin tratat prin metode de consolidare	402-428
<i>Houssam KHELALFA</i>	
A Review Regarding the Heat Recovery from Wastewater O revizuire cu privire la recuperarea căldurii din apele uzate	429-438
<i>Amjed ALBAIYATI</i>	
Software programs used in designing of low voltage electrical distribution panels Programe software utilizate în proiectarea tablourilor electrice de distribuție de joasă tensiune	439-446
<i>Cristina Gabriela SĂRĂCIN, Diana PARAIPAN</i>	
Modeling the Drying Shrinkage of Structural Concretes Modelarea contracției prin uscare a betoanelor structurale	447-463
<i>Abderraouf KEBIR, Abdelmalek BRAHMA</i>	
Analiza implementării măsurilor de apărare împotriva incendiilor în clădiri civile Analysis of the implementation of fire protection measures in civil buildings	464-481
<i>Aurel TROFIN, Mihai Ciprian MITREA</i>	
Metodă eficientă de încălzire cu microunde pentru fabricarea spumei de sticlă din deșeu de sticlă Effective microwave heating method for manufacturing glass foam from glass waste	482-491
<i>Lucian PĂUNESCU, Sorin Mircea AXINTE, Marius Florin DRĂGOESCU, Bogdan Valentin PĂUNESCU</i>	
Expansion of glass waste by the double effect of liquid and solid foaming agents for manufacturing the cellular glass gravel (CGG) in a 10 kW-microwave oven Expandarea deșeurii de sticlă prin dublul efect al agenților de spumare lichid și solid pentru fabricarea pietrișului din spumă de sticlă (CGG) într-un cuptor cu microunde de 10 kW	492-503
<i>Lucian PĂUNESCU, Sorin Mircea AXINTE, Marius Florin DRĂGOESCU, Bogdan Valentin PĂUNESCU</i>	

**MATRIX ROM**  
**OP CHIAJNA CP 2**  
**077040 – ILFOV**  
**Tel. 021 4113617 Fax. 021 4114280**  
**e-mail: [office@matrixrom.ro](mailto:office@matrixrom.ro)**  
**[www.matrixrom.ro](http://www.matrixrom.ro)**

#### **EDITORIAL BOARD**

Ph.D. R.S.AJIN, *Kerala State Disaster Management Authority, India*  
Ph.D.Prof.Eng. Ioan BOIAN, *Transilvania University of Brasov, Romania*  
Ph.D.Prof.Eng. Ioan BORZA, *Polytechnic University of Timisoara, Romania*  
Ph.D.Assoc.Prof.Eng. Vasilică CIOCAN, *Gh. Asachi Technical University of Iași, Romania*  
Ph.D.Prof. Stefano CORGNATI, *Politecnico di Torino, Italy*  
Ph.D.Assoc.Prof.Eng. Andrei DAMIAN, *Technical University of Constructions Bucharest, Romania*  
Ph.D.Prof. Yves FAUTRELLE, *Grenoble Institute of Technology, France*  
Ph.D.Prof.Eng. Carlos Infante FERREIRA, *Delft University of Technology, The Netherlands*  
Ph.D.Prof. Manuel GAMEIRO da SILVA, *University of Coimbra, Portugal*  
Ph.D.Prof.Eng. Dragoș HERA, *Technical University of Constructions Bucharest, Romania, honorary member*  
Ph.D. Jaap HOGELING, *Dutch Building Services Knowledge Centre, The Netherlands*  
Ph.D.Prof.Eng. Ovidiu IANCULESCU, *Romania, honorary member*  
Ph.D.Lawyer Cristina Vasilica ICOCIU, *Polytechnic University of Bucharest, Romania*  
Ph.D.Prof.Eng. Anica ILIE, *Technical University of Constructions Bucharest, Romania*  
Ph.D.Prof.Eng. Gheorghe Constantin IONESCU, *Oradea University, Romania*  
Ph.D.Prof.Eng. Florin IORDACHE, *Technical University of Constructions Bucharest, Romania – director editorial*  
Ph.D.Prof.Eng. Vlad IORDACHE, *Technical University of Constructions Bucharest, Romania*  
Ph.D.Prof.Eng. Karel KABELE, *Czech Technical University, Prague, Czech Republic*  
Ph.D.Prof. Birol KILKIS, *Baskent University, Ankara, Turkey*  
Ph.D.habil. Assoc.Prof. Zoltan MAGYAR, *Budapest University of Technology and Economics, Hungary*  
Ph.D.Assoc.Prof.Eng. Carmen MĂRZA, *Technical University of Cluj Napoca, Romania*  
Ph.D.Prof.Eng. Ioan MOGA, *Technical University of Cluj Napoca, Romania*  
Ph.D.Assoc.Prof.Eng. Gilles NOTTON, *Pascal Paoli University of Corsica, France*  
Ph.D.Prof.Eng. Daniela PREDA, *Technical University of Constructions Bucharest, Romania*  
Ph.D.Prof.Eng. Adrian RETEZAN, *Polytechnic University of Timisoara, Romania*  
Ph.D. Boukarta SOUFIANE, *Institute of Architecture and Urban Planning, BLIDAI, Algeria*  
Ph.D.Assoc.Prof.Eng. Daniel STOICA, *Technical University of Constructions Bucharest, Romania*  
Ph.D.Prof. Branislav TODORVIĆ, *Belgrad University, Serbia*  
Ph.D.Prof. Marija S. TODORVIĆ, *Academy of Engineering Sciences of Serbia*  
Ph.D.Eng. Ionuț-Ovidiu TOMA, *Gh. Asachi Technical University of Iași, Romania*  
Ph.D.Prof.Eng. Ioan TUNS, *Transilvania University of Brasov, Romania*  
Ph.D.Assoc.Prof.Eng. Constantin ȚULEANU, *Technical University of Moldova Chisinau, Republic of Moldova*  
Ph.D.Assoc.Prof.Eng. Eugen VITAN, *Technical University of Cluj Napoca, Romania*

**Romanian Journal of Civil Engineering is founded, published and funded by  
publishing house MATRIX ROM  
Executive Director: mat. Iancu ILIE**

**Online edition ISSN 2559-7485**

**Print edition ISSN 2068-3987; ISSN-L 2068-3987**

## Influence of illumination and tracers on Particle Image Velocimetry measurements on open flow channels

Influența iluminării și a trasoarelor asupra măsurătorilor de velocimetrie a imaginii particulelor pe canalele de curgere deschise

Ilinca Nastase<sup>1</sup>, Mihnea Sandu<sup>1</sup>, Marius Iliescu<sup>1</sup>, Amjed Albaiyati<sup>1,2</sup>

<sup>1</sup> CAMBI Research Center, Technical University of Civil Engineering Bucharest  
021414 Bucharest, Romania  
aamjed1@yahoo.com

<sup>2</sup> Kut Technical Institute, Middle Technical University  
Iraq

DOI: 10.37789/rjce.2021.12.4.1

**Abstract.** *Within the study of free surface flows, measurements in the vertical planes of the flow are desired. Using Particle Image Velocimetry, usually measurements are performed with the laser sheet through the bottom of the channel in order to avoid the optical perturbations on the laser light sheet, generating light scattering and measurement artefacts. There are however a number of cases where this is not possible since the transparence of the bottom cannot be ensured. In the present study we wanted to check the influence of the illumination on the velocity fields distribution, through the bottom of the channel or through the free surface, on a very simple flow on a plane plate placed on the bottom of a circular channel. We also checked the influence on using conventional silver hollow glass spheres and fluorescent particles.*

*The results allowed us to conclude that in the cases where the study is focused on the boundary layer close to the solid surface and the observed perturbations of the free surface are not important, top illumination of the open channel might be considered as an option if perturbations of the free surface are not observed.*

**Key words:** *PIV, free surface flows, optical techniques*

### 1. Introduction

Particle Image Velocimetry (PIV) represents a reference tool for the analysis of a wide range of flows. A wide range of three-dimensional applications, including free surface flows, can be found in the recent literature.

The application of PIV for experimental studies in open-channel flows can be challenging due to the presence of strong velocity gradients and the inclusion of moving interfaces in the captured images. This way, understanding the performance

and limitations of the PIV technique under these conditions is critical for optimizing experimental parameters and robust interpretation of data. The accuracy and precision of PIV measurements is highly affected by the quality of the captured images which in its turn depends on several conditions that should be accomplished by the channel and the fluid. Thus, besides complying with the conditions imposed by ensuring geometrical similitude, the experimental models for internal flows must comply with two specific conditions: the ability of the tracer particles to follow the instantaneous motion of the continuous phase and to scatter light on one hand and the transparency and the refraction index of the channel.

When working with free surface flows, usually measurements in the vertical planes of the flow are desired. In this case it is somehow acknowledged as common sense that the laser sheet would pass through the bottom of the channel. Indeed, the presence of the strongly perturbed free surface would act inducing optical perturbations on the laser light sheet, generating parasite scattering as well. There are however cases where this is not possible since the transparency of the bottom cannot be ensured.

Studies of our colleagues [1, 2] regarded for instance the flow characteristics of artificially roughened channels simulating deposits on sewer pipes. Other studies were interested on the flow around bodies immersed near the free surface of the channel [3].

In these two examples is impossible to insure illumination through the bottom of the channel. During an experimental campaign related to an extension of the analysis performed in [1, 2], we wanted to check the influence of the illumination on the velocity fields distribution, through the bottom of the channel or through the free surface, on a very simple flow on a plane plate placed on the bottom of a circular channel (Fig. 1). We also checked at the occasion the influence on using conventional silver hollow glass spheres and fluorescent particles.

## 2. Methodology

In this study it has been considered a system which generates a free surface flow in a circular sewage pipe, with deposit material at the bottom. The interior pipe diameter is  $D_i=144$  mm, pipe length is 3,9 m made of poly acrylate. The experimental setup is presented in Figure 1. The water is pumped from the tank (1) towards the tank (5). This one is a free surface tank and from here we obtain a free surface flow through the main poly acrylate pipe from the tank (5) towards the tank (1). The flow rate is determined with an ultrasonic flow meter (6) and it may be varied using a regulation valve. A plane plate was fixed on the bottom of the channel to simulate the deposits on the bottom of the pipe.

In this study, we have employed a Dantec Particle Image Velocimetry (PIV) system for the velocity field measurements. This system is composed of one high sensitivity Flow Sense EO camera of  $4 \times 10^6$  pixels resolution and of a Dual Power 200 mJ laser having the wavelength of 532 nm. The acquisition frequency of the PIV

Influence of illumination and tracers on Particle Image Velocimetry measurements on open flow channels  
 system was 5 Hz. The image calibration gave a spatial resolution of  $160\text{ }\mu\text{m}$  per pixel, which corresponds to a  $270 \times 270\text{ mm}^2$  field of view.

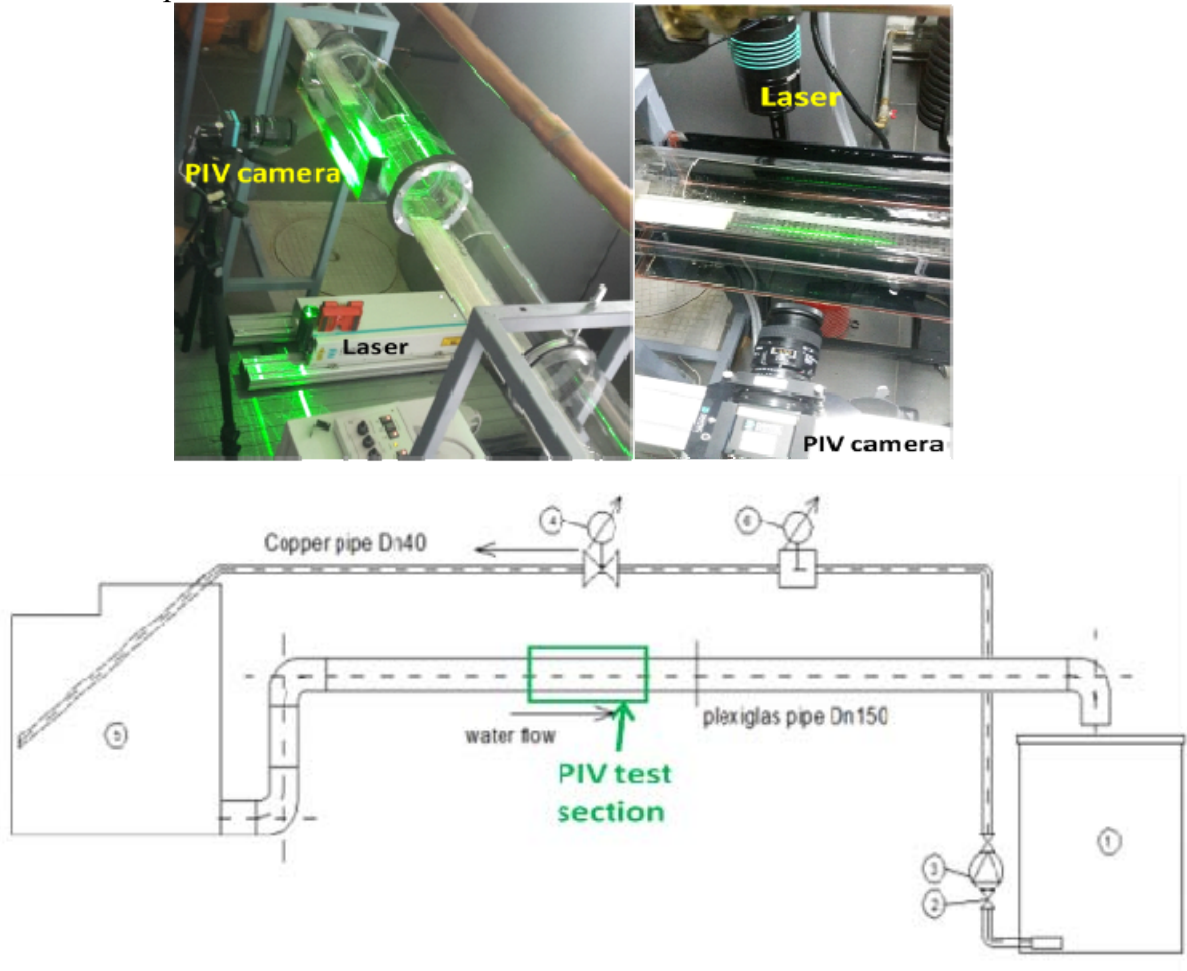


**Fig. 1** Experimental set-up using the laser illumination from the bottom of the channel and from the top of the channel through the free surface

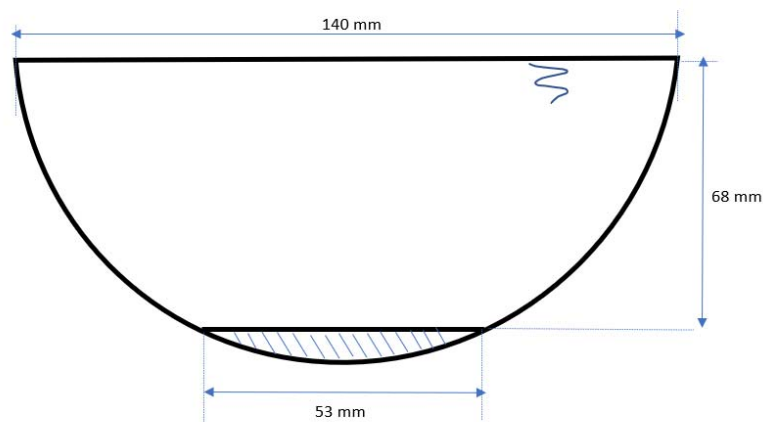


**Fig. 2** Plate plane on the bottom of the channel simulating deposits

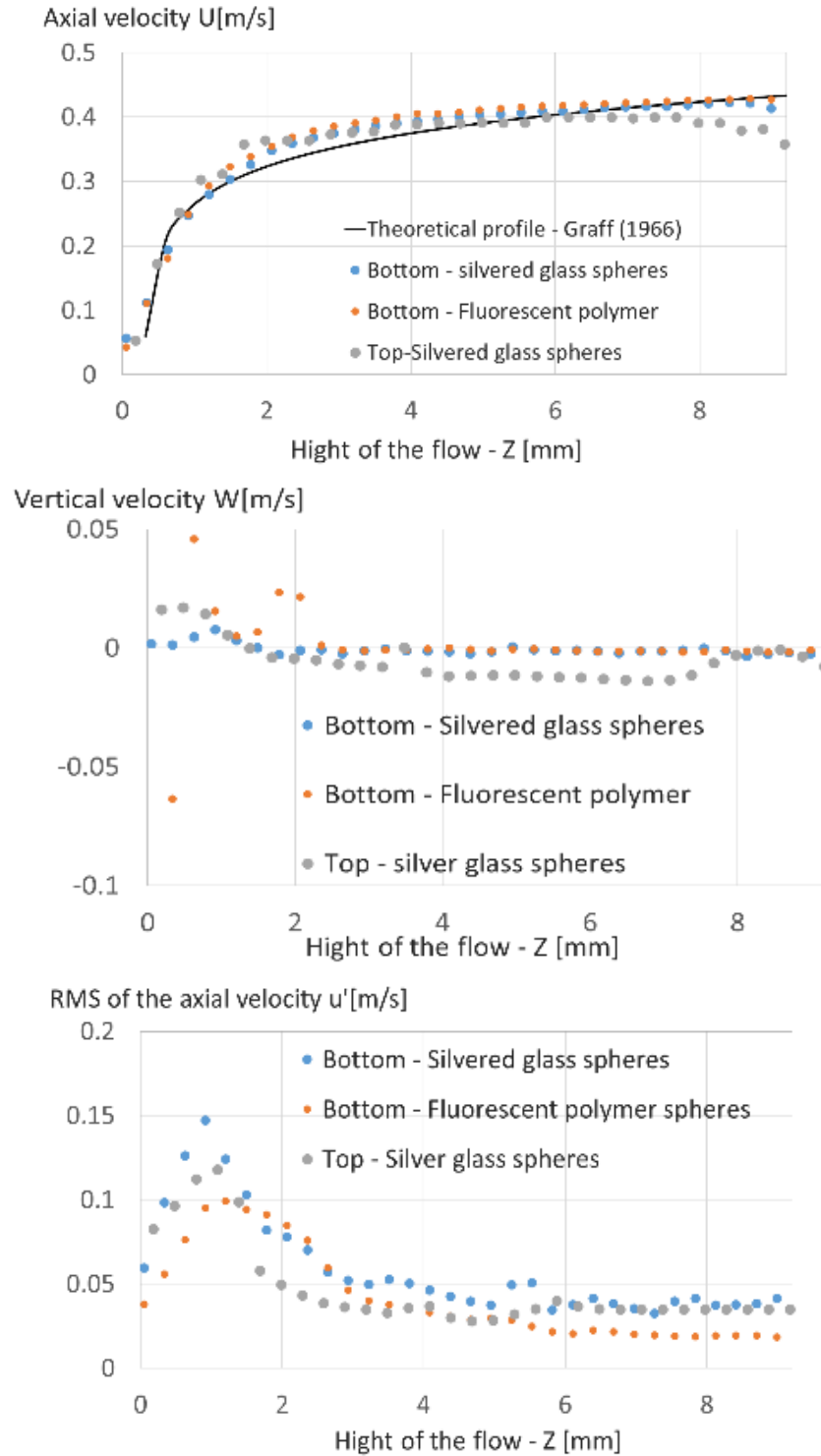


**Fig. 3** Comparison of the axial and vertical velocity profiles and of the RMS of the axial velocity for one of the studied flow rates corresponding to a free stream velocity of 0.3m/s

As we wanted to check the influence of the position of the laser plane on the velocity fields distribution, passing through the bottom of the channel or through the free surface, we chose to use this on a very simple flow on the plane plate placed on the bottom of a circular channel (Fig. 1). We also wanted to compare the influence on using conventional silver hollow glass spheres and fluorescent particles.

To this end two types of tracer particles were compared along with two laser illumination strategies: a) the laser plane was incident from the bottom of the channel and silvered glass micro-spheres were used, b) the laser plane was incident from the bottom of the channel and fluorescent polymer micro-spheres were used, c) the laser plane was incident from the top of the channel and silvered glass micro-spheres were used.

### 3. Results

The axial velocity profiles presented in Fig. 3 display differences only next to the free surface. We observed this phenomenon for several flow rates corresponding to free stream velocities of respectively: 0.3m/s, 0.5m/s, 0.6m/s, 0.7m/s. The surface velocity seems to display slight smaller values for the lowest flowrates in the case with top illumination. This gap is much reduced for higher flowrates.

Using the empirical profile proposed by Graf [4] one could observe that the top illumination cases are display closer values to the ones preconized by the theory. It is important to note here that we couldn't observe, with the naked eye, perturbations of the free surface of the flow.

Concerning the vertical velocities and the RMS values of the velocity components, values are quite different for the different seedings as well as for the two positions of the illuminations. However, these differences fall into the measurement method incertitude.

We have to note also that the polymer fluorescent particles have a slightly higher density than the one of the water, while the hollow silvered glass spheres have a slightly lower density and this could also influence the velocity profile distribution observed in the previous figures.

### Conclusions

Within the study of free surface flows, measurements in the vertical planes of the flow are desired. Using Particle Image Velocimetry, usually measurements are performed with the laser sheet through the bottom of the channel in order to avoid the optical perturbations on the laser light sheet, generating light scattering and measurement artefacts. There are however a number of cases where this is not possible since the transparence of the bottom cannot be ensured. In the present study we wanted to check the influence of the illumination on the velocity fields distribution, through the bottom of the channel or through the free surface, on a very simple flow on a plane

plate placed on the bottom of a circular channel. We also checked the influence on using conventional silver hollow glass spheres and fluorescent particles.

The results allowed us to conclude that in the cases where the study is focused on the boundary layer close to the solid surface and the observed perturbations of the free surface are not important, top illumination of the open channel might be considered as an option if perturbations of the free surface are not observed.

## References

1. Iliescu, M., et al., *An Experimental Approach Regarding the Sewage Self-Cleansing Conditions*. Energy Procedia, 2016. **85**: p. 266-272.
2. Iatan, E., et al., *Numerical Study for Open-channel Flow over Rows of Hemispheres*. Energy Procedia, 2016. **85**: p. 260-265.
3. Tanase, N.O., D. Broboana, and C. Balan, *Flow around an immersed cylinder in the presence of free surface*. U.P.B. Sci. Bull. Series D, 2014 **76**(2).
4. Graf, W.H., *Hydraulics of Sediment Transport*, McGraw-Hill, New York. 1966.



# Steady heat transfer by natural (free) convection and radiation, for a horizontal circular pipe surrounded by air, using the Mathcad® software

Transfer constant de căldură prin convecție naturală (liberă) și radiație, pentru o țevă circulară orizontală înconjurată de aer, folosind software-ul Mathcad®

Gelu-Adrian CHISĂLIȚĂ<sup>1</sup>, Raluca MOLDOVAN<sup>2</sup>

<sup>1</sup>Technical University of Cluj-Napoca, Romania  
Faculty of Building Services Engineering, Department of Building Services Engineering  
e-mail: [gelu.chisalita@insta.utcluj.ro](mailto:gelu.chisalita@insta.utcluj.ro)

<sup>2</sup>Technical University of Cluj-Napoca, Romania  
Faculty of Building Services Engineering, Department of Building Services Engineering  
e-mail: [raluca.moldovan@insta.utcluj.ro](mailto:raluca.moldovan@insta.utcluj.ro)

DOI: 10.37789/rjce.2021.12.4.2

**Abstract.** *The paper presents a study on the heat transfer in steady state, by natural convection and radiation, from a circular pipe to the surrounding air. Using the Mathcad® software application, the calculation procedure for the average heat transfer coefficient on the surface by convection, radiation and combined was implemented on the computer, as well as the determination of the heat flux density (the rate of heat transfer per unit time per unit length) taking into account various values of the outer surface temperature of the pipe. The results of the study show that neglecting the heat transfer by thermal radiation, even for low temperatures with values in the range of 40°C...90°C, can lead to relatively high technical errors in estimating the heat loss of pipes. In these situations, is necessary to take into account the combined heat transfer by natural convection and thermal radiation.*

**Keywords:** heat, transfer, steady state, natural convection, radiation, Mathcad

**Rezumat.** *Lucrarea prezintă un studiu privind transmiterea căldurii în regim termic staționar, prin convecție termică liberă și radiație, de la o conductă cu secțiune circulară către aerul înconjurător. Cu ajutorul aplicației software Mathcad®, a fost implementată pe calculator procedura de calcul pentru coeficienții de transfer termic superficiali prin convecție, radiație și combinat, precum și determinarea valorii fluxului termic unitar raportat la unitatea de lungime transmis mediului ambiant, având în vedere diverse valori ale temperaturii pe suprafața exterioară a conductei. Rezultatele studiului indică faptul că neglijarea transferului de căldură prin radiație termică, chiar în cazul unor temperaturi având valori cuprinse în intervalul 40°C...90°C, poate conduce la erori tehnice relativ ridicate privind estimarea pierderilor de căldură ale conductelor, fiind necesar a lua în calcul în aceste situații transferul termic combinat prin convecție și radiație.*

**Cuvinte cheie:** transfer, căldură, staționar, convecție termică, liberă, radiație termică, Mathcad

## 1. Introduction

The general approach of studying and solving a case of thermal convection is usually done by using empirical correlations indicated in the literature, characteristic of a class, category, type etc. of a convection phenomenon analyzed, such as: thermal convection with or without phase change, natural (free) convection or forced convection, thermal convection in open spaces (unlimited spaces or large volumes) or thermal convection in closed spaces (limited spaces or small volumes) etc.

For the case of natural (free) convection that occurs in open spaces, the commonly used empirical correlation has the general form (1) [1], [2], [3], [4] etc.

$$Nu = C \cdot (Gr \cdot Pr)^m \text{ or } Nu = C \cdot Ra^m \quad (1)$$

where:

- Nu – Nusselt number;
- Gr – Grashof number;
- Pr – Prandtl number;
- Ra – Rayleigh number ( $Ra = Gr \cdot Pr$ );
- C, m – Dimensionless constants depending on the fluid flow regime.

The average Nusselt number (Nu) is expressed by the general definition relationship (2) [1], [4], [5], [6], [7] etc.

$$Nu = \frac{\alpha}{\lambda} \cdot l_c \quad (2)$$

where:

- $\alpha$  – Convection heat transfer coefficient [ $W/m^2 \cdot K$ ];
- $\lambda$  – Thermal conductivity of the fluid [ $W/m \cdot K$ ];
- $l_c$  – Characteristic length [m].

The Grashof number (Gr) can be determined using the formula (3) [1], [4], [5] etc.

$$Gr = \frac{g \cdot l_c^3}{\nu^2} \cdot \beta \cdot \Delta t \quad (3)$$

where:

- g – Acceleration due to gravity [ $m/s^2$ ];
- $l_c$  – Characteristic length [m];
- $\nu$  – Kinematic viscosity [ $m^2/s$ ];
- $\beta$  – Isobaric volume expansion coefficient [ $1/K$ ];
- $\Delta t$  – Temperature difference  $\Delta t = t_f - t_s$  (or vice versa) [ $^{\circ}C$ ].

The Prandtl number (Pr) is expressed using the relationship (4) [1], [3], [4], [5], [6] etc.

$$Pr = \frac{\nu}{a} \quad (4)$$

where:

- $\nu$  – Kinematic viscosity [ $m^2/s$ ];
- a – Thermal diffusivity (heat diffusivity) [ $m^2/s$ ].

Usually, the Prandtl number is determined from the tables of properties for various fluids, depending on the temperature.

Steady heat transfer by natural (free) convection and radiation, for a horizontal circular pipe surrounded by air, using the Mathcad® software

Knowing the value of the Nu number, one can calculate from relationship (1) the heat transfer coefficient by convection  $\alpha_C$ , using the formula (5) [1], [4], [5], [7] etc.

$$\alpha_C = \frac{Nu \cdot \lambda}{l_c} \quad (5)$$

and then, from Newton's law (6) is obtained the rate of heat transfer by natural convection (heat flux)  $\dot{Q}$  [1], [2], [3], [4], [5], [6] etc.

$$\dot{Q} = \alpha_C \cdot A \cdot (t_f - t_s) \text{ [W]} \quad (6)$$

where:

- $\alpha_C$  – Average heat transfer coefficient by convection [W/m<sup>2</sup>·K];
- $t_f$  – Temperature of the fluid [°C];
- $t_s$  – Temperature of the contact surface between solid and fluid [°C];
- $A$  – Heat transfer surface area [m<sup>2</sup>].

In order to determine the heat flux density  $\dot{q}$  per unit length (the rate of heat transfer per unit time per unit length), in the case of a circular pipe with diameter  $d$ , we can use the relationship (7) [4], [8], [9] etc.

$$\dot{q}_C = \alpha_C \cdot (\pi \cdot d) \cdot (t_f - t_s) \left[ \frac{\text{W}}{\text{m}} \right] \quad (7)$$

where the product  $(\pi \cdot d)$  represents the lateral heat transfer surface area corresponding to a pipe length  $L=1.0$  m.

If heat transfer by thermal radiation is also taken into account, a heat transfer coefficient by radiation  $\alpha_R$  can be determined, using the general relationship (8) [4], [5], [8], [9] etc.

$$\alpha_R = \frac{\varepsilon_{12} \cdot C_0 \cdot \left[ \left( \frac{T_1}{100} \right)^4 - \left( \frac{T_2}{100} \right)^4 \right]}{T_1 - T_2} \left[ \frac{\text{W}}{\text{m}^2 \cdot \text{K}} \right] \quad (8)$$

where:

- $\varepsilon_{12}$  – Reciprocal emission-absorption coefficient [–];
- $T_1, T_2$  – Absolute temperatures of surfaces [K];
- $C_0$  – The radiation coefficient of the absolute black body,  $C_0=5.67 \text{ W/m}^2 \cdot \text{K}^4$ .

The reciprocal emission-absorption coefficient  $\varepsilon_{12}$  is calculated with the relationships indicated in the literature, characteristic of a certain case of thermal radiation [2], [3], [4], [5], [6], [8] §.a.

For example, for the case of two surfaces  $S_1$  and  $S_2$ , enclosed in each other, one can use the general relationship (9) [4], [5], [8] etc.

$$\varepsilon_{12} = \frac{1}{\frac{1}{\varepsilon_1} + \frac{S_1}{S_2} \left( \frac{1}{\varepsilon_2} - 1 \right)} \text{ [–]} \quad (9)$$

where  $\varepsilon_1$  represents the emission-absorption coefficient of surface  $S_1$  and  $\varepsilon_2$  is the emission-absorption coefficient of surface  $S_2$ .

The heat flux density  $\dot{q}_R$  (per unit length), transferred by thermal radiation in the case of a cylindrical body having a diameter  $d$ , for example a pipe with a circular section, is calculated by using the formula (10) [4], [5], [8], [9] etc.

$$\dot{q}_R = \varepsilon_{12} \cdot C_0 \cdot \left[ \left( \frac{T_1}{100} \right)^4 - \left( \frac{T_2}{100} \right)^4 \right] \cdot (\pi \cdot d) \left[ \frac{\text{W}}{\text{m}} \right] \quad (10)$$

Considering the simultaneous action of the two fundamental modes of heat transfer: thermal convection and thermal radiation, to determine the heat flux density  $\dot{q}_{CR}$  (per unit length) transferred by both convection and radiation, a combined heat transfer coefficient by convection and radiation  $\alpha_{CR}$  is calculated using the formula (11) [4], [5] etc.

$$\alpha_{CR} = \alpha_C + \alpha_R \quad (11)$$

and then applying the relationship (7), for example in form (12) or (13)

$$\dot{q}_{CR} = \alpha_{CR} \cdot (\pi \cdot d) \cdot (t_f - t_s) \left[ \frac{W}{m} \right] \quad (12)$$

$$\dot{q}_{CR} = \frac{t_f - t_s}{\frac{1}{\pi \cdot d \cdot \alpha_{CR}}} \left[ \frac{W}{m} \right] \quad (13)$$

As an alternative calculation or as a verification procedure, if the two-heat flux density  $\dot{q}_C$  and  $\dot{q}_R$  were previously determined using relationships (7) and (10), the heat flux density  $\dot{q}_{CR}$  (per unit length), transferred by convection and radiation, is calculated using the formula (14)

$$\dot{q}_{CR} = \dot{q}_C + \dot{q}_R \left[ \frac{W}{m} \right] \quad (14)$$

This paper presents a study on how to solve a case of combined heat transfer, by natural (free) convection in open spaces and thermal radiation, for a circular pipe with an outside diameter  $d_e$ , surrounded by a fluid (air) as in figure 1.

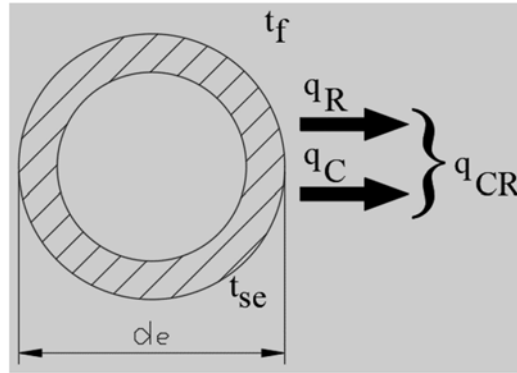


Fig. 1. Circular pipe surrounded by fluid (air)

The implementation of the problem-solving procedure was performed using the Mathcad® software application, taking into account the representation capabilities of this computer program regarding the following:

- Describing the calculation relationships mentioned above using a language as close as possible with the natural one;
- Enhanced possibilities to operate with various measurement units and their combinations;
- Efficient management of the thermophysical properties of the working fluids;
- Creating some general functions, more simple or more complex, used in calculations;
- Stylish presentation of the numerical and/or graphical results obtained etc.

Steady heat transfer by natural (free) convection and radiation, for a horizontal circular pipe surrounded by air, using the Mathcad® software

The method of problem-solving presented in this paper is quite easy to implement on computer and has the advantage of quickly obtaining the pursued numerical and/or graphical results.

Also, the indicated method is particularly useful especially in cases where some data of the problem may undergo a series of changes, compared to the initial situation treated in a solving phase. For example, the outer surface temperature of the pipe  $t_{se}$  can vary in a certain technical range of interest, the fluid temperature  $t_f$  with which the heat exchange occurs may have certain reference values, the pipe geometry is modified or the material from which it is made is changed etc.

## 2. Methodology of solving the heat transfer problem

The technical application proposed for solve in this paper has the initial data and requirements specified by the following statement:

*A pipe  $\phi 1'' (25 \times 2.5 \text{ mm})$ , having a length  $L = 1 \text{ m}$ , it is placed horizontally in calm air. Knowing that the outer surface temperature of the pipe is  $t_{se} = 50^\circ\text{C}$  and the fluid (air) temperature is  $t_f = 10^\circ\text{C}$ , determine the followings:*

- The heat transfer coefficient by convection from the pipe surface to air;*
- The heat flux transferred by convection from the pipe surface to air;*
- The heat transfer coefficient by radiation;*
- The heat flux transferred by radiation;*
- The heat transfer coefficient by convection and radiation;*
- The heat flux transferred by convection and radiation.*

The creation of the automatic spreadsheet used to solve the proposed case involves performing several successive work steps, which will be described below.

### DATELE PROBLEMEI

ORIGIN  $\equiv 1$  °C  $\equiv 1$  K  $\equiv$  °C

#### Caracteristici fluid

Tipul Fluid := "Aer"

Temperatura  $t_f := 10 \cdot ^\circ\text{C}$

#### Caracteristici corp

Diametru exterior  $d_e := 25 \cdot \text{mm}$

Grosime perete  $\delta := 2.5 \cdot \text{mm}$

Lungime  $L := 1 \cdot \text{m}$

Temperatura suprafata  $t_{se} := 50 \cdot ^\circ\text{C}$

#### Coeficienti de emisie-absorbtie

Corp  $\epsilon_{s1} := 0.8$

Mediu ambiant  $\epsilon_{s2} := 1$

Coeficient de radiatie al corpului negru absolut

$$C_0 := 5.67 \cdot \frac{\text{W}}{\text{m}^2 \cdot \text{K}^4}$$

Constanta Stefan-Boltzmann

$$\sigma := 5.67 \cdot 10^{-8} \cdot \frac{\text{W}}{\text{m}^2 \cdot \text{K}^4}$$

Fig. 2. The implementation of the initial data

First, the initial data of the problem are specified and implemented. These are represented by: the characteristics of the working fluid, the geometric and thermal characteristics of the pipe, the emission-absorption coefficients of the body and the environment, as well as the values of the radiation coefficient of the absolute black body, respectively the Stefan-Boltzmann constant (figure 2).

Because a series of initial data such as: outer surface temperature of the pipe  $t_{se}$ , fluid temperature  $t_f$ , emission-absorption coefficients, geometry of the pipe etc. may undergo various changes, it is preferable specify them as separate variables instead of using constant values entered directly in calculation formulas.

The function for calculating the heat transfer coefficient by convection  $\alpha_c$  shall be introduced in accordance with relationship (5) and the functions used for the determination by linear interpolation of the thermophysical properties of the working fluid (figure 3) shall be introduced using the properties table from figure 4 [8], [9] etc.

*a) Coeficientul de convecție de la corp la fluid*

$$\text{Criteriul Nusselt } Nu = \frac{\alpha}{\lambda} \cdot l_c \quad \text{Coeficientul de convecție } \alpha = Nu \cdot \frac{\lambda}{l_c} \quad \text{fn\_}\alpha(Nu, \lambda, l_c) := Nu \cdot \frac{\lambda}{l_c}$$

*Funcțiile proprietăților fizice*

$$\text{fn\_}\rho(\text{Temp}, \text{Densitate}, \text{ValTemp}) := \text{linterp}(\text{Temp}, \text{Densitate}, \text{ValTemp}) \cdot \frac{\text{kg}}{\text{m}^3}$$

$$\text{fn\_}\lambda(\text{Temp}, \text{Cond\_termica}, \text{ValTemp}) := \text{linterp}(\text{Temp}, \text{Cond\_termica}, \text{ValTemp}) \cdot \frac{\text{W}}{\text{m} \cdot ^\circ\text{C}}$$

$$\text{fn\_}\nu(\text{Temp}, \text{Visc\_cinematica}, \text{ValTemp}) := \text{linterp}(\text{Temp}, \text{Visc\_cinematica}, \text{ValTemp}) \cdot \frac{\text{m}^2}{\text{s}}$$

$$\text{fn\_Pr}(\text{Temp}, \text{Prandtl}, \text{ValTemp}) := \text{linterp}(\text{Temp}, \text{Prandtl}, \text{ValTemp})$$

$$\text{fn\_}\beta(\text{Temp}, \beta\_Coef\_Dil\_Vol\_p\_ct, \text{ValTemp}) := \text{linterp}(\text{Temp}, \beta\_Coef\_Dil\_Vol\_p\_ct, \text{ValTemp}) \cdot \frac{1}{\text{K}}$$

Fig. 3.  $\alpha$  function and linear interpolation functions

The mean fluid temperature shall be determined using the usual relationship (15)

$$t_m = \frac{t_f + t_s}{2} [^\circ\text{C}] \quad (15)$$

which is implemented by the generic function  $\text{fn\_}t_m(t_1, t_2)$  and corresponding to its value the thermophysical properties of the working fluid are calculated: thermal conductivity ( $\lambda_f$ ), kinematic viscosity ( $\nu_f$ ) and Prandtl number ( $\text{Pr}_f$ ).

The results given in figure 5 were obtained, where the characteristic length  $l_c$  used in the calculations below is also stated.

Steady heat transfer by natural (free) convection and radiation, for a horizontal circular pipe surrounded by air, using the Mathcad® software

Proprietati fizice pentru aer uscat  $p=1 \text{ atm}$

	$t[\text{C}]$	$\rho[\text{kg/m}^3]$	$c_p[\text{kJ/kgK}]$	$\lambda[\text{W/mK}]$	$\eta[\text{Ns/m}^2]$	$\nu[\text{m}^2/\text{s}]$	Pr
PropFiziceAer :=	1	2	3	4	5	6	7
6	0	1.293	1.005	0.024	$1.72 \cdot 10^{-5}$	$1.328 \cdot 10^{-5}$	0.707
7	10	1.247	1.005	0.025	$1.76 \cdot 10^{-5}$	$1.416 \cdot 10^{-5}$	0.705
8	20	1.205	1.005	0.026	$1.81 \cdot 10^{-5}$	$1.506 \cdot 10^{-5}$	0.703
9	30	1.165	1.005	0.027	$1.86 \cdot 10^{-5}$	$1.6 \cdot 10^{-5}$	0.701
10	40	1.128	1.005	0.028	$1.91 \cdot 10^{-5}$	$1.696 \cdot 10^{-5}$	0.699
11	50	1.093	1.005	0.028	$1.96 \cdot 10^{-5}$	$1.795 \cdot 10^{-5}$	0.698
12	60	1.06	1.005	0.029	$2.01 \cdot 10^{-5}$	$1.897 \cdot 10^{-5}$	0.696
13	70	1.029	1.009	0.03	$2.06 \cdot 10^{-5}$	$2.002 \cdot 10^{-5}$	...

Index\_t := 1   Index\_rho := 2   Index\_cp := 3   Index\_lambda := 4   Index\_eta := 5   Index\_nu := 6   Index\_Pr := 7

Fig. 4. The thermophysical properties of air [8], [9] etc

$$\begin{aligned}
 \text{Temperatura medie } t_m &= \frac{t_1 + t_2}{2} & \text{fn\_tm}(t_1, t_2) &:= \frac{t_1 + t_2}{2} \\
 t_m &:= \text{fn\_tm}(t_{se}, t_f) & t_m &= 30^\circ\text{C} \\
 \text{Proprietatile fizice pentru Fluid} &= \text{"Aer"} \text{ la temperatura medie } t_m = 30^\circ\text{C} \\
 \lambda_f &:= \text{fn\_}\lambda(\text{PropFiziceAer}^{\langle \text{Index\_}\lambda \rangle}, \text{PropFiziceAer}^{\langle \text{Index\_}t \rangle}, t_m) & \lambda_f &= 2.67 \times 10^{-2} \cdot \frac{\text{W}}{\text{m} \cdot ^\circ\text{C}} \\
 \nu_f &:= \text{fn\_}\nu(\text{PropFiziceAer}^{\langle \text{Index\_}\nu \rangle}, \text{PropFiziceAer}^{\langle \text{Index\_}t \rangle}, t_m) & \nu_f &= 1.6 \times 10^{-5} \cdot \frac{\text{m}^2}{\text{s}} \\
 \text{Pr}_f &:= \text{fn\_Pr}(\text{PropFiziceAer}^{\langle \text{Index\_}t \rangle}, \text{PropFiziceAer}^{\langle \text{Index\_}Pr \rangle}, t_m) & \text{Pr}_f &= 0.701 \\
 \text{Lungimea caracteristica } l_c &= d_e & l_c &:= d_e \\
 & & l_c &= 0.025 \text{ m}
 \end{aligned}$$

Fig. 5. The calculus of mean temperature  $t_m$  and thermophysical properties of the fluid (air)

The function for calculating the Gr number shall be introduced in accordance with relationship (3), where the volume expansion coefficient at constant pressure (isobaric volume expansion coefficient)  $\beta$  is calculated using formula (16), approximating the behavior of fluid (air) with a perfect/ideal gas (GP/I)

$$\beta \approx \frac{1}{T_m} \left[ \frac{1}{\text{K}} \right] \quad (16)$$

and  $T_m$  represents the mean absolute temperature of the fluid.

For the determination of the fluid flow regime, using relationship (17) [1], [2], [3], [4], [6] etc. the value of product  $\text{Gr} \cdot \text{Pr}$  or the Ra number shall be calculated (figure 6)

$$\text{Ra} = \text{Gr} \cdot \text{Pr} \quad (17)$$

$$\begin{aligned}
 \text{Criteriul Grashof} \quad Gr &= \frac{g \cdot l_c^3}{\nu^2} \cdot \beta \cdot (t_1 - t_2) & \text{fn\_Gr}(l_c, \nu, \beta, t_1, t_2) &:= \frac{g \cdot l_c^3}{\nu^2} \cdot \beta \cdot |(t_1 - t_2)| \\
 \text{Coeficientul de dilatare volumica} & & & \\
 \text{la presiune constanta pentru gaz} \quad \beta &= \frac{1}{T} & \text{fn\_}\beta_{\text{Gaz}}(T) &:= \frac{1}{T} \cdot \frac{1}{K} \\
 \beta &:= \text{fn\_}\beta_{\text{Gaz}}(t_m + 273.15) & & \beta = 3.2987 \times 10^{-3}, \frac{1}{K} \\
 Gr &:= \text{fn\_Gr}(l_c, \nu_f, \beta, t_{se}, t_f) & & Gr = 7.89775 \times 10^4 \\
 \text{Criteriul Rayleigh (produsul Gr*Pr)} \quad Ra_f &= Gr_f \cdot Pr_f & \text{fn\_Ra}(Gr, Pr) &:= Gr \cdot Pr \\
 Ra &:= \text{fn\_Ra}(Gr, Pr_f) & & Ra = 5.53632 \times 10^4
 \end{aligned}$$

Fig. 6. The calculus of the Gr number and the product Gr·Pr (the Ra number)

In solving the case of heat transfer by natural convection in open spaces, consideration was given to the use of an empirical correlation with general form (1), in which dimensionless constants C and m are chosen with respect to the fluid flow regime according to table 1 [1], [4], [5], [8], [9] etc.

*Table 1*  
**C and m constants characteristic to the empirical correlation (1) [1], [4], [5], [8], [9] etc.**

Crt no.	Flow regime	Gr·Pr	C	m
1	Film	$10^{-4} \dots 10^{-3}$	0.50	0
2	Transient	$10^{-3} \dots 500$	1.18	1/8
3	Laminar	$500 \dots 2 \cdot 10^7$	0.54	1/4
4	Turbulent	$2 \cdot 10^7 \dots 10^{13}$	0.135	1/3

The results obtained for the Nu number and the heat transfer coefficient by convection  $\alpha_C$  are shown in figure 7.

$$\begin{aligned}
 &\text{Constantele ecuatiei criteriale (formule MIHEEV)} \\
 &\text{fn\_C}(Ra) := \text{if}(Ra < 2 \cdot 10^7, 0.54, 0.135) & \text{fn\_m}(Ra) &:= \text{if}\left(Ra < 2 \cdot 10^7, \frac{1}{4}, \frac{1}{3}\right) \\
 &\underline{C} := \text{fn\_C}(Ra) & & C = 0.54 \\
 &\text{const\_m} := \text{fn\_m}(Ra) & & \text{const\_m} = 0.25 \\
 &\text{Criteriul Nusselt} \quad Nu = C \cdot (Gr \cdot Pr)^m & \text{fn\_Nu}(C, Ra, m) &:= C \cdot Ra^m \\
 &Nu := \text{fn\_Nu}(C, Ra, \text{const\_m}) & & Nu = 8.283 \\
 &\alpha_C := \text{fn\_}\alpha(Nu, \lambda_f, l_c) & & \alpha_C = 8.8465 \cdot \frac{W}{m^2 \cdot K}
 \end{aligned}$$

Fig. 7. The calculus of the Nu number and the heat transfer coefficient by convection  $\alpha_C$



Steady heat transfer by natural (free) convection and radiation, for a horizontal circular pipe surrounded by air, using the Mathcad® software

To verify the final results obtained and also to calculate in other situations directly the heat transfer coefficient by convection  $\alpha_C$ , including for other fluids e.g., liquids the synthetic calculation function shown in figure 8 have been created.

*Funcție sintetică pentru calculul coeficientului de convecție liberă în spații nelimitate (deschise); relații Miheev*

*Definirea identificatorului fluidului*      **Gaz := 1    Lichid := 2**

$\text{fn\_}\alpha_{\text{ConvLib\_SpDes}}(t_f, t_s, l_c, \text{Fluid}, \text{PropFizice}) :=$

$t_m \leftarrow \frac{t_f + t_s}{2}$ $\text{Vector\_Temp} \leftarrow \text{PropFizice}^{(\text{Index}_t)}$ $\text{Vector}_\rho \leftarrow \text{PropFizice}^{(\text{Index}_\rho)}$ $\text{Vector}_\lambda \leftarrow \text{PropFizice}^{(\text{Index}_\lambda)}$ $\text{Vector}_\nu \leftarrow \text{PropFizice}^{(\text{Index}_\nu)}$ $\text{Vector\_Pr} \leftarrow \text{PropFizice}^{(\text{Index}_\text{Pr})}$ $\text{Vector}_\beta \leftarrow \text{PropFizice}^{(\text{Index}_\beta)}$ $\lambda \leftarrow \text{linterp}(\text{Vector\_Temp}, \text{Vector}_\lambda, t_m) \cdot \frac{\text{W}}{\text{m} \cdot \text{K}}$ $\nu \leftarrow \text{linterp}(\text{Vector\_Temp}, \text{Vector}_\nu, t_m) \cdot \frac{\text{m}^2}{\text{s}}$ $\text{Pr} \leftarrow \text{linterp}(\text{Vector\_Temp}, \text{Vector\_Pr}, t_m)$ $\beta \leftarrow \frac{1}{t_m + 273.15} \cdot \frac{1}{\text{K}} \quad \text{if Fluid} = \text{Gaz}$ $\text{if Fluid} = \text{Lichid}$ $\rho_f \leftarrow \text{linterp}(\text{Vector\_Temp}, \text{Vector}_\rho, t_f) \cdot \frac{\text{kg}}{\text{m}^3}$ $\rho_s \leftarrow \text{linterp}(\text{Vector\_Temp}, \text{Vector}_\rho, t_s) \cdot \frac{\text{kg}}{\text{m}^3}$ $\beta_{\text{formula}} \leftarrow \frac{\rho_f - \rho_s}{\rho_f (t_s - t_f)}$ $\beta \leftarrow \text{linterp}(\text{Vector\_Temp}, \text{Vector}_\beta, t_m)$ $\text{Gr} \leftarrow \frac{g \cdot l_c^3}{\nu^2} \cdot \beta \cdot  t_f - t_s $ $\text{Ra} \leftarrow \text{Gr} \cdot \text{Pr}$ $\text{Nu} \leftarrow \begin{cases} 0.5 & \text{if } \text{Ra} \leq 10^{-3} \\ \left( 1.18 \cdot \text{Ra}^{\frac{1}{8}} \right) & \text{if } 10^{-3} < \text{Ra} \leq 500 \\ \left( 0.54 \cdot \text{Ra}^{\frac{1}{4}} \right) & \text{if } 500 < \text{Ra} \leq 2 \cdot 10^7 \\ \left( 0.135 \cdot \text{Ra}^{\frac{1}{3}} \right) & \text{otherwise} \end{cases}$ $\alpha \leftarrow \text{Nu} \cdot \frac{\lambda}{l_c}$ $\text{return } \alpha$	$\text{error}(\text{"Eroare: Fluid = Gaz (1) sau Lichid (2)"} ) \quad \text{otherwise}$
---	---

$\alpha_{C\_verif} := \text{fn\_}\alpha_{\text{ConvLib\_SpDes}}(t_f, t_{se}, l_c, \text{Gaz}, \text{PropFiziceAer})$        $\alpha_{C\_verif} = 8.8465 \cdot \frac{\text{W}}{\text{m}^2 \cdot \text{K}}$

Fig. 8. Synthetic function for direct calculus of the heat transfer coefficient by convection  $\alpha_C$

The calculus of the heat flux density  $\dot{q}_C$  (per unit length), transferred by natural convection, was performed by implementing the relationship (7) and the value from figure 9 was obtained.

*b) Fluxul termic transferat prin convecție de la corp la fluid*

*Fluxul termic unitar transmis  
prin convecție de la un fluid  
la un perete cilindric*

$$q_{\text{Conv\_PC}} = \frac{t_f - t_s}{\frac{1}{\pi \cdot d \cdot \alpha}} \quad \text{fn\_qConv\_PC}(\alpha, d, t_f, t_s) := \alpha \cdot \pi \cdot d \cdot |(t_f - t_s)|$$

*Fluxul termic total transferat  
printr-un perete cilindric*

$$Q = q \cdot L \quad \text{fn\_QPC}(q, L) := q \cdot L$$

$$q_{\text{conv}} := \text{fn\_qConv\_PC}(\alpha_C, d_e, t_f, t_{se})$$

$$q_{\text{conv}} = 27.792 \cdot \frac{\text{W}}{\text{m}}$$

$$Q_{\text{conv}} := \text{fn\_QPC}(q_{\text{conv}}, L)$$

$$Q_{\text{conv}} = 27.792 \cdot \text{W}$$

Fig. 9. The calculus of the heat flux density  $\dot{q}_C$  (per unit length)

To obtain the heat transfer coefficient by radiation  $\alpha_R$ , the reciprocal emission-absorption coefficient  $\epsilon_{12}$  (figure 10) has been calculated beforehand using the formula (9), in which the surface  $S_2$  of the environment has been considered infinite ( $S_2 = \infty$ ).

*c) Coeficientul de TRO superficial prin radiație*

$\alpha_R$

*Coeficientul reciproc de emisie  
pentru 2 suprafețe cuprinse una în  
cealalta  $S_1 < S_2$*

$$\epsilon_{12\_S1S2} = \frac{1}{\frac{1}{\epsilon_1} + \frac{S_1}{S_2} \cdot \left( \frac{1}{\epsilon_2} - 1 \right)}$$

$$\text{fn\_}\epsilon_{12\_S1S2}(\epsilon_1, \epsilon_2, S_1, S_2) := \frac{1}{\frac{1}{\epsilon_1} + \frac{S_1}{S_2} \cdot \left( \frac{1}{\epsilon_2} - 1 \right)}$$

*Arie laterala corp*

$$S_1 := \pi \cdot d_e \cdot L$$

$$S_1 = 0.079 \text{ m}^2$$

*Suprafata mediu ambiant (infinita)*

$$S_2 := \infty \text{ m}^2$$

$$\epsilon_{12\_S1S2} := \text{fn\_}\epsilon_{12\_S1S2}(\epsilon_{s1}, \epsilon_{s2}, S_1, S_2)$$

$$\epsilon_{12\_S1S2} = 0.8$$

Fig. 10. The calculus of the reciprocal emission-absorption coefficient  $\epsilon_{12}$

The heat transfer coefficient by radiation  $\alpha_R$  (figure 11) was determined using the relationship (8), in which the absolute temperatures  $T_s$  (surface temperature) and  $T_e$  (outer fluid temperature), expressed in Kelvin degrees, were determined using the common transformation formula

$$T [\text{K}] = t [^\circ\text{C}] + 273.15 \quad (18)$$

which was implemented in the form of the function  $\text{fn\_T}(t)$ .

Steady heat transfer by natural (free) convection and radiation, for a horizontal circular pipe surrounded by air, using the Mathcad® software

*Coefficientul de transfer de caldura superficial prin radiatie*

$$\alpha_R = \frac{\varepsilon_{pf} \cdot C_0 \cdot \left[ \left( \frac{T_s}{100} \right)^4 - \left( \frac{T_f}{100} \right)^4 \right]}{T_s - T_f} \quad \text{fn\_}\alpha_R(\varepsilon_{pf}, C_0, T_s, T_f) := \frac{\varepsilon_{pf} \cdot C_0 \cdot \left[ \left( \frac{T_s}{100} \right)^4 - \left( \frac{T_f}{100} \right)^4 \right]}{T_s - T_f}$$

*Temperatura absoluta*  $T = t + 273.15 \cdot K$   $\text{fn\_}T(t) := (t + 273.15) \cdot K$

$$T_s := \text{fn\_}T(t_{se}) \quad T_e := \text{fn\_}T(t_f) \quad T_s = 323.15 \cdot K \quad T_e = 283.15 \cdot K$$

$$\alpha_R := \text{fn\_}\alpha_R(\varepsilon_{12\_S1S2}, C_0, T_s, T_e) \quad \alpha_R = 5.077 \cdot \frac{W}{m^2 \cdot K}$$

Fig. 11. The calculus of the heat transfer coefficient by radiation  $\alpha_R$

The heat flux density  $\dot{q}_R$  (per unit length), transferred by thermal radiation, was calculated using the relationship (10) and the results shown in figure 12 were obtained. For its verification, one can use as an alternative calculation the formula (19)

$$\dot{q}_R = \varepsilon_{12} \cdot \sigma \cdot S_{1u} \cdot (T_1^4 - T_2^4) \left[ \frac{W}{m} \right] \quad (19)$$

where  $\sigma$  represents the Stefan-Boltzmann constant  $\sigma = 5.67 \cdot 10^{-8} \frac{W}{m^2 \cdot K^4}$ , and  $S_{1u}$  denotes the heat transfer lateral surface area per unit length ( $S_{1u} = \pi \cdot d_e$ ).

*d) Fluxul termic transmis prin radiatie*

*Fluxul termic unitar transmis prin radiatie intre 2 suprafete cilindrice*

$$q_R = \varepsilon_{12} \cdot C_0 \cdot \left[ \left( \frac{T_1}{100} \right)^4 - \left( \frac{T_2}{100} \right)^4 \right] \cdot \pi \cdot d_1 \quad \text{fn\_}q_{R\_SC}(\varepsilon_{12}, C_0, T_1, T_2, d) := \varepsilon_{12} \cdot C_0 \cdot \left[ \left( \frac{T_1}{100} \right)^4 - \left( \frac{T_2}{100} \right)^4 \right] \cdot \pi \cdot d$$

$$q_R := \text{fn\_}q_{R\_SC}(\varepsilon_{12\_S1S2}, C_0, T_s, T_e, d_e) \quad q_R = 15.949 \cdot \frac{W}{m}$$

*Fluxul termic total transmis prin radiatie*  $Q_R := q_R \cdot L \quad Q_R = 15.949 \cdot W$

*Variantă de calcul*

$$q_R = \varepsilon_{12} \cdot \sigma \cdot S_{1u} \cdot (T_1^4 - T_2^4) \quad \text{fn2\_}q_R(\varepsilon_{12}, \sigma, S_{1u}, T_1, T_2) := \varepsilon_{12} \cdot \sigma \cdot S_{1u} \cdot (T_1^4 - T_2^4)$$

$$q_{2R} := \text{fn2\_}q_R(\varepsilon_{12\_S1S2}, \sigma, \pi \cdot d_e, T_s, T_e) \quad q_{2R} = 15.949 \cdot \frac{W}{m}$$

$$Q_R = \varepsilon_{12} \cdot \sigma \cdot S_1 \cdot (T_1^4 - T_2^4) \quad \text{fn2\_}Q_R(\varepsilon_{12}, \sigma, S_1, T_1, T_2) := \varepsilon_{12} \cdot \sigma \cdot S_1 \cdot (T_1^4 - T_2^4)$$

$$Q_{2R} := \text{fn2\_}Q_R(\varepsilon_{12\_S1S2}, \sigma, S_1, T_s, T_e) \quad Q_{2R} = 15.949 \cdot W$$

Fig. 12. The calculus and verification of the heat flux density  $\dot{q}_R$  transferred by thermal radiation

Considering the simultaneous action of the two modes of heat transfer by thermal convection and thermal radiation, the combined heat transfer coefficient by convection and radiation  $\alpha_{CR}$  was calculated using the relationship (11), and then using the formula

(12) the heat flux density  $\dot{q}_{CR}$  (per unit length) transferred by convection and radiation shall be calculated (figure 13).

Having previously calculated the partial results for the two-heat flux density  $\dot{q}_C$  and  $\dot{q}_R$ , the heat flux density  $\dot{q}_{CR}$  is checked using the relationship (14).

*e) Coeficientul de TRO superficial prin convectie si radiatie*

*Coeficientul de transfer de caldura superficial prin convectie si radiatie*

$$\alpha_{CR} = \alpha_C + \alpha_R \quad \text{fn\_}\alpha_{CR}(\alpha_C, \alpha_R) := \alpha_C + \alpha_R$$

$$\alpha_{CR} := \text{fn\_}\alpha_{CR}(\alpha_C, \alpha_R)$$

$$\alpha_{CR} = 13.923 \cdot \frac{\text{W}}{\text{m}^2 \cdot \text{K}}$$

*Fluxul termic transmis prin convectie si radiatie*

$$q_{CR} := \text{fn\_}q_{\text{Conv\_PC}}(\alpha_{CR}, d_e, t_f, t_{se})$$

$$q_{CR} = 43.741 \cdot \frac{\text{W}}{\text{m}}$$

$$Q_{CR} := \text{fn\_}Q_{\text{PC}}(q_{CR}, L)$$

$$Q_{CR} = 43.741 \cdot \text{W}$$

**Verificare**

$$q_{CR\_verif} := q_{\text{conv}} + q_R$$

$$q_{CR\_verif} = 43.741 \cdot \frac{\text{W}}{\text{m}}$$

$$Q_{CR\_verif} := Q_{\text{conv}} + Q_R$$

$$Q_{CR\_verif} = 43.741 \cdot \text{W}$$

Fig. 13. The calculus of the combined heat transfer coefficient  $\alpha_{CR}$  and heat flux density  $\dot{q}_{CR}$  transferred by convection and radiation

For a comparative analysis and a better interpretation of the main results obtained, they have been summarized as shown in figure 14.

$$\text{Centralizare rezultate} \quad M_{CRrez} := \text{augment} \left( \frac{\alpha_C}{\frac{\text{W}}{\text{m}^2 \cdot \text{K}}}, \frac{\alpha_R}{\frac{\text{W}}{\text{m}^2 \cdot \text{K}}}, \frac{\alpha_{CR}}{\frac{\text{W}}{\text{m}^2 \cdot \text{K}}}, \frac{q_{\text{conv}}}{\frac{\text{W}}{\text{m}}}, \frac{q_R}{\frac{\text{W}}{\text{m}}}, \frac{q_{CR}}{\frac{\text{W}}{\text{m}}} \right)$$

	$\alpha_C$ [W/m <sup>2</sup> K]	$\alpha_R$ [W/m <sup>2</sup> K]	$\alpha_{CR}$ [W/m <sup>2</sup> K]	$q_{\text{conv}}$ [W/m]	$q_R$ [W/m]	$q_{CR}$ [W/m]
$M_{CRrez} =$	1	2	3	4	5	6
	8.846	5.077	13.923	27.792	15.949	43.741

Fig. 14. Summary of the main results obtained for the coefficients  $\alpha_C$ ,  $\alpha_R$ ,  $\alpha_{CR}$  and the heat flux densities  $\dot{q}_C$ ,  $\dot{q}_R$  and  $\dot{q}_{CR}$

### 3. Studied cases and results obtained

Using the software tool shown above, the heat transfer problem proposed in the paper has been successfully solved, operating with a certain set of initial data.

Its usefulness is particularly proven in similar cases, where there are several changes in the application data compared to the reference situation under consideration,

Steady heat transfer by natural (free) convection and radiation, for a horizontal circular pipe surrounded by air, using the Mathcad® software

for example the outer surface temperature of the pipe  $t_{se}$  changes, the fluid temperature  $t_f$  with which the heat exchange occurs changes, the outside diameter of the pipe or the pipe material changes etc.

The software tool presented has been used to analyze how the main results in figure 14 vary, for several cases where the outer surface temperature of the pipe  $t_{se}$  changes within a range of technical interest, with values between  $t_{se}=40^{\circ}\text{C}\dots 90^{\circ}\text{C}$ , using a temperature step  $\Delta t_{se}=5^{\circ}\text{C}$ .

The outside air temperature was considered to be constant, as in the proposed example, at  $t_f=10^{\circ}\text{C}$  and the pipe geometry remained unchanged, the heat transfer being sought for the same steel pipe  $\phi 1''(25\times 2.5\text{ mm})$ .

The numeric results from the study were processed using the Microsoft Excel® software and are summarized in figure 15.

	te [C]	tse [C]	Alfa_conv [W/mpK]	Alfa_rad [W/mpK]	Alfa_conv_rad [W/mpK]	q_conv [W/m]	q_rad [W/m]	q_conv_rad [W/m]
	10.0	40.0	8.268	4.821	13.089	19.482	11.359	30.841
	10.0	45.0	8.574	4.947	13.522	23.570	13.600	37.170
	10.0	50.0	8.846	5.077	13.923	27.792	15.949	43.741
	10.0	55.0	9.099	5.209	14.308	32.159	18.410	50.569
	10.0	60.0	9.331	5.344	14.675	36.641	20.986	57.627
	10.0	65.0	9.544	5.482	15.026	41.228	23.680	64.909
	10.0	70.0	9.743	5.623	15.366	45.914	26.497	72.411
	10.0	75.0	9.910	5.767	15.677	50.593	29.440	80.033
	10.0	80.0	10.066	5.914	15.980	55.342	32.512	87.854
	10.0	85.0	10.212	6.064	16.276	60.156	35.717	95.873
	10.0	90.0	10.350	6.217	16.566	65.029	39.060	104.089
Media	10.000	65.000	9.449	5.497	14.946	41.628	24.292	65.920
Variatie		125.000%	25.18%	28.96%	26.56%	233.790%	243.868%	237.502%

Fig. 15. The numeric results for the coefficients  $\alpha_C$ ,  $\alpha_R$ ,  $\alpha_{CR}$  and the heat fluxes density  $\dot{q}_C$ ,  $\dot{q}_R$  and  $\dot{q}_{CR}$  for a variation of the temperature  $t_{se}$  in the range  $[40^{\circ}\text{C}\dots 90^{\circ}\text{C}]$

It is noted that, at a change of 125% in the outer surface temperature of the pipe  $t_{se}$  (from  $t_{se}=40^{\circ}\text{C}$  to  $t_{se}=90^{\circ}\text{C}$ ), the value of the coefficient  $\alpha_C$  is changed by about 25%, the value of the coefficient  $\alpha_R$  by about 29%, resulting in a variation of the combined heat transfer coefficient by convection and radiation  $\alpha_{CR}$  of about 26.5%.

Also, for the same temperature variation range of  $t_{se}$ , there are significant increases in the heat fluxes density  $\dot{q}_C$ ,  $\dot{q}_R$  and  $\dot{q}_{CR}$ , their variations are about 234%, 244% and 237.5% respectively.

The graphical representation of the variation of the coefficients  $\alpha_C$ ,  $\alpha_R$  and  $\alpha_{CR}$  with temperature  $t_{se}$  is given in figures 16, 17 and 18, and the variation of the heat fluxes density  $\dot{q}_C$ ,  $\dot{q}_R$  and  $\dot{q}_{CR}$  with temperature  $t_{se}$  is shown graphically in figures 19, 20 and 21.

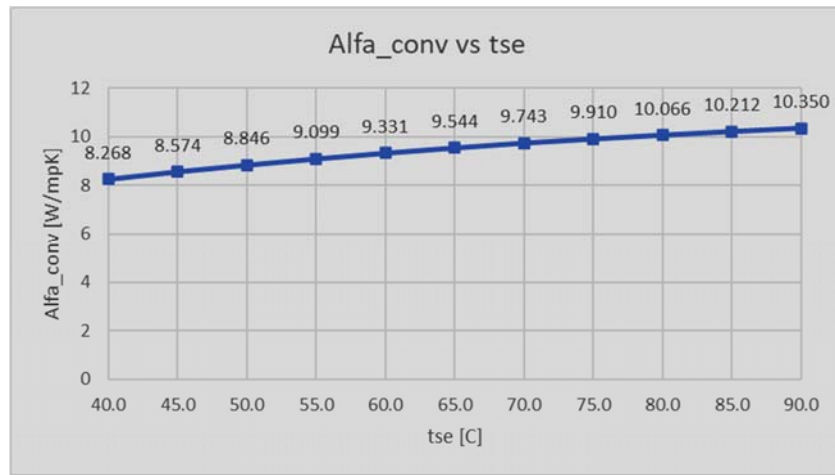


Fig. 16. The variation of coefficient  $\alpha_C$  with temperature  $t_{se}$

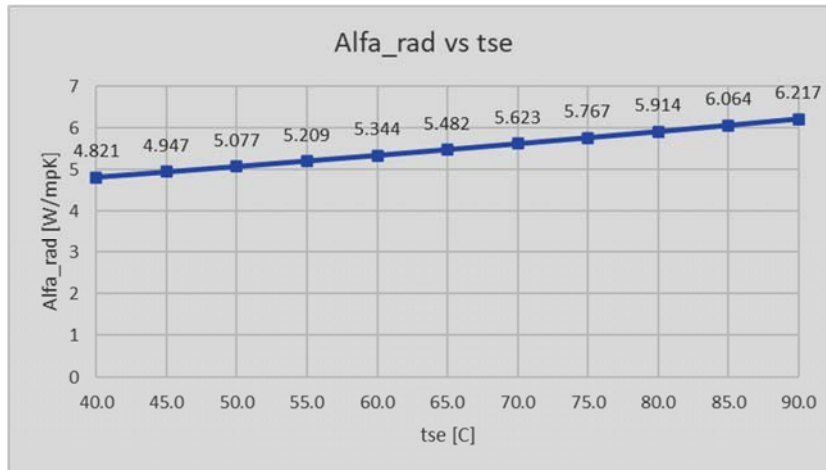


Fig. 17. The variation of coefficient  $\alpha_R$  with temperature  $t_{se}$

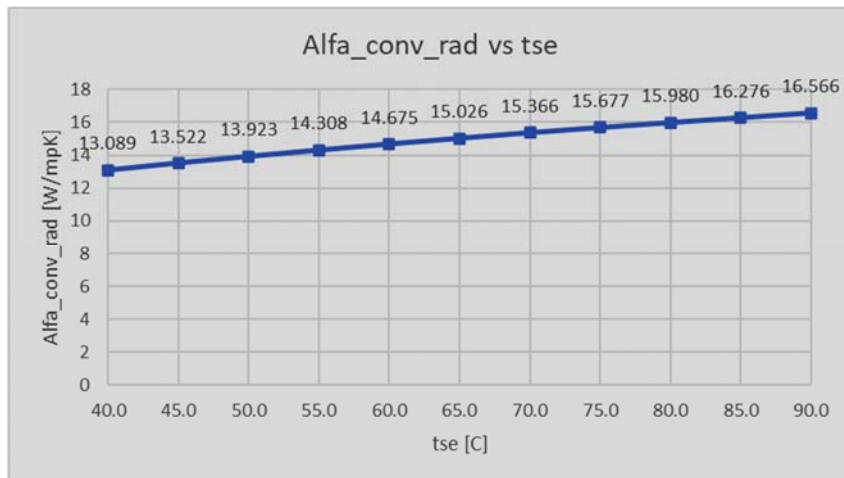


Fig. 18. The variation of coefficient  $\alpha_{CR}$  with temperature  $t_{se}$

Steady heat transfer by natural (free) convection and radiation, for a horizontal circular pipe surrounded by air, using the Mathcad® software

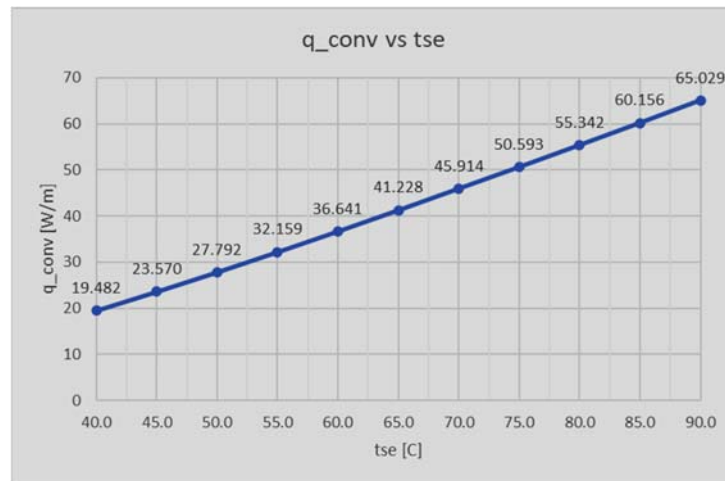


Fig. 19. The variation of heat flux density  $\dot{q}_C$  with temperature  $t_{se}$

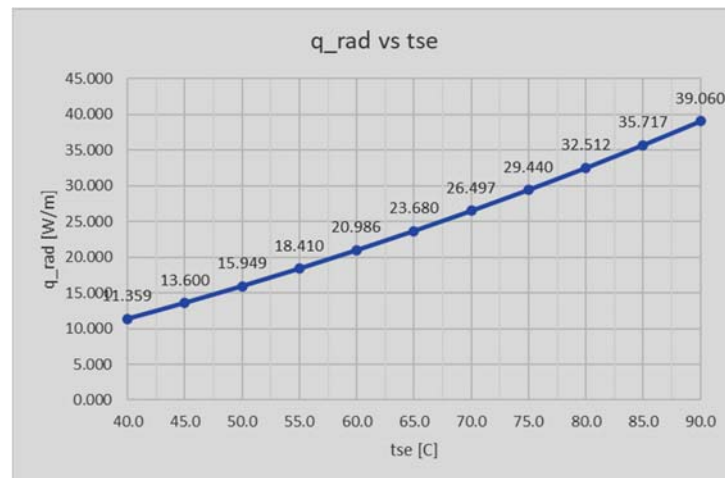


Fig. 20. The variation of heat flux density  $\dot{q}_R$  with temperature  $t_{se}$

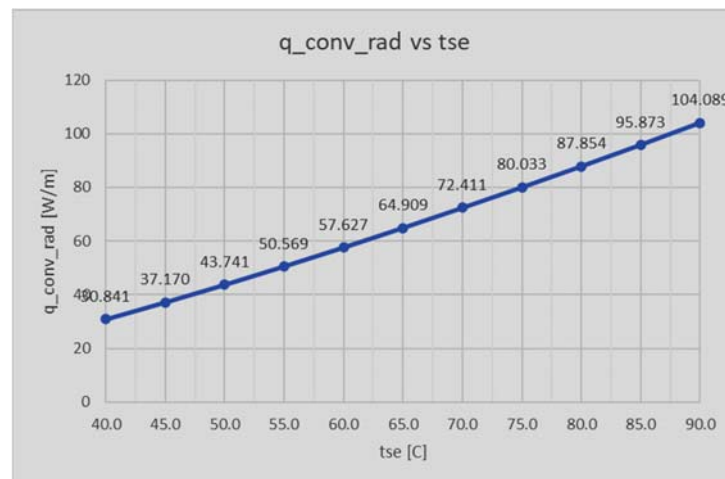


Fig. 21. The variation of heat flux density  $\dot{q}_{CR}$  with temperature  $t_{se}$

At the same time, the contribution of natural thermal convection and thermal radiation, to the combined transmission of heat through the two fundamental modes has been studied.

The numeric results are shown in figure 22 and their graphical representation in figure 23 (comparative) and figure 24 (combined).

	te [C]	tse [C]	q_conv din q_conv_rad [%]	q_rad din q_conv_rad [%]
	10.0	40.0	63.169%	36.831%
	10.0	45.0	63.411%	36.589%
	10.0	50.0	63.538%	36.462%
	10.0	55.0	63.594%	36.406%
	10.0	60.0	63.583%	36.417%
	10.0	65.0	63.517%	36.482%
	10.0	70.0	63.407%	36.593%
	10.0	75.0	63.215%	36.785%
	10.0	80.0	62.993%	37.007%
	10.0	85.0	62.746%	37.254%
	10.0	90.0	62.474%	37.526%
<b>Media</b>	10.000	65.000	63.241%	36.759%
Variatie			-1.100%	1.886%

Fig. 22. The share of natural thermal convection and thermal radiation in the transmission of heat flux density  $\dot{q}_{CR}$ , for different values of temperature  $t_{se}$

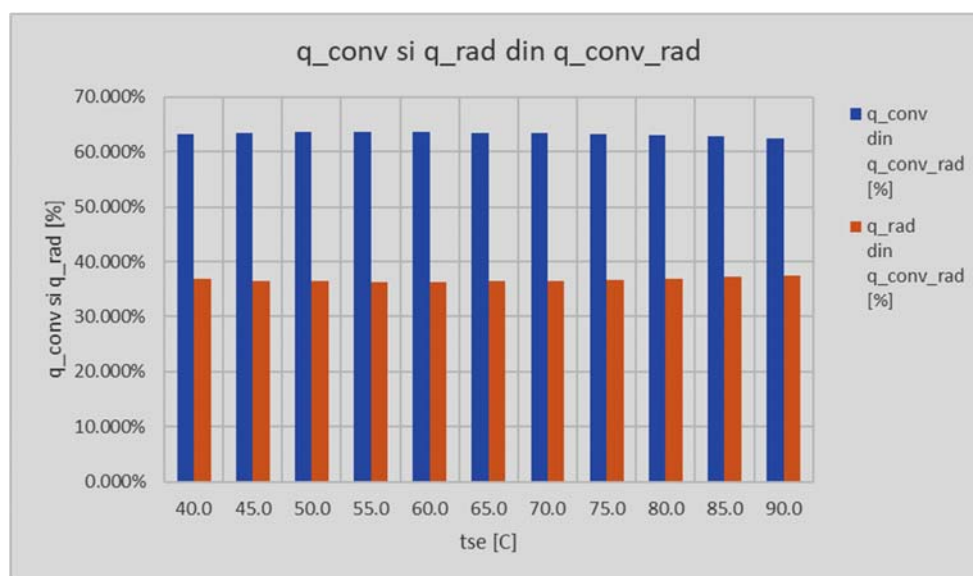


Fig. 23. The share of natural thermal convection and thermal radiation in the transmission of heat flux density  $\dot{q}_{CR}$  (comparative representation)



Steady heat transfer by natural (free) convection and radiation, for a horizontal circular pipe surrounded by air, using the Mathcad® software

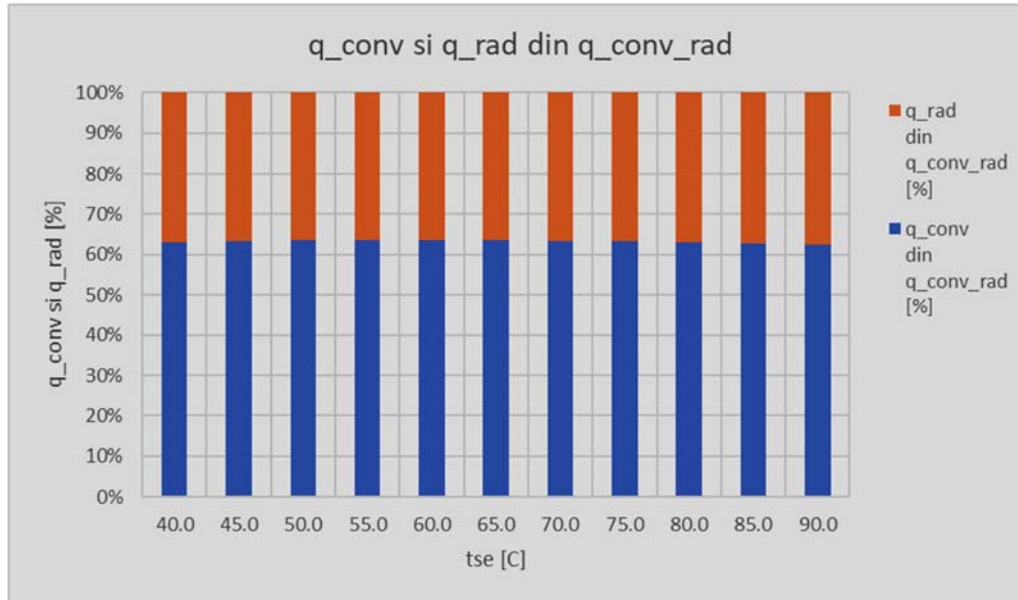


Fig. 24. The share of natural thermal convection and thermal radiation in the transmission of heat flux density  $\dot{q}_{CR}$  (combined representation)

It is noted that in the temperature range studied  $t_{se}=40^{\circ}\text{C}\dots90^{\circ}\text{C}$ , the natural thermal convection accounts for about 62-63% and the remaining 38-37% is the transmission of heat by thermal radiation.

It has also been noted that for values of temperature  $t_{se}$  higher than  $55\text{--}60^{\circ}\text{C}$ , the contribution of natural thermal convection has a slight decrease from 63.59% to 62.47% and thermal radiation has slightly increased from 36.4% to 37.52% of the total transferred heat flux density  $\dot{q}_{CR}$ .

With lower values of the outer surface temperature of the pipe, usually below  $100^{\circ}\text{C}$ , there is generally a tendency to neglect the effect of thermal radiation by considering it less important and the calculation of the transferred heat flux density  $\dot{q}$  is based mainly on the treatment of the phenomenon of natural thermal convection ( $\dot{q} \approx \dot{q}_C$ ).

Considering the above results, neglecting the effect of thermal radiation, even in the case of values of temperature  $t_{se}$  within the usual technical range of  $40^{\circ}\text{C}\dots90^{\circ}\text{C}$ , may lead primarily to a relatively erroneous assessment of the value of the heat transfer coefficient  $\alpha$ , and then, to the estimation with a high technical error of about 37% (figure 22) of the transferred heat flux density  $\dot{q}$ , which actually represents the heat loss to the environment.

#### 4. Conclusions

The solution of an application of steady heat transfer by natural (free) convection and thermal radiation is generally a slightly more complex one, which requires treatment of both fundamental modes of heat transfer and then combining the results to obtain the final values of the heat transfer coefficient and the heat flux density or total heat flux transferred.

Implementation of the solution to the proposed problem and the development of the study presented in the paper have been carried out using the MathCAD® software application, taking into account the benefits of this computer program in terms of describing calculation relationships in a language close to the natural one, ability to operate with different measurement units, creation of functions used in calculations, management of fluid thermophysical properties, presentation of obtained numerical and/or graphical results etc.

Preparation to solve the studied case was made by entering the initial data of the problem represented by working fluid characteristics, geometrical and thermal characteristics of the pipe, emission-absorption coefficients of the body and the environment, the value of the radiation coefficient of the absolute black body and the Stefan-Boltzmann constant (figure 2).

The approach to heat transmission by natural convection was carried out using appropriate empirical correlations specified in the literature having the general form (1), in which the Grashof (Gr) and the Prandtl (Pr) numbers are calculated with the established relationships (3) and (4).

The determination of the thermophysical properties of the working fluid shall be carried out using the reference temperature indicated in the empirical correlation tables, the tabular values for fluid properties and the use of required linear interpolation functions (figure 3 and figure 4). The determination of the fluid flow regime is made by calculating the value of product  $Gr \cdot Pr$  or the Ra number (figure 6), then identifying the C and m constants of the empirical correlation. One will compute the value of Nusselt number (Nu) and using the relationship (5) the heat transfer coefficient by natural convection  $\alpha_C$  is obtained (figure 7). A synthetic calculation function shown in figure 8 was created to verify the result obtained and/or to calculate in other situations directly the heat transfer coefficient by natural convection.

The heat flux density  $\dot{q}_C$  (per unit of length), transferred by natural convection, was calculated by the implementation of the relationship (7) and the results were displayed in figure 9.

The approach to heat transmission by thermal radiation is carried out by determining the heat transfer coefficient by radiation  $\alpha_R$  (figure 11) using the relationship (8), first calculating the reciprocal emission-absorption coefficient  $\varepsilon_{12}$  with the relationship (9) and then using the relation (10) the heat flux density  $\dot{q}_R$  (per unit of length) transferred by thermal radiation, which has the value shown in figure 12.

Steady heat transfer by natural (free) convection and radiation, for a horizontal circular pipe surrounded by air, using the Mathcad® software

Considering the simultaneous action of the two modes of heat transfer by natural convection and thermal radiation, using the relationship (11) the combined heat transfer coefficient by convection and radiation  $\alpha_{CR}$  shall be calculated, and then using the formula (12) the heat flux density  $\dot{q}_{CR}$  (per unit of length) transferred by convection and radiation shall be determined (figure 13).

Since partial results have been determined for the heat fluxes density  $\dot{q}_C$  and  $\dot{q}_R$ , the resulting heat flux density  $\dot{q}_{CR}$  can be verified by using the relationship (14).

Using the software tool presented in the paper, a number of cases have been investigated, where for the same steel pipe  $\phi 1''$  (25×2.5 mm) and a temperature of outside air of  $t_f=10^\circ\text{C}$ , the temperature of the outer surface of the pipe  $t_{se}$  changes in a range  $t_{se}=40^\circ\text{C} \dots 90^\circ\text{C}$ . A temperature step  $\Delta t_{se}=5^\circ\text{C}$  has been selected to determine the following results:

- The heat transfer coefficient by convection  $\alpha_C$ ;
- The heat transfer coefficient by radiation  $\alpha_R$ ;
- The combined heat transfer coefficient by convection and radiation  $\alpha_{CR}$ ;
- The heat flux density transferred by natural convection  $\dot{q}_C$ ;
- The heat flux density transferred by radiation  $\dot{q}_R$ ;
- The heat flux density transferred by natural convection and radiation  $\dot{q}_{CR}$ .

The numeric results obtained are summarized in figure 15. The graphical representation of the variation of the coefficients  $\alpha_C$ ,  $\alpha_R$  and  $\alpha_{CR}$  with temperature  $t_{se}$  is given in figures 16, 17 and 18, and the variation of the heat fluxes density  $\dot{q}_C$ ,  $\dot{q}_R$  and  $\dot{q}_{CR}$  with temperature  $t_{se}$  is shown graphically in figures 19, 20 and 21.

From the results obtained it was noted that a change in the value of the outer surface temperature of the pipe  $t_{se}$  by 125%, from  $40^\circ\text{C}$  to  $90^\circ\text{C}$ , corresponds to a change in the value of the  $\alpha_C$  coefficient of about 25%, the value of the  $\alpha_R$  coefficient by about 29% and the value of the combined heat transfer coefficient by convection and radiation  $\alpha_{CR}$  by about 26.5%.

The share of natural convection and thermal radiation in combined heat transfer through the two fundamental modes, was also analyzed. The numerical results are shown in figure 22 and their graphical representation has been shown comparative in figure 23 and combined in figure 24.

It has been noted that in the temperature range studied  $t_{se}$ , the natural convection accounts for approximately 62-63% and the remaining approximately 38-37% is the transmission of heat by thermal radiation. At the same time, it is noted that for values of temperature  $t_{se}$  higher than  $55-60^\circ\text{C}$ , the contribution of natural thermal convection has a slight decrease from 63.59% to 62.47% and thermal radiation has slightly increased from 36.4% to 37.52% of the total transferred heat flux density  $\dot{q}_{CR}$ .

Considering the results presented above, it is assessed that neglecting the heat transfer by radiation, even in the case of temperature  $t_{se}$  within a technical range normally encountered in building services engineering ( $40^\circ\text{C} \dots 90^\circ\text{C}$ ), may lead to a relatively erroneous assessment of the value of the heat transfer coefficient  $\alpha$  (figure 15).

In direct correlation with this, due to Newton's law (6), the determination with a high technical error of approximately 37% of the heat flux density  $\dot{q}$  (figure 22) transferred to the external fluid will then be found, which represents for the cases studied in the paper the heat loss to the environment.

Considering the current context, where particular emphasis is placed on the most efficient use of energy, the use of clean alternative energy sources, the reduction of heat losses, the efficiency increases of thermal equipment and installations, the reduction of environmental pollution etc., the estimation of heat transfer as close as possible to reality in situations like those presented in the paper is becoming an increasingly important goal.

While taking into account the heat transfer by radiation at low temperatures also requires an additional calculation effort, being necessary to determine in addition other heat transfer quantities such as: the coefficient by radiation  $\alpha_R$ , the combined heat transfer coefficient by convection and radiation  $\alpha_{CR}$ , the heat flux density transferred by radiation  $\dot{q}_R$ , the heat flux density transferred by convection and radiation  $\dot{q}_{CR}$ , the results of this more complex mathematical model better approximate the way in which the heat transfer is actually occurring, generating much more reliable results from a technical point of view.

The solution of the example proposed in the paper and the software tool developed for the analysis of the combined heat transfer by free convection and thermal radiation is useful both to students at the Faculties of Building Services Engineering, who study the heat transfer, as well as specialists in the field interested in the practical solution of these engineering applications.

## Bibliography

- [1] Chisăliță, G.A., Transmiterea căldurii, Note de curs, 2010-2021.
- [2] Bergman, T.L., Lavine, A.S., Incropera, F.P., Dewitt D.P., Fundamentals of Heat and Mass Transfer, 7th edition, ISBN 978-0470-50197-9, John Wiley & Sons, Inc., 2011, pp. 594-616, 862-895.
- [3] Cengel, Y.A., Ghajar A.J., Heat and Mass Transfer: Fundamentals and Applications, 5th edition, ISBN 978-0073398181, McGraw-Hill Education, 2014, pp. 459-473, 606-641.
- [4] Leonăchescu, N., Termotehnică, E.D.P, București, 1981, pp. 413-418, 458-467.
- [5] Oprețoiu, A., Termotehnică și aparate termice – Transmiterea căldurii, Litografia I.P.C.-N., Cluj-Napoca, 1992, pp. 111-121, 186-197.
- [6] Lienhard IV, J.H., Lienhard V, J.H., A Heat Transfer Textbook, 4th edition, ISBN 0-486-47931-5, Dover Publications Inc., 2011, pp. 399-429, 538-565.
- [7] Popa B., Vintilă C., Transfer de căldură în procese industriale, Editura Dacia, Cluj-Napoca, 1975, pp. 111-142, 257-280.
- [8] Leonăchescu, N. ș.a., Probleme de termotehnică, E.D.P, București, 1977, pp. 277-281, 439, 515-524.
- [9] Muntea, C., Câmpăanu, A., Transfer de căldură – Probleme, ISBN 973-95386-2-2, Editura Ana, Cluj-Napoca, 1997, pp. 54-70, 89-95, 141, 194-195.

## Theoretical aspects regarding energy efficiency in foods refrigeration and freezing

Aspecte teoretice privind eficiența energetică în refrigerarea și congelarea alimentelor

Alina GIRIP<sup>a</sup>, Răzvan CALOTĂ<sup>b</sup>, Mădălina NICHITA<sup>c</sup>, Anica ILIE, <sup>d</sup>

*a,b,c,d, Technical University of Civil Engineering of Bucharest, Faculty of Building Services, Pache Protopopescu 66, Bucharest, Romania*

*alina.girip@utcb.ro ; razvan.calota@utcb.ro, madalina.nichita@utcb.ro, ilie.anica@utcb.ro*

DOI: 10.37789/rjce.2021.12.4.3

### Abstract

This paper presents a technical study on energy consumption and performance of a refrigeration system used for food products refrigeration and congelation. The authors compared the two-stage refrigeration system with the cascade refrigeration system. The analysis was based on the thermodynamic cycles corresponding to each one of the proposed solutions. For the booster system several refrigerants were considered in the analysis for the upper loop, respectively R717, R404A, R407C and R417A. Based on the total energy consumption of the installation (compressor, fans, recirculation pumps), the overall performance coefficient of the installation was determined. The study showed that the lowest electrical energy consumption corresponds to the cascade refrigeration system with R717-R744 and the two-stage compression refrigeration system with R717. The difference between the 2 optimal variants is only 4.6%. Therefore, it is recommended that the choice of the final scheme to be made on the basis of an LCC (Life cycle cost) analyze, which takes into account the refrigerant charge, the initial investment cost, the operating costs and the electricity cost.

**Keywords:** ammonia, carbon dioxide, power consumption, coefficient of performance

### 1. Introduction

Refrigeration systems with mechanical vapor compression having two compression stages and two vaporization temperatures are used in food products freezing and refrigeration processes. The main reasons for adopting the refrigeration system mentioned above are related to energy savings, due to the decrease in the discharge temperature of refrigerant vapors and the possibility of using cold, at the temperature level corresponding to the open intercooler. The refrigerant used in refrigeration

installations with mechanical vapor compression, with two stages and two vaporization temperatures can be ammonia or a type of freon. Refrigeration installations generate, during their operation, CO<sub>2</sub> emissions due to refrigerant leaks in the atmosphere attributed to equipment performance (direct emissions), but also mainly due to their energy consumption (indirect emissions). Thus, they contribute significantly to both direct and indirect greenhouse gas emissions. Greenhouse gas emissions can occur directly through the leakage of refrigerants with a high global warming potential (GWP), which can account for up to 30% of the system load per year [1]. Therefore, there is a global concern about the use of refrigeration equipment with high energy efficiency as well as with lower GWP, which could halve the CO<sub>2</sub> emissions [2].

Choosing one appropriate refrigerant for a particular application, which must comply with regulatory policies to reduce greenhouse gas emissions, seems quite a challenge. When considering refrigerant alternatives for future decision makers, the public and manufacturers must select refrigerants with the best balance between:

- Safety for consumers and service technicians (flammability, toxicity and high pressure)
- Reducing CO<sub>2</sub> emissions by increasing the equipment energy efficiency
- Environmental concerns about reducing ozone depleting potential (ODP).

Indirect emissions are also significant, as these systems are large consumers of electricity and are reported to consume about 4 MtCO<sub>2</sub>e per year, where CO<sub>2</sub>e is the equivalent of carbon dioxide [3]. In recent years, natural refrigerants have been proposed as an environmentally friendly solution for the refrigeration industry, due to the inevitable future elimination of HFCs [4]. Refrigerants like ammonia, hydrocarbons, carbon dioxide (R744) do not contribute to ozone depletion and have a low impact on global warming (low GWP), so they offer a long-term solution, suitable for refrigeration/ freezing applications [5].

## **2. Methodology**

The technical economic study was carried out for a refrigeration installation, which provides the refrigeration load of 100kW and the freezing load of 75 kW. The vaporization temperature for refrigeration is -15°C respectively -40°C for freezing. For the cascade type refrigeration system the following pairs of refrigerants were evaluated: CO<sub>2</sub> - NH<sub>3</sub>; CO<sub>2</sub> - R404A; CO<sub>2</sub> - R407C; CO<sub>2</sub> - R417A. The scheme of the cascade refrigeration plant is presented in Figure 1.

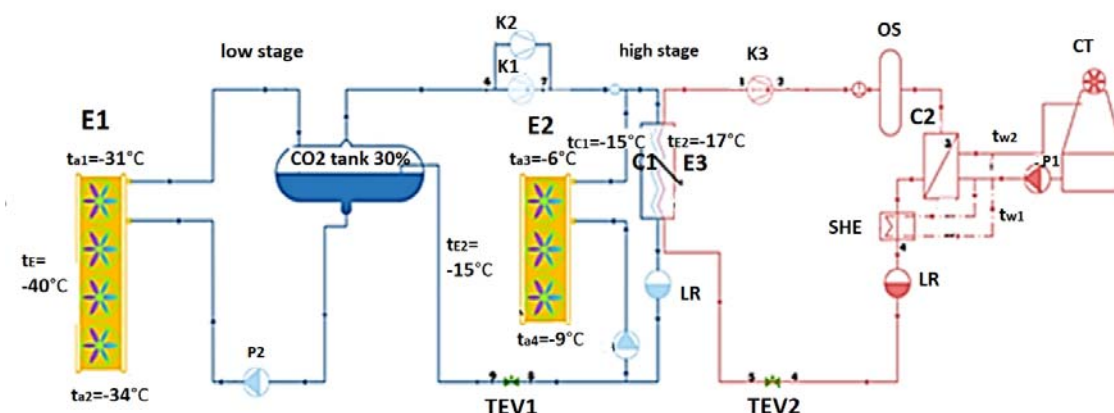


Figure 1. Cascade refrigeration installation, with two vaporization temperatures

The second option consists in a mechanical vapor compression plant having two compression stages, an intermediate open intercooler and working with two vaporization temperatures. The corresponding scheme is presented in Figure 2 [6].

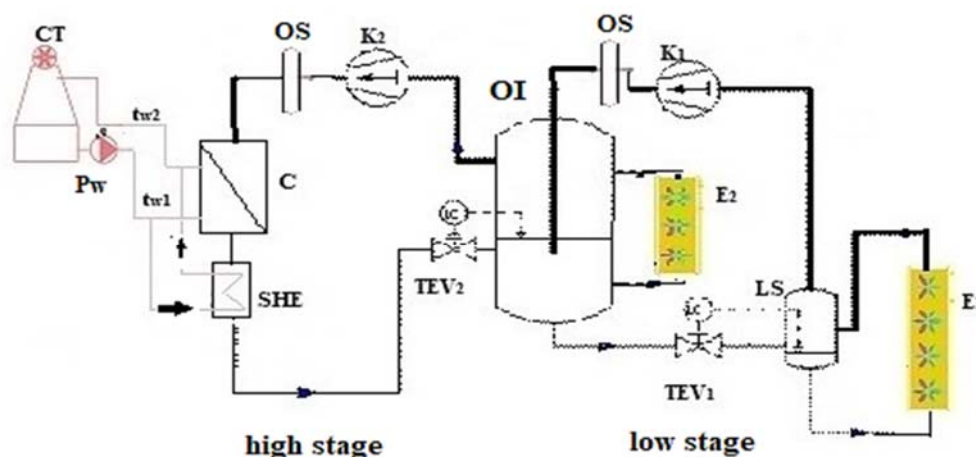


Figure 2. Refrigeration plant in two stages, with open intercooler and two vaporization temperatures

Thermodynamic cycles were plotted for each pair of agents: R744 - R717; R744 - R404A / R407C / R417A according to the input data from Table 1, using the Coolpak program [7].

Tabel 1. Input data for cascade refrigeration system

Refrigerant pair	R744-R717	R744 – R404A/ R407C/ R417A
$t_c$ [°C]	30	42
$t_{01}$ [°C]	-40	-40
$t_{02}$ [°C]	-15	-17
Overheating in the evaporator [°C]	-	5
Overheating in the internal heat exchanger [°C]	-	12

Condenser subcooling [°C]	5	5
Isentropic efficiency [-]	0.7	0.7
$\Phi_{01 \text{ low stage, [kW]}}$	75	
$\Phi_{02 \text{ CO}_2 \text{ high stage [kW]}}$	100	
$\Phi_{03 \text{ condenser/evaporator [kW]}}$	<b>186.15</b>	

Thermal load of the low stage condenser / high stage evaporator ( $\Phi_{03 \text{ condenser/evaporator}}$ ) was determined from the following equations:

$$\Phi_{01 \text{ CO}_2 \text{ low stage}} = 75 \text{ kW} = \dot{m}_1 \cdot (h_1 - h_4) \Rightarrow \dot{m}_1 \text{ at } t_0 = -40^\circ\text{C} \quad (1)$$

$$\Phi_{02 \text{ CO}_2 \text{ low stage}} = 100 \text{ kW} = \dot{m}_2 \cdot (h_2 - h_3) \Rightarrow \dot{m}_2 \text{ at } t_0 = -15^\circ\text{C} \quad (2)$$

$$\Phi_{03 \text{ condenser/evaporator}} = \Phi_{c1} = \Phi_{02 \text{ CO}_2 \text{ low stage}} + \dot{m}_1 \cdot (h_2 - h_3) \quad (3)$$

Based on the thermodynamic cycles, the electrical energy consumption for compressor operation was calculated, as well as the performance coefficient of the installation, in each constructive variant: cascade with two refrigerants and with two compression stages with two vaporization temperatures. For an extended analysis, in addition to the electricity consumption necessary to operate the compressor other types of consumers should be taken into account:

- fans from air-cooled condensers;
- fans from air cooling batteries (evaporators);
- fans from the cooling tower (in the case of the ammonia condenser);
- the liquid refrigerant circulation pumps of the coolant in the cooling tower circuit.

The equipment and components of the refrigeration systems were chosen based on the thermal loads required by the evaporators and condensers, in each constructive variant while the electrical energy consumption was extracted from the technical sheets. The total energy consumption resulted by summing up all the consumptions related to the equipment components of the respective refrigeration installation. The overall efficiency of the refrigeration system was determined as the ratio between the total refrigeration power (refrigeration circuit + freezing circuit) and the total electrical power.

### 3. Results

#### 3.1. Booster system

The comparative analysis was performed in terms of electrical energy consumption, performance coefficient, effect on the environment (ozone depletion - ODP and global warming - GWP). The values of the parameters and quantities characteristic of the thermodynamic cycles, when operating in the cascade variant, as well as the values of the calculated quantities are included in Table 2.



Table 2. Parameters and quantities for the cascade refrigeration system

Refrigerant	R744	R717	R417A	R407C	R404A
Parameter					
$t_0$ [°C]	-40	-17	-17	-17	-17
$p_0$ [bar]	10	2.17	2.15	2.65	3.36
$t_c$ [°C]	-15	30	42	42	42
$p_c$ [bar]	22.9	11.67	14.21	17.32	19.04
Compression ratio low stage [-]	2.29	-	-	-	-
Compression ratio high stage [-]	-	5.37	6.61	6.54	5.67
$v_{asp}$ [m <sup>3</sup> /kg]	0.0381	0.5507	0.0928	0.0887	0.0631
$V_{asp}$ [m <sup>3</sup> /h]	37	329.1	495.1	389.9	365.1
$q_0$ [kJ/kg]	269.4	1124.7	125.6	152.5	115.87
$q_c$ [kJ/kg]	319.09	1451.3	181.75	220.18	169.94
$l_k$ [kJ/kg]	49.67	350.14	56.12	67.66	54.06
$\dot{m}_{AF}$ [kg/s]	0.270	0.166	1.482	1.221	1.607
$\Phi_0$ [kW]	75	186.15	186.15	186.15	186.15
$\Phi_c$ [kW]	186.15	240.22	269.30	268.75	273.02
ODP [-]	0	0	0	0	0
GWP [-]*	1	0	2117	1624	3943

\*According to AR5 values [8]

By analyzing the data presented in Table 1, it can be noticed that the highest values for condensing pressure in the high stage corresponds to R404A. This aspect leads to the conclusion that the energy consumption on this circuit will have the highest value, fact sustained by the calculated mechanical work. Regarding the refrigerant mass flow it can be observed that it has the highest value for the high stage circuit when operating with R404A. The high flow rates in circulation determine large dimensions of the component equipment and increased emissions in the case of damages. The volume flow rate aspirated by the compressor on the high stage circuit, with implications of the compressor size, has the highest value for R417A. The pressure of the low stage for R744 is higher than atmospheric pressure, respectively 10 bar. So is no chance to entry of air from low side leakage and the operating problems are related.

The electrical energy consumption of the R744 - R717 / R417A / R407C / R404A cascade system is included in Tables 3, 4 and 5.

Table 3. Electric power consumption on the R744 circuit (low stage)

Refrigeration circuit	Evaporator fan (Model: SOLO80 384F 3 x Ø 800 / 6PH) [kW]	3.6
	Liquid CO <sub>2</sub> pump, [kW]	0.054
Congelation circuit	Evaporator fan (Model: SOLO60 484E 4 x Ø 630 / 4PH) [kW]	3.2
	Liquid CO <sub>2</sub> pump [kW]	0.074

Table 4. Electric power consumption on the R717 circuit (High Stage)

Water-cooled condenser and cooling tower, [kW]	Fans	2.2
	Recirculating pump condenser-cooling tower ( $m_{rec}=11m^3/h$ )	0.254
Compressor, [kW]		57.95

Table 5. Electric power consumption on R417A / R407C / R404A circuit (High Stage)

	R417A	R407C	R404A
Compressor, [kW]	83.15	82.58	86.85
Fans – air-cooled condenser, [kW]	4.4	6.6	8.8

From Tables 3, 4 and 5 it can be observed that the major share of energy consumption is at the compressor, regardless of the constructive system considered.

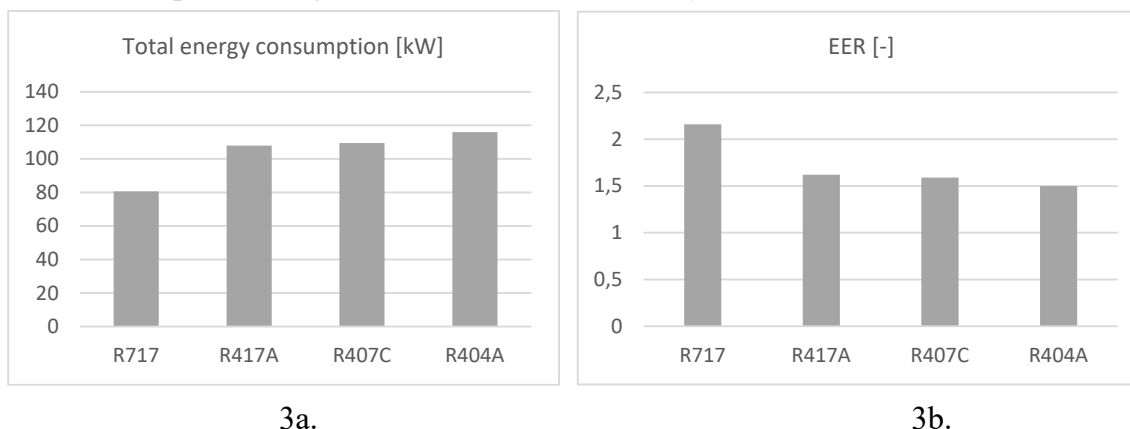


Figure 3. Total energy consumption and EER values output for different constructive solutions

From Figure 3 it can be concluded that in the case of the refrigeration installation in the cascade, with ammonia in the high stage, the lowest electrical energy consumption is registered and the performance coefficient, for the entire installation, also has the highest value. For the case of the other 3 refrigerants analyzed, the energy consumption registers increase between  $33.6 \div 43.6\%$ , while the global performance coefficient decreases. This is explained by the fact that the refrigeration load at the consumer remains the same and the energy consumption increases on the high stage circuit to obtain the same useful effect at the consumer.

### 3.2. 2-stage refrigeration system, with closed intercooler and 2 vaporization temperatures

The values of the parameters and quantities characteristic of the thermodynamic cycles as well as the calculated quantities are included in Table 6.

Table 6. Characteristic parameters for R717 and R417A systems

Refrigerant	R717	R417A
Parameter		
$t_{01}$ [°C]	-39	-40
$t_{02}$ [°C]	-15	15
$p_{01}$ [bar]	0.715	1
$p_{02}$ [bar]	2.36	2.75
Compression ratio low stage [-]	3.3	2.75
Compression ratio high stage [-]	4.95	7.2
$t_c$ [°C]	30	42
$p_c$ [bar]	11.702	20
$v_{asp}$ [m <sup>3</sup> /kg]	1.66	0.23
$m_{LS}$ [kg/s]	0.068	0.38
$m_{HS}$ [kg/s]	0.18	1.98
$q_c$ [kJ/kg]	1442.9	150.7
$l_{k,LS}+l_{k,HS}$ [kJ/kg]	556.4	109.0
$P_{k,LS}+P_{k,HS}$ [kW]	76.77	142.69
$\Phi_0$ [kW]	286.15	286.15
$\Phi_c$ [kW]	264.8	299.6
EER [-]	2.28	1.22
ODP [-]	0	0
GWP [-]*	0	1950

\*According to AR5 values [8]

The pressure of the low stage for R717 is lower than atmospheric pressure, respectively 0.715 bar. So is chance to entry the air from low side and is necessary to use automatic air purger with control (instrument, valve, pipes, thermal insulation) to resolve this problem of entry of non-condensable air in the system.

The R744 has a much lower vapour specific volume at low temperature (0.0381 m<sup>3</sup>/kg) compared R717 (1.66 m<sup>3</sup>/kg). This is approximately 44% less at a saturated vapour of -40 °C.

Greater vapour volume flow rate requirement for low stage means larger compressor for R717 that is required. For R744 the compressor size for low stage is drastically reduced from 406.4 m<sup>3</sup>/h to 37m<sup>3</sup>/h. Thus, the compressor size for R744 low stage side is smaller as compared to the low stage ammonia. The suction line size is smaller (smaller suction valve, strainer, fitting etc.) and the thermal insulation requirement will be also less.

The compression ratio required for low stage is much lower for R744; it's approximately 31% less than low stage ammonia.

Electrical energy consumption related to equipment is included in Table 7.

Table 7. Electrical energy consumption

Equipment type	R717	R417A
Compressor low and high stage [kW]	76.77	142.69
Water cooled condenser and cooling tower [kW]	2.2	-
Air cooled condenser fan [kW]	-	4.4
Recirculating pump condenser-cooling tower with a flow of 11m <sup>3</sup> /h [kW]	0.254	-
Evaporator fan, freezing circuit [kW]	3.6	3.6
Evaporator fan, refrigeration circuit [kW]	3.2	3.2
Total electrical energy consumption [kW]	86.024	153.88
EER [-]	2.03	1.137

From Table 6 it can be seen that the lowest electrical energy consumption corresponds to R717 for which the performance coefficient also has the highest value. By using R417A as a refrigerant, energy consumption increased by 78.9%, while the overall coefficient of performance decreased by 54%.

#### 4. Comparative analysis

In the following, a comparative analysis will be performed between the two solutions that have the highest efficiency in each case. Thus, for the cascade cooling system, the pair of carbon dioxide - ammonia was chosen and for the installation with two refrigeration stages, ammonia was chosen as the refrigerant, which in both situations obtained the highest performances in terms of EER and the lowest electrical energy consumption.

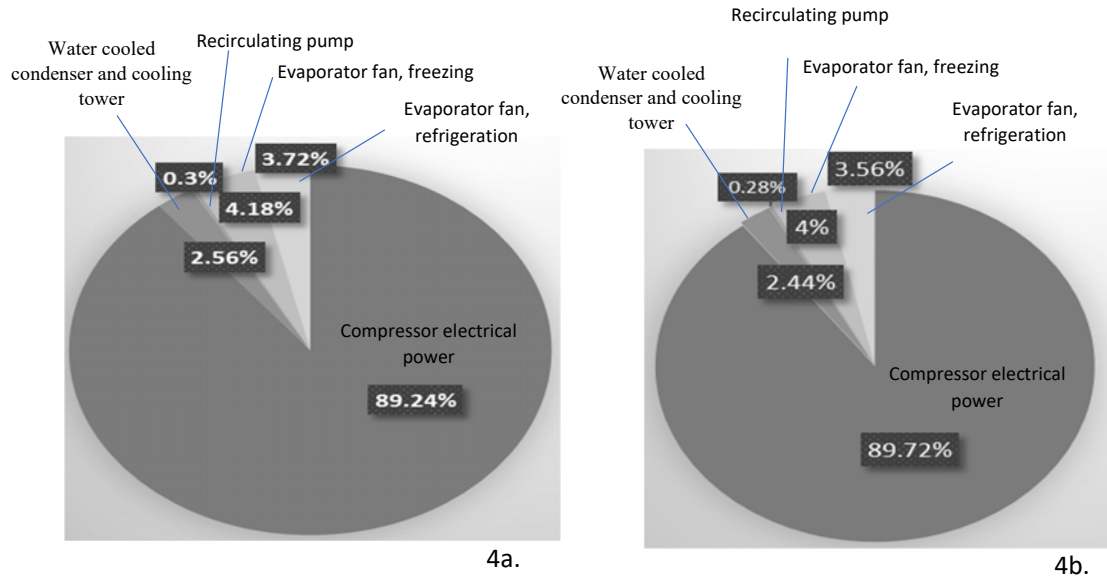


Figure 4. Share of electrical power consumed in the refrigeration system; 4a. R717 4b. R744-R717

From Figure 4 and Table 8 it can be seen that both types of installation have a very similar electrical energy consumption with a slightly higher value in the case of the booster type system. The largest contribution to energy consumption is made by the compressor in each situation, with a percentage of about 90% of the total energy consumption.

Table 8. Parameters defining energy efficiency

Refrigerant	R717	R744-R717
Total electrical energy consumption [kW]	86.024	90
EER [-]	2.03	1.94

Adopting one of the options can be influenced not only by energy consumption but also by investment and maintenance costs.

## 5. Conclusions

The technical analysis performed highlights the following aspects:

- Although the desired useful effect (cooling power on refrigeration and freezing) is the same, the energy consumption is different, even in the case of the same constructive variant of refrigeration system. As the analysis of thermodynamic cycles shows, the characteristic parameters depend on the refrigerant.
- For the cascade refrigeration system, the refrigerant from the high stage, which meets the criteria regarding the lowest electrical energy consumption, the best coefficient of

performance, zero ozone depletion effect, as well as zero effect on global warming, is ammonia.

- For the refrigeration system with two compression stages and two vaporization temperatures, the optimal variant from the point of view of the consumed electrical energy is the one with ammonia.
- The implementation of each one of the analyzed refrigeration systems has advantages in terms of environmental impact. Refrigerants are natural, without the potential to destroy the ozone layer and with minimal impact on global warming.
- the shaft power at compressors (low stage + high stage) represents about 90% from total value of electrical consumption. The fans and pumps give a smaller value, respectively about 10%.
- The difference regarding the electrical energy consumption between the 2 optimal variants is small, around 4.6%. Therefore, it is recommended that the choice of the final variant to be made on the basis of an LCC (Life cycle cost) analyze, which takes into account the refrigerant charging, the initial investment cost, the operating costs and the electricity cost. CO<sub>2</sub> is approximately 37% cheaper than ammonia. Thus, there will be additional benefit in future cost saving.

#### *Nomenclature*

l – specific mechanical power consumption by compressor [kJ/kg]	t – temperature [°C]
m – refrigerant mass flow rate [kg/s]	v – specific volume [m <sup>3</sup> /kg]
q – specific thermal power [kJ/kg]	
Φ - thermal power [kW]	
p – pressure[bar]	
P – Compressor electrical power [kW]	

V –volume flow [m<sup>3</sup>/h]

EER – coefficient of performance [-]

GWP – warming global potential [-]

ODP – ozon depletion potential [-]

#### *subscripts*

0 – evaporation

Theoretical aspects regarding energy efficiency in foods refrigeration and freezing

C – condensation

K - compressor

LS – low stage temperature or freezing

HS – high stage temperature or cooling

AF – refrigerant

suc – suction

## REFERENCES

- [1] Stephen Anthony Kujak, Panayu Robert Srichai, Kenneth J. Schultz: Life Cycle Climate Performance (LCCP) Tools For HVAC&R Applications With The Latest Next Generation Refrigerant Technology, 2014 International Refrigeration and Air Conditioning Conference, Purdue
- [2] IIR-7e Note d'Information sur le froid et l'alimentation: L'empreinte carbone de la chaîne du froid, aprilie 2021
- [3] Tassou SA, Ge Y, Hadawey A, et al. Energy consumption and conservation in food retailing. Research paper, Brunel University, 2007.
- [4] Kuijper L. Refrigeration within a climate regulatory framework. In: 23rd IIR International Congress of Refrigeration, Prague, Czech, 21–26 August 2011
- [5] I. Colombo\*, G. G. Maidment, I. Chaer and J. M. Missenden: Carbon dioxide refrigeration with heat recovery for supermarkets, International Journal of Low-Carbon Technologies 2014, 9, 38–44
- [6] D Hera, A Girip - Instalații frigorifice: Scheme și cicluri frigorifice, 2007 , Ed. Matrix Rom, pp 407.
- [7] [www.ipu.dk](http://www.ipu.dk) Coolpack software
- [8] AR 5 – Climate Change 2014 Synthesis Report

# In-situ and Laboratory Analysis of Treated Marine Soil by Consolidation Methods

Analiza in situ și de laborator a solului marin tratat prin metode de consolidare

Houssam KHELALFA. <sup>(1)</sup> <sup>(2)</sup>,

1 Civil Engineering and Environment Laboratory (LGCE), University of Jijel , Algeria.

2 Department of civil engineering, Faculty of engineering and technology, Selinus university of science and literature (SUSL), Bologna, Italy.

E-mail: khelalfahoussam@gmail.com

ORCID: 0000-0002-8052-6947

DOI: 10.37789/rjce.2021.12.4.4

## Abstract

The methods of improvement of vibroflotation (VF), dynamic compaction (DC) and the preloading took a scale in Algeria these last years, they are applied at the port of DjenDjen in Jijel province, object of our study, in the framework of its extension and its development, in order to improve the support soil which will receive the foundations of the protections structures and the container terminal in caissons. The main objective is to understand and apprehend these techniques, as well as the sensitivity of the intervening factors on its realization, and their effect on the behavior of the soil during and after its implementation. In addition, this treatment to minimize the risk of liquefaction and instability of the protective structure, However, the advantage of speed of execution and reasonable cost compared to the importance of the project, thus no negative effects have been reported on the environment. The effectiveness of these soil treatment methods has been demonstrated by the results of the available in-situ tests, in particular the SPT tests which made it possible to check the capacity of the support soil before and after its completion, as well as the settlement surveys confirm the efficiency of these techniques in terms of improving the bearing capacity of the seabed.

**Keywords:** Harbours, Vibroflotation, Dynamic compaction, Preloading, Soil improvement.

## 1. Introduction:

The construction of a port, its equipment, the layout of its access, the protection of the shoreline from the action of the sea constitute a complex set of operations, usually referred to as "maritime works" [1,2]. It was therefore quickly considered to study the mechanisms of rupture to increase their bearing capacity and eliminate settlements and risks of liquefaction [3]. Soil improvement methods are one of the tools available to the engineer to solve the stability problems or deformations he encounters when developing a project.



The dike consists of blocks or caissons of reinforced concrete, or prestressed, which with their own weight resist the forces imposed by the swell: they must be large enough to be heavy enough. When the foundation soil offers good resistance, the quays are made in the form of massive structures capable of withstanding the forces, horizontal (towards the ground, caused by the berthing of the ships and towards the basin, caused by the thrusting of embankments and mooring of ships) and vertical forces due to their own weight [1]. Ruptures are usually due either to the action of the swell or to geotechnical factors which are influenced by the self weight, the hydraulic actions and the seismic actions. There must be checks for each of these potential failure modes.

## 2. Consolidation methods for soil improvement:

In the feasibility study of a project, the use of soil treatment methods implies knowledge of their respective performances and limits. A question then arises: how to easily represent the application fields of each process? It has been chosen to represent the ability of a method to treat a soil according to the grain size distribution of the latter. It has the advantage of only using identification criteria obtained by simple laboratory measurements [4].

## 3. Analysis of Soil sample Behaviour of DjenDjen port Sites during the Laboratory tests:

The Agitation Study showed that the development of a container terminal with caisson's quay wall necessitates the extension of the protection structures (breakwaters) of the 400 m north dike and the 250 m East dike with the creation of a Groin of 100 m, to reduce the width of the entrance pass (figure 1). The protective structures adopted is of the vertical breakwater type.

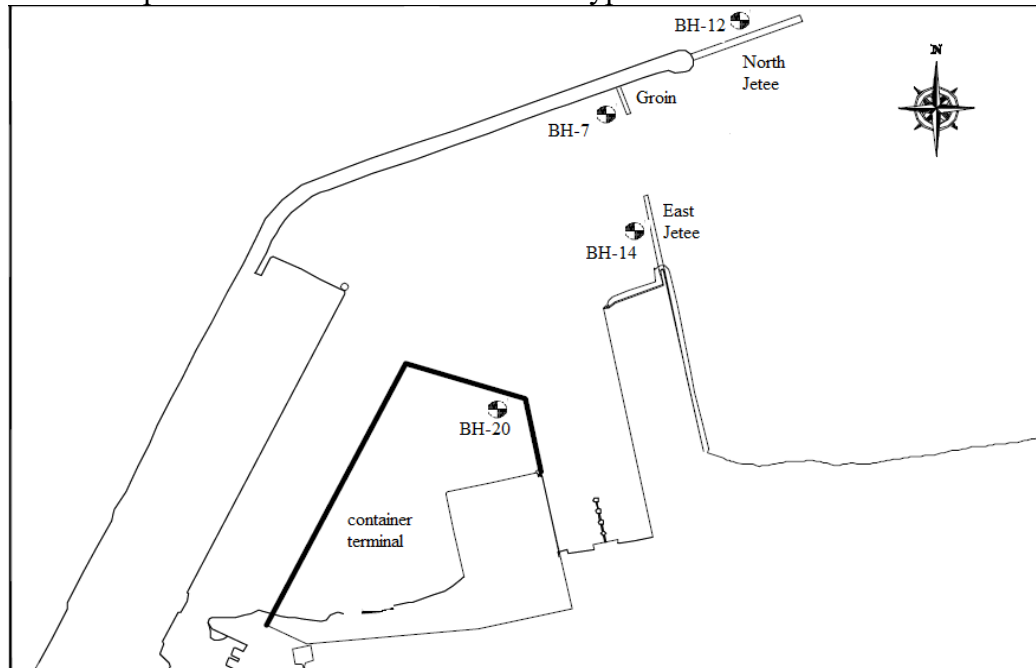


Figure-1: Ground plan of the DjenDjen port.

The purpose of this study is to verify the stability of the protective structures, as well as the quay wall of the container terminal at the port of Djen-Djen in Algeria during the extension works. To ensure the stability and strength of the foundations of the structure and to determine the effect of consolidation methods on marine soil improvement.

We conducted a drilling study, physical research and tests at the initial site on the project area; seeking to know the state of the layers on the ground base, the physical and dynamic characteristics of the soil, we conducted tests below to offer mechanical data on ground necessary during the design. We conducted a drilling study for a total of 4 wells (Figure 1) (1 hole on the north dike, 1 hole on the east dike, 1 hole on the groin, 1 hole in the container terminal section). In the dike and terminal sections, drilling was done on 5 meters of marl.

### 3.1 Basement conditions:

The geotechnical survey and the results of the laboratory tests showed that the soil in the study area consisted, in order and depending on the depth, of sandy and gravelly sedimentary layers and marl (Figure 2). In general, silty sand is predominant, and beneath, layers of gravel or gravelly sand are observed. In the area of the East Jetty, found among the upper layers of sand, sand mixed layers of rocks.

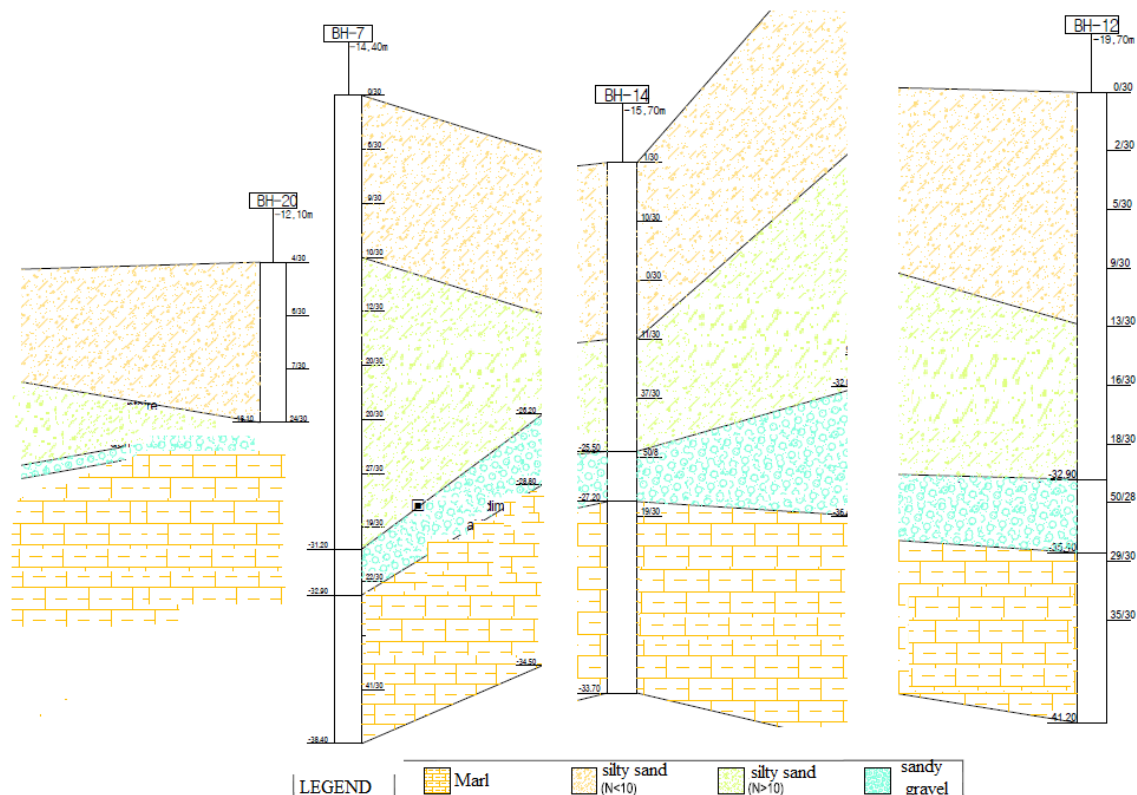


Figure-2: lithological section of the port site.

### 3.1.1 North Jetty (BH-12):

Figure 2 shows the cross-section of the north dike section. Based on the results of the in-situ study and laboratory tests, drilling results of 21.5 m maximum are as follows:

□ ***Very loose to loose silty sand***

The upper part consists of weak silty sand of gray and brown color. This sand is 6.0 to 8.0 m (PWD -25.3m ~ -28.0m) from the surface of the seabed. The  $N_{SPT}$  is from 0 to 10/30, and the natural water content is from 24.33 to 30.19%. Located in the upper part of the sedimentary layers, this layer is considered inadequate for settlement and bearing capacity.

□ ***Dense to very dense silty sand***

It is a moderately or very dense silty sand of gray and brown color below a muddy and weak sand; the thickness is 4.7 to 7.2m, and it lies at -32.2m to -33.2m of PWD. The  $N_{SPT}$  is 11 to 39/30, and the natural water content is 26.07 to 28.47%.

□ ***Compact to very compact sandy gravel***

It is a thin layer of pebbles located under medium and very dense muddy sand; it lies between -34.1 and -35.7m of PWD. The  $N_{SPT}$  is very high: 50/28 to 50/18.

□ ***Stiff marly***

This layer is located in the lower part according to the depth of the study, and it is of a gray or brown color. This layer appears between -34.1 and -35.7m of PWD, and has been observed up to 5.5 to 6.5 m. It is a cohesive soil corresponding to CL according to the unified classification.  $N_{SPT}$  is very high: 25 to 36/30.

Table 1: BH-12

Soil Layer	Prof.		SPT N		Density humid, $\gamma_h$ (kN/m <sup>3</sup> )	Cohesion Cu (kPa)	Friction Angle $\phi$ , (DEG)	Deformed Modulus E (MPa)	Velocity (m/s)		Poisson's Ratio $\mu_d$	Shear Modulus $G_d$ (kN/m <sup>2</sup> )	Dynamic Modulus $E_d$ (kN/m <sup>2</sup> )	Constrained Modulus, $K_d$ (kN/m <sup>2</sup> )
	GL- (m)	PWD (m)	measured	average					P-wave	S-Wave				
silty Sand (N <10)	-	- 19.7	0	4	17	5<	27	0.2	1.248	63	0.499	6.94E+03	2.08E+04	3.47E+06
	2.0	-21.7	2		17	5<	28	0.8	1.373	94	0.498	1.52E+04	4.54E+04	3.79E+06
	4.0	- 23.7	5		17	5<	29	2.0	1.462	121	0.497	2.52E+04	7.55E+04	4.20E+06
	6.0	- 25.7	9		17	5<	30	3.6	1.522	142	0.496	3.50E+04	1.05E+05	4.36E+06
silty Sand (N >10)	8.0	-27.7	13	16	18	10<	31	5.2	1.560	157	0.495	4.54E+04	1.36E+05	4.53E+06
	10	-29.7	16		18	10<	32	6.4	1.583	167	0.494	5.10E+04	1.52E+05	4.23E+06
	13.2	-32.9	18		18	10<	32	7.2	1.595	172	0.494	5.44E+04	1.63E+05	4.52E+06
Gravel	15.7	-35.4	54	60	19	5<	43	37.5	1.719	233	0.491	1.05E+05	3.14E+05	5.81E+06
Marl	16	-35.7	29	33	20	181.3	15<	13.9	1.832	276	0.488	1.56E+05	4.63E+05	6.43E+06
	18	-37.7	35		20	218.8	15<	10.6	1.861	285	0.488	1.66E+05	4.94E+05	6.86E+06
	20.5	-40.2	35		20	218.8	15<	12.8	1.861	285	0.488	1.66E+05	4.94E+05	6.86E+06

### 3. 1. 2 Groin (BH-7) et East Jetty (BH-14):

Figure 2 shows the cross-section of the East dike and groin section. Based on the results of the in-situ study and laboratory tests, drilling results of 28.5 m maximum are as follows:

□ **Very loose to loose silty sand**

The entire upper part consists of low silty sand gray and brown color. This sand is 6.0 to 8.0 m (PWD -10.6m ~ -22.5m) from the seabed surface.  $N_{SPT}$  is 0 to 10/30, and the natural water content is 27.28 to 41.76%. Located in the upper part of the sedimentary layers, this layer is considered inadequate for settlement and bearing capacity.

□ **Dense to very dense silty sand**

It is a moderately or very dense muddy sand of gray and brown color below a muddy and weak sand; the thickness is 3.7 to 12.6m, and it lies at -23.2m to -31.2m of PWD.  $N_{SPT}$  is 11.30 to 50/25, and the natural water content is 27.45 to 28.47%.

□ **Compact to very compact sandy gravel**

It is a thin layer of pebbles located under medium and very dense muddy sand; it lies between -27.2 and -32.9m of PWD.  $N_{SPT}$  is very high: 22/30 to 50/10.

□ **Stiff marly**

This layer is located in the lower part depending on the depth of the study, and it is a gray or brown color. This layer appears between -27.2 and -32.9m of PWD, and has been observed up to 5.5 to 7.8m. It is a cohesive soil corresponding to CL according to the unified classification.  $N_{SPT}$  is very high: 29/30 to 43/30.

Table 2: BH-14

Soil Layer	Prof.		SPT N		Density humid, $\gamma_h$ (kN/m <sup>3</sup> )	Cohesion Cu (kPa)	Friction Angle $\phi$ , (DEG)	Deformed Moulus E (MPa)	Velocity (m/s)		Poisson's Ratio $\mu_d$	Shear Modulus $G_d$ (kN/m <sup>2</sup> )	Dynamic Modulus Ed (kN/m <sup>2</sup> )	Constrained Moduls, Kd (kN/m <sup>2</sup> )
	GL- (m)	PWD (m)	measured	average					P-wave	S-Wave				
silty Sand (N <10)	-	-15.7	1	6	17	5<	27	0.4	1.310	77	0.498	1.03E+04	3.09E+04	2.58E+06
	2.0	-17.7	10		17	5<	30	4.0	1.533	146	0.495	3.71E+04	1.11E+05	3.70E+06
	4.0	-19.7	0		17	5<	27	0.2	1.248	63	0.499	6.94E+03	2.08E+04	3.47E+06
	6.0	-21.7	11		17	5<	30	4.4	1.543	150	0.495	3.91E+04	1.17E+05	3.90E+06
silty Sand (N >10)	9.8	-25.5	37	37	18	10<	38	14.8	1.676	210	0.492	8.12E+04	2.42E+05	5.05E+06
Gravel	11.5	-27.2	188	60	19	5<	45	131.3	1.872	330	0.484	2.11E+05	6.26E+05	6.53E+06
Marl	12.0	-27.7	19	19	20	118.8	15<	81.9	1.769	257	0.489	1.35E+05	4.01E+05	6.08E+06
	15.	-30.7	19		20	118.8	15<	83.5	1.769	257	0.489	1.35E+05	4.01E+05	6.08E+06
	18.0	-33.7	19		20	118.8	15<	85.2	1.769	257	0.489	1.35E+05	4.01E+05	6.08E+06

Table 3: BH- 7

Soil Layer	Prof.		SPT N		Density humid, $\gamma_h$ (kN/m <sup>3</sup> )	Cohesion Cu (kPa)	Friction Angle $\phi$ , (DEG)	Deformed Moulus E (MPa)	Velocity (m/s)		Poisson's Ratio $\mu_d$	Shear Modulus $G_d$ (kN/m <sup>2</sup> )	Dynamic Modulus Ed (kN/m <sup>2</sup> )	Constrained Moduls, Kd (kN/m <sup>2</sup> )
	GL- (m)	PWD (m)	measure d	average					P-wave	S-Wave				
silty Sand (N <10)	-	-14.4	0	6	17	5<	27	0.2	1.248	63	0.499	6.94E+03	2.08E+04	3.47E+06
	2.0	-16.4	6		17	5<	29	2.4	1.480	127	0.496	2.79E+04	8.35E+04	3.48E+06
	4.0	-18.4	9		17	5<	30	3.6	1.522	142	0.496	3.50E+04	1.05E+05	4.36E+06
	6.0	-20.4	10		17	5<	30	4.0	1.533	146	0.495	3.71E+04	1.11E+05	3.70E+06
silty Sand (N >10)	8.0	-22.4	12	20	18	10<	31	4.8	1.552	154	0.495	4.34E+04	1.30E+05	4.33E+06
	10	-24.4	20		18	10<	33	8.0	1.607	177	0.494	5.77E+04	1.72E+05	4.79E+06
	12.0	-26.4	20		18	10<	33	8.0	1.607	177	0.494	5.77E+04	1.72E+05	4.79E+06
	14.0	-28.4	27		18	10<	35	10.8	1.640	193	0.493	6.82E+04	2.04E+05	4.85E+06
Gravel	16.8	-31.2	19	19	19	5<	33	13.3	1.601	175	0.494	5.92E+04	1.77E+05	4.91E+06
Marl	18.5	-32.9	22	35	20	137.5	15<	20.3	1.791	263	0.489	1.42E+05	4.22E+05	6.39E+06
	20.0	-34.4	35		20	218.8	15<	7.0	1.861	285	0.488	1.66E+05	4.94E+05	6.86E+06
	22.0	-36.4	41		20	256.3	15<	72.5	1.886	293	0.488	1.75E+05	5.21E+05	7.24E+06
	24.0	-38.4	41		20	256.3	15<	73.5	1.886	293	0.488	1.75E+05	5.21E+05	7.24E+06

### 3.1.3 Container terminal areas (BH-20):

To check the deeper layer, we examined 17.0m for BH-20. The layer within 6m of the upper part in the filling section is revealed as a layer of sand and weak sandy below 10 N; there is clay in the layer. Figure 2 shows the cross section of this area.

Table 4: BH-20.

Soil Layer	Prof.		SPT N		Density humid, $\gamma_h$ (kN/m <sup>3</sup> )	Cohesion Cu (kPa)	Friction Angle $\phi$ , (DEG)	Deformed Moulus E (MPa)	Velocity (m/s)		Poisson's Ratio $\mu_d$	Shear Modulus $G_d$ (kN/m <sup>2</sup> )	Dynamic Modulus Ed (kN/m <sup>2</sup> )	Constrained Moduls, Kd (kN/m <sup>2</sup> )
	GL- (m)	PWD (m)	measure d	average					P-wave	S-Wave				
silty Sand (N <10)	-	-5.7	3	5	17	5<	28	1.2	1.412	105	0.497	1.90E+04	5.69E+04	3.16E+06
	2.0	-7.7	7		17	5<	29	2.8	1.496	132	0.496	3.04E+04	9.10E+04	3.79E+06
	4.9	-10.6	6		17	5<	29	2.4	1.480	127	0.496	2.79E+04	8.35E+04	3.48E+06
silty Sand (N >10)	6.0	-11.7	50	21	18	10<	42	20.0	1.711	229	0.491	9.60E+04	2.86E+05	5.30E+06
	8.0	-13.7	31		18	10<	36	12.4	1.656	200	0.493	7.36E+04	2.20E+05	5.23E+06
	10.0	-15.7	16		18	10<	32	6.4	1.583	167	0.494	5.10E+04	1.52E+05	4.23E+06
	12.0	-17.7	21		18	10<	33	8.4	1.612	180	0.494	5.93E+04	1.77E+05	4.92E+06
	14.0	-19.7	20		18	10<	33	8.0	1.607	177	0.494	5.77E+04	1.72E+05	4.79E+06
	17.5	-23.2	27		18	10<	35	10.8	1.640	193	0.493	6.82E+04	2.04E+05	4.85E+06

# In-situ and Laboratory Analysis of Treated Marine Soil by Consolidation Methods

Gravel	18.0	-23.7	115	89	19	5<	45	80.8	1.811	288	0.487	1.61E+05	4.79E+05	6.15E+06
	20.0	-25.7	62		19	5<	45	43.4	1.736	243	0.490	1.14E+05	3.40E+05	5.67E+06
	22.0	-27.7	125		19	5<	45	87.5	1.821	295	0.487	1.69E+05	5.01E+05	6.42E+06
Marl	24.0	-29.7	37	35	20	231.3	15<	19.8	1.870	288	0.488	1.69E+05	5.03E+05	6.99E+06
	26.0	-31.7	34		20	212.5	15<	25.2	1.857	284	0.488	1.64E+05	4.89E+05	6.79E+06
	27.8	33.5	34		20	212.5	15<	28.9	1.857	284	0.488	1.64E+05	4.89E+05	6.79E+06

The following conclusions are drawn from this investigation:

- The layers in the area of this project are of a following order: low sandy soil, medium and very dense sandy soil, marl. The weak sandy soil that is important in mechanics is 6.0 to 8.0m thick, and the  $N_{SPT}$  is less than 10/30.

- According to the results of the PDL test, the correlation with the standard penetration test is  $N_d = 1.93N_{SPT}$ . This correlation will help to understand the resistance after soil improvement.

- According to the results of the assessment on the possibility of liquefaction, it is expected that the liquefaction will take place in the area where the  $N_{SPT}$  is less than 10.

- According to the results of the calculation for the permitted lift according to the PDL results, it appears that the sandy and weak soil layer does not have enough lift; hence the need for soil improvement.

- The amount of immediate settlement will occur during and after the work. it will require a supervision on the settlement during the works. In general, compressive settlement takes place on the muddy and weak soil; the amount of compressive settlement will not be large for the solid marl in the area of this project. Even if the quantity is large, the time of compression is long; the amount of settlement will not be large during the life of the structures.

- Depending on the results of the liquefaction assessment and the base lift calculation, consolidation techniques are recommended. To apply these techniques requires a detailed examination of the current state of the soil; granulometry, setting the goal for soil improvement and checking for improvement effects during and after the works.

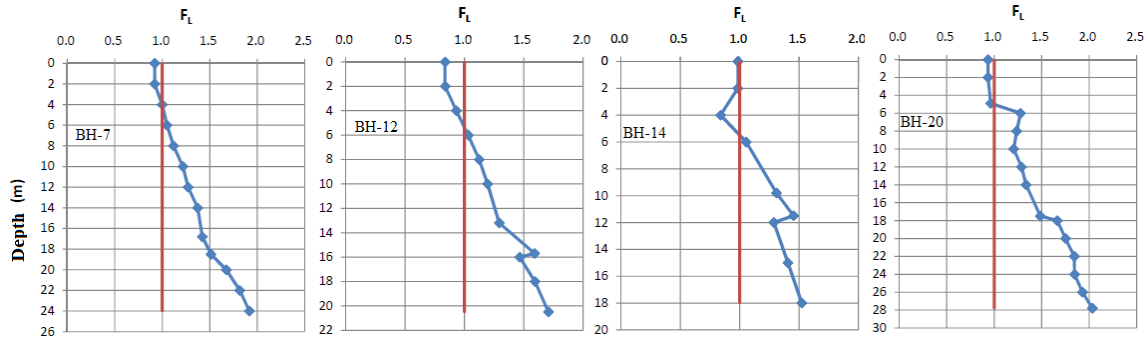


Figure 3: Liquefaction potential in different DjenDjen port areas before soil treatment.

For the detailed soil liquefaction assessment, we used the results of the standard penetration test and the vibration and triaxial compression test. As for the maximum acceleration of the surface of the earth  $a_{max}$ , we applied 0.200g. Figure (3) shows the stability rate for liquefaction versus depth for each location. According to a detailed examination, the liquefaction is less than 1 stability rate below 10  $N_{SPT}$ . It is therefore necessary measures against liquefaction.

### 3.2 Cyclic Triaxial Test:

During the study, in order to prevent the collapse of the borehole wall, an envelope was installed up to the top of the marl, and based on the speed of advance during a drilling, the condition of the silt, the color of the flowing water, samples extracted by SPT and N numbers, the layer distribution status was checked, and the order and thickness of the layers were discovered. During a standard penetration test, disturbed samples were collected by Split Spoon sampler. From the samples collected, we selected the representative sample from each layer according to the ASTM/ NF P regulations.

The cyclic triaxial test is carried out to calculate the resistance to liquefaction of the soil by including the characteristics related to the pressure and the deformation occurring on the ground during an earthquake; the earthquake deformation characteristics occurring during an earthquake are calculated by selecting the number of repetitions corresponding to the earthquake dimension. This test is used to calculate the shear stress ratio of the vibration resistance and the shear strength of the detailed liquefaction forecasting method.

Liquefaction resistance is calculated on the basis of the initial liquefaction that occurs when the effective confining pressure becomes zero; for high density sand and sandy and muddy soil, initial liquefaction does not occur; the resistance is defined according to the axial strain ratio.

### 3.2.1 Stress–strain behavior, failure modes, Strain energy and cyclic resistance:

A series of cyclic triaxial tests was conducted to investigate the combined effect of cyclic shear on the undrained behavior of saturated loose sand. Magnitude cycles have been imposed to simulate the responses of sand subject to cyclic loadings, and distinctly different behaviors have been observed. The excess PWP generation is one of the main concerns when assessing the liquefaction potential of sandy sites during cyclic loading. Some studies [5, 6] have shown that residual pore pressures due to plastic deformation under undrained conditions or equivalent to changes in plastic volume under drained conditions can be mathematically related to density. The cumulative energy density during deviatoric stress cycles is represented by the area of the hysteresis loop formed by a series of charges. The failure can be characterized by a large residual deformation, which differs from the flux liquefaction with a strong transient axial stress on the extension side. This type of failure with excessive accumulated cyclic stress on the compression side may be called residual deformation failure [7, 8]. A single amplitude residual deformation criterion (5%) is adopted to designate the state of failure [7, 9, 10].

The behavior of the luminous sand with different relative density (DR-30, 50, 80) in different applied pressures, The typical effective stress path, the excess PWP generation and the axial strain with the load cycles are shown in the Figures (4-6). These tests were performed on consolidated samples with different cyclic loading modes with a CSR ranging from 0.25 to 0.4 and two different damping amplitudes (DA5%, DA10%). The sample under cyclic loading shows different responses of Figure 4 to 6, although the effective stress decreases with the number of cycles, the excess of PWP builds up moderately and stabilizes after the application of large number of cycles, and the sample does not fail with the initial liquefaction because the effective stress is always greater than zero. The development of axial deformations and its rate accelerates when the generated PWP approaches the final value. Increasing trends in axial deformation appear to be similar, also leading to failure of flow liquefaction, as evidenced by the effective stress path and stress-strain curve. Axial deformation progressively accumulates on the side of the initial static shear stress, indicating that residual deformation failure is triggered as a result of undrained cyclic loading. A similar trend with interstitial pressure responses is also seen in the figures, in which the PWP builds rapidly in the incipient loading cycles and quickly becomes stabilized with a constant end value. In addition, the cyclic loading results in the reduction of the shear modulus, which is signed by the flattened hysteresis cycle. This may be due to a decrease in the confining pressure due to the excessive pressure of interstitial water. Meanwhile, low soil resistance is not sufficient to retain liquefaction during cyclic loading. The hysteresis cycle resulting from the propagation of the wave shows that there is no insignificant reduction of the shear modulus. This indicates that the effective confining pressure is not significantly reduced due to excessive pore water pressure.



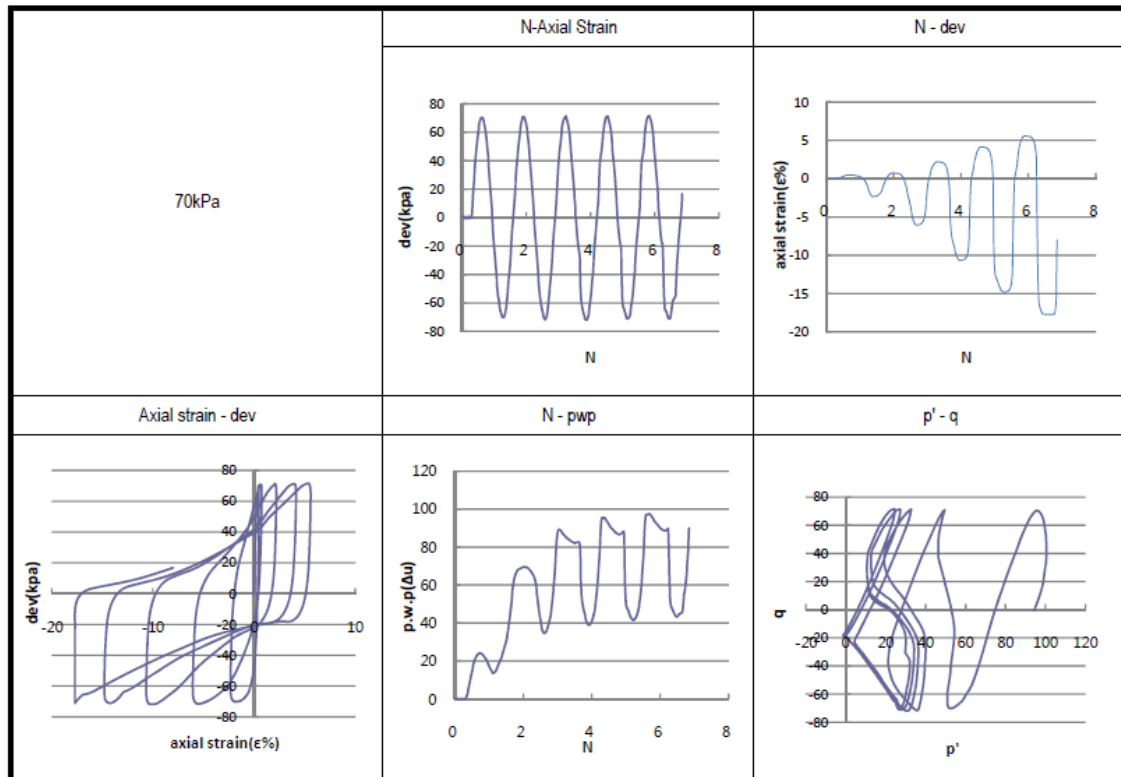
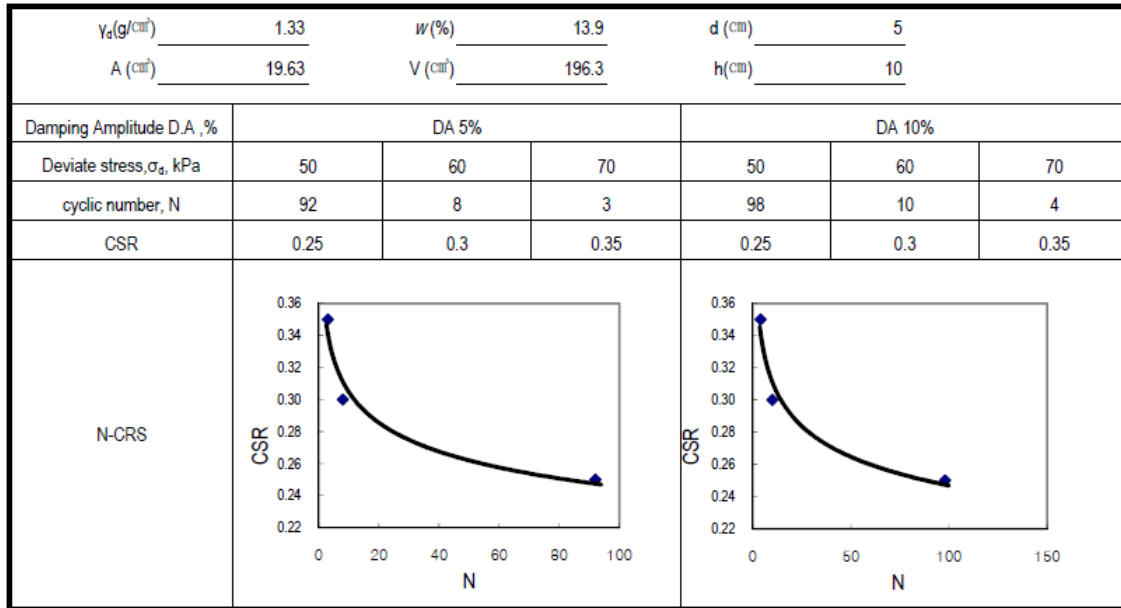
The increase in excess pore water pressure (PWP) production is shown in Figures (4-6), which indicates the gradual increase of the excess PWP ratio during cyclic loading. As shown in these Figures, the variation of the deflection stress with axial deformation (hysteresis loops) represents the degradation of the damping ratio and the shear stiffness of the soil with increasing number of loading cycles (N). During undrained cyclic loading, the rise of the PWP in saturated sand results in the reduction of intergranular forces, resulting in a reduction in soil stress and stiffness [11, 12]. The stress-strain responses of saturated samples obtained from monotonic tests at different applied loading and relative density DR are presented. It is observed that the maximum deflection stresses and the associated deformation levels are significantly affected by the variation of Confining Pressure and the relative density. In view of confining pressure, the increase in maximum deviation stress is important for increasing relative density. Therefore, it can be argued that the effect of the variation of confining pressure is greater for sands at low relative density, that is to say in the range of dense to medium-dense sands. The figures represent the exponential decay of the deviating stress with an increase of (N) which can be attributed to the deformation of the soil sample.

The distinctly different liquefaction resistance observed shows the importance of evaluating the cyclic resistance of sand under irregular loading conditions encountered in engineering proprieties. Unlike the test results of the samples with a moderate CSR, the development of axial deformations of samples with higher CSR values starts at an early stage of the stress cycles. Sufficient soil resistance provided by increasing relative density could maintain soil stability during cyclic loading. Although the results of the cyclic triaxial tests indicate that the irregularity of the load plays an important role in the cyclic behavior of sand, it has been shown that the modes of deformation and failure depend only on the type of consolidation. The following conclusions are drawn from this test:

- Two failure modes are identified for sand samples subjected to cyclic loading, namely flow liquefaction and residual deformation failure. The liquefaction of the flow occurs for the isotropically consolidated samples, accompanied by a sharp increase in pore pressure and axial strain, bringing the samples to initial liquefaction. Residual deformation failure is triggered for samples with initial static shear due to anisotropic consolidation, and failure could be defined as residual axial deformation greater than 5% on the compression side.
- Resistance to liquefaction of sand is greatly affected by the irregularity of the load. The results of the tests performed under load conditions indicate that the number of cycles (N) required for the failure is related to the CSR. It has been found that the presence of the initial static shear differs failures and is therefore beneficial for the cyclic resistance of the sand.
- There is a unique relationship between the residual PWP and the strain energy accumulated during the cyclic triaxial loading, irrespective of the cyclic stress

# In-situ and Laboratory Analysis of Treated Marine Soil by Consolidation Methods

amplitude. A standardized version of the test data for pore pressure and strain energy in a narrow band suggests that the trend is independent of the loading path.



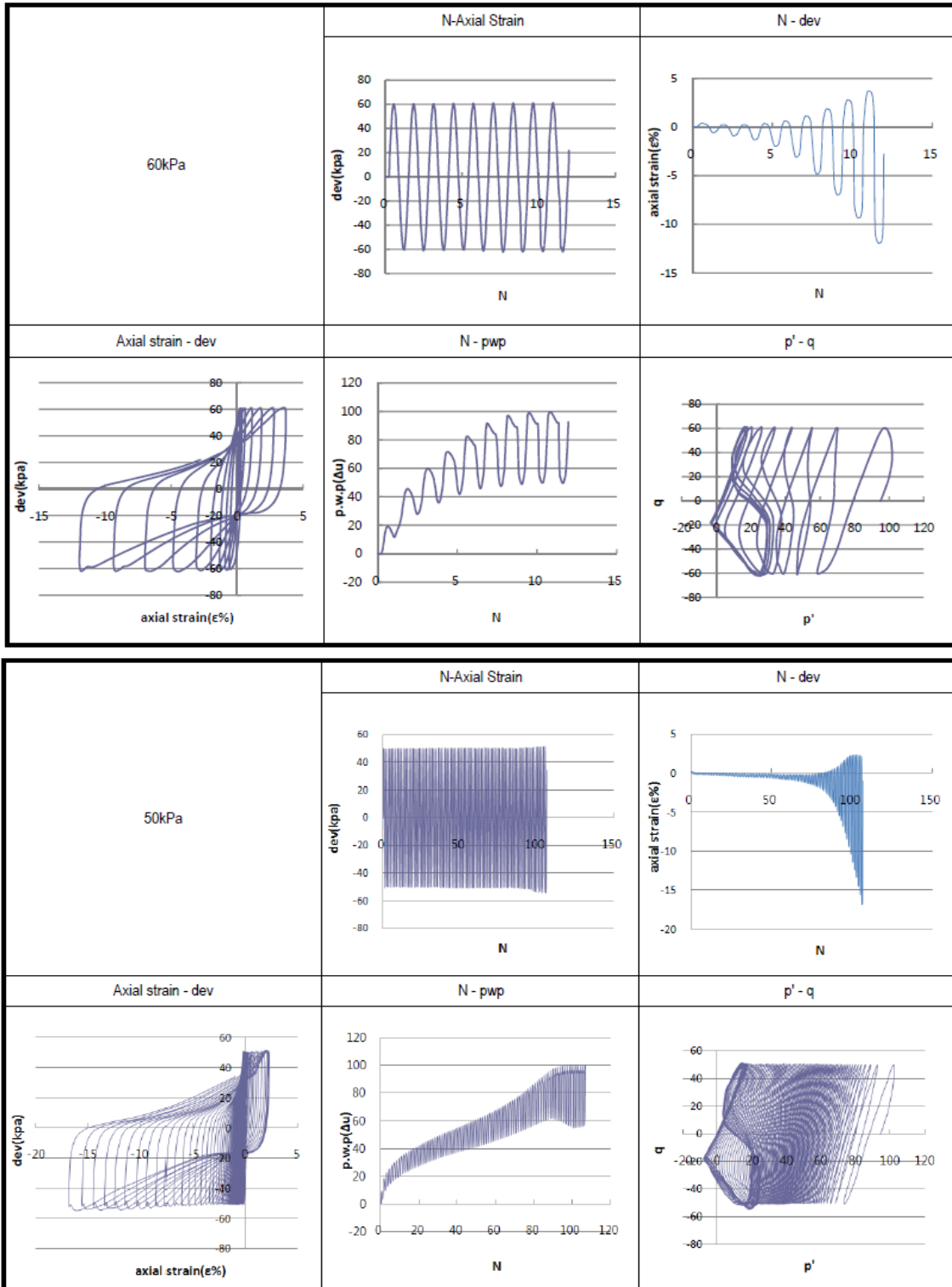
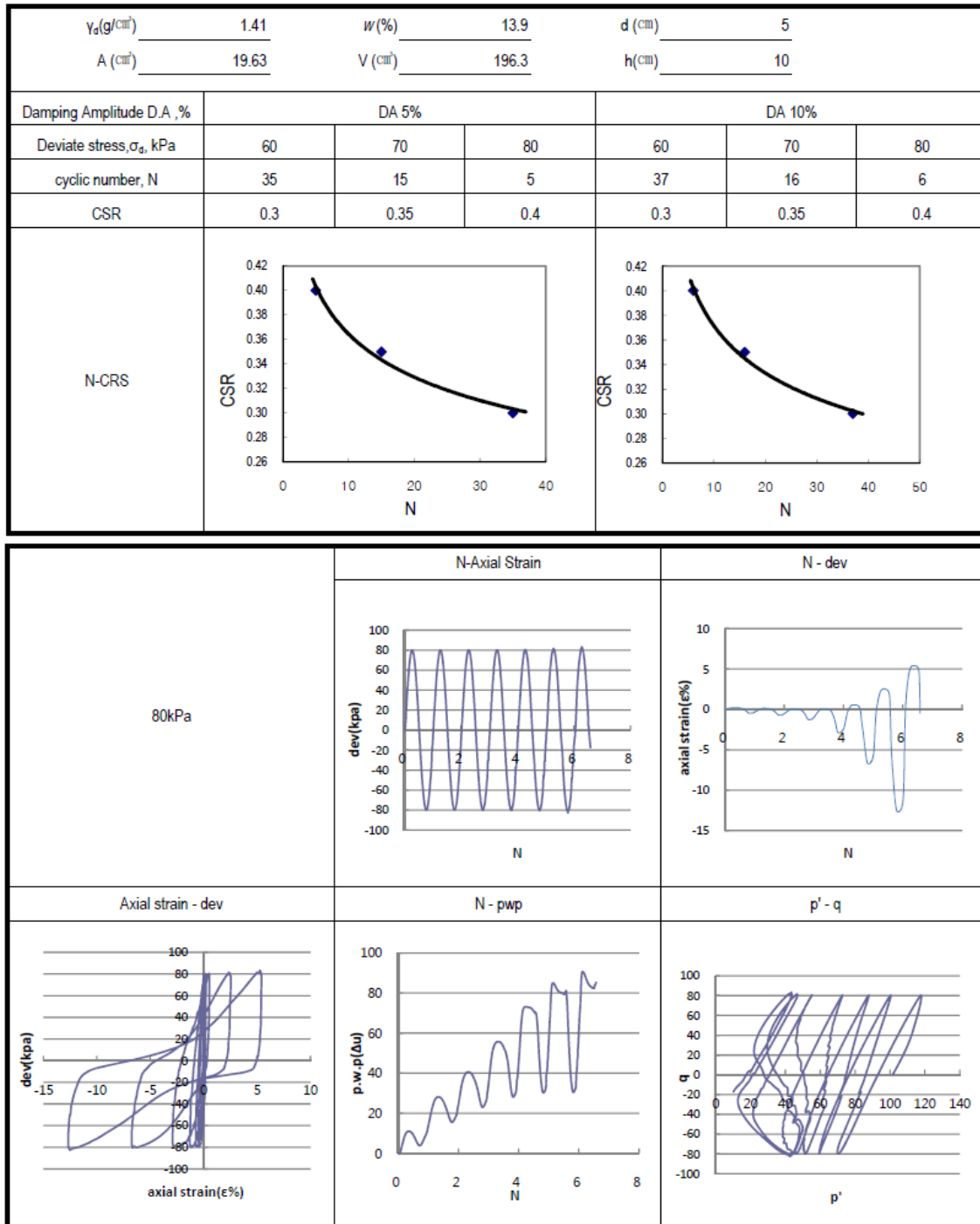


Figure 4: Cyclic response of sand (silty sand DR-30) under Cyclic loading in DjenDjen port: (a): axial strain vs N. (b) axial strain; and (c) stress- strain curve. (d) excess pore-water pressure; (e) effective stress path;

# In-situ and Laboratory Analysis of Treated Marine Soil by Consolidation Methods



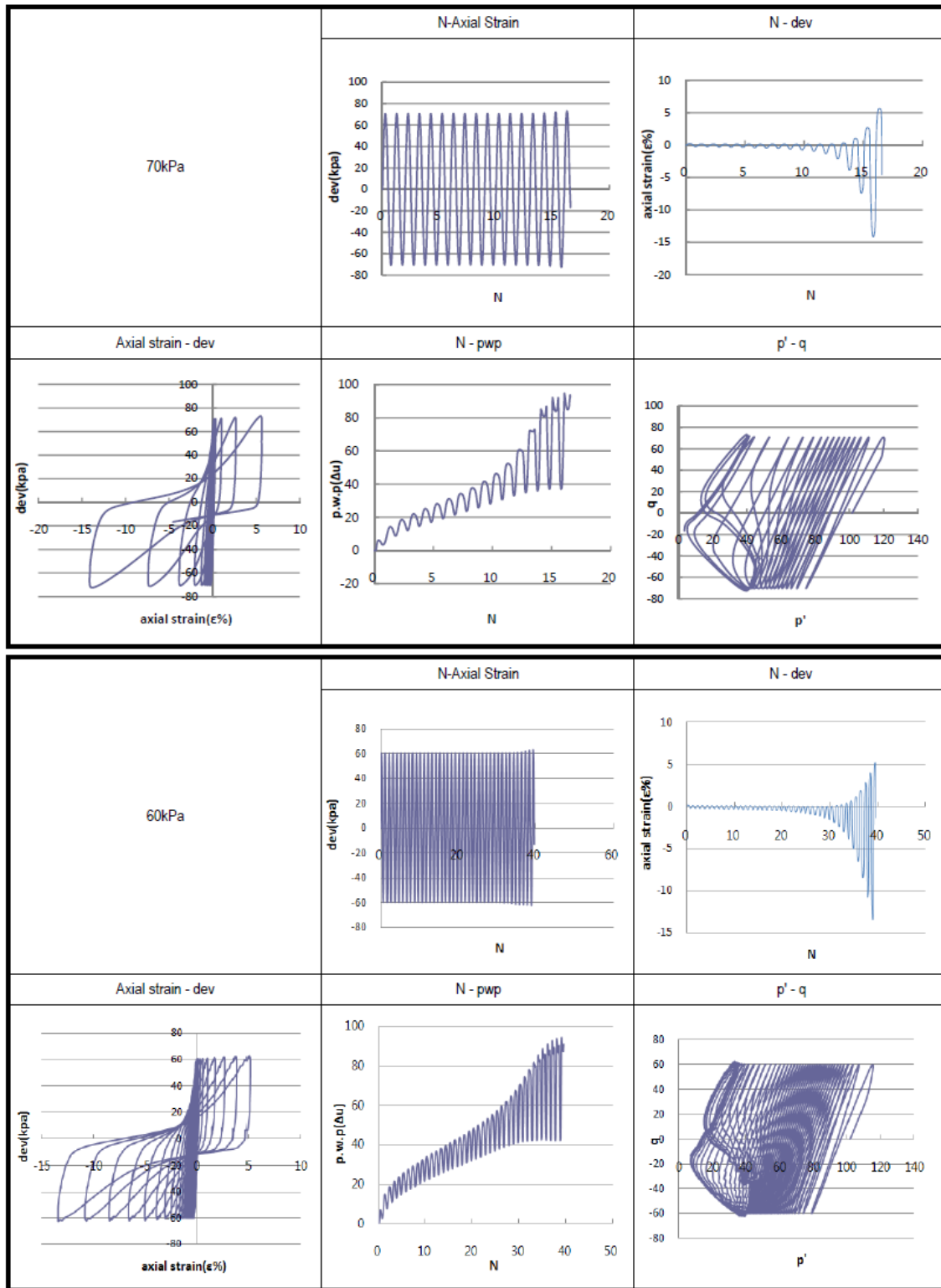
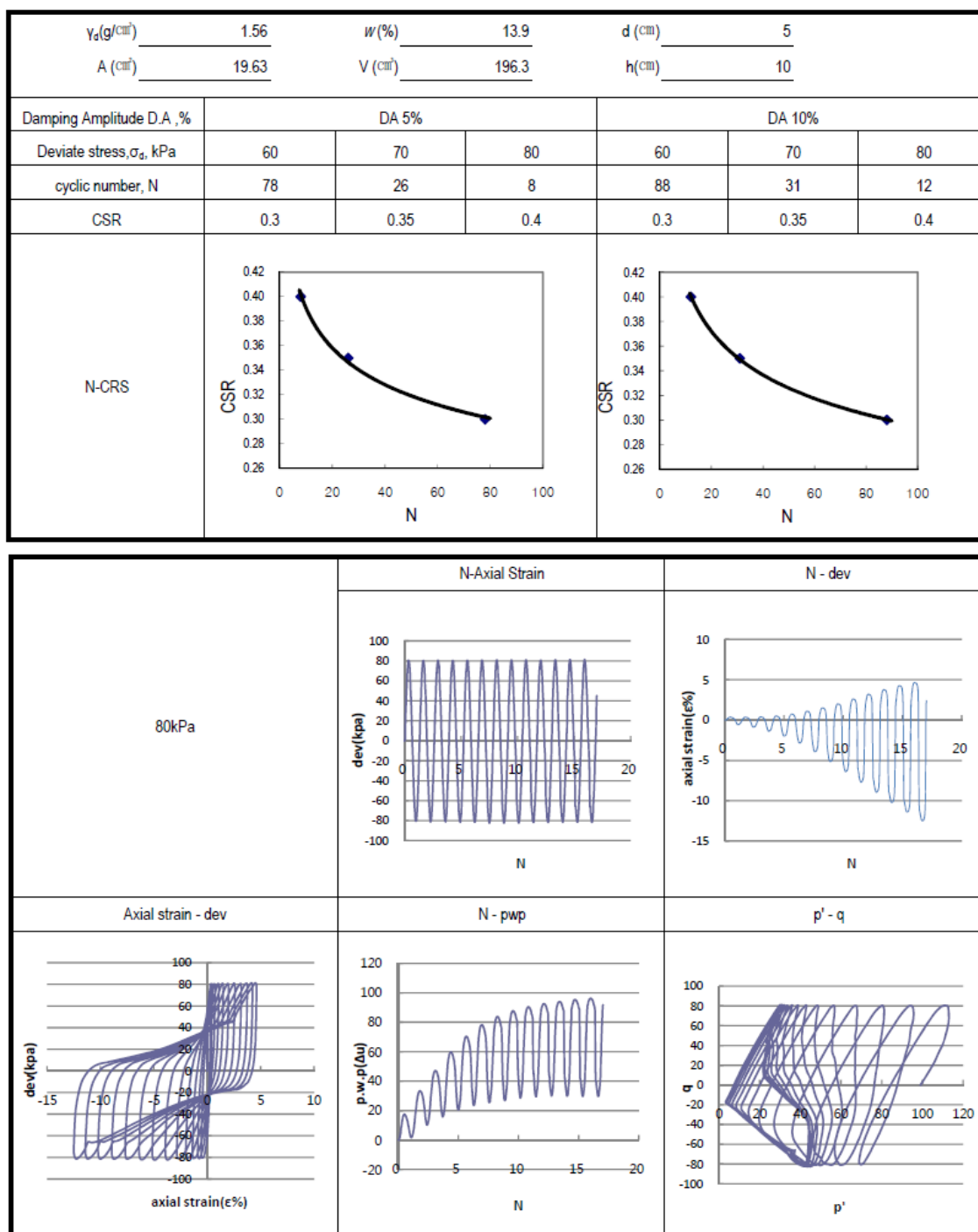


Figure 5: Cyclic response of sand (silty sand DR-50) under Cyclic loading in DjenDjen port: (a): axial strain vs N. (b) axial strain; and (c) stress- strain curve. (d) excess pore-water pressure; (e) effective stress path;

# In-situ and Laboratory Analysis of Treated Marine Soil by Consolidation Methods



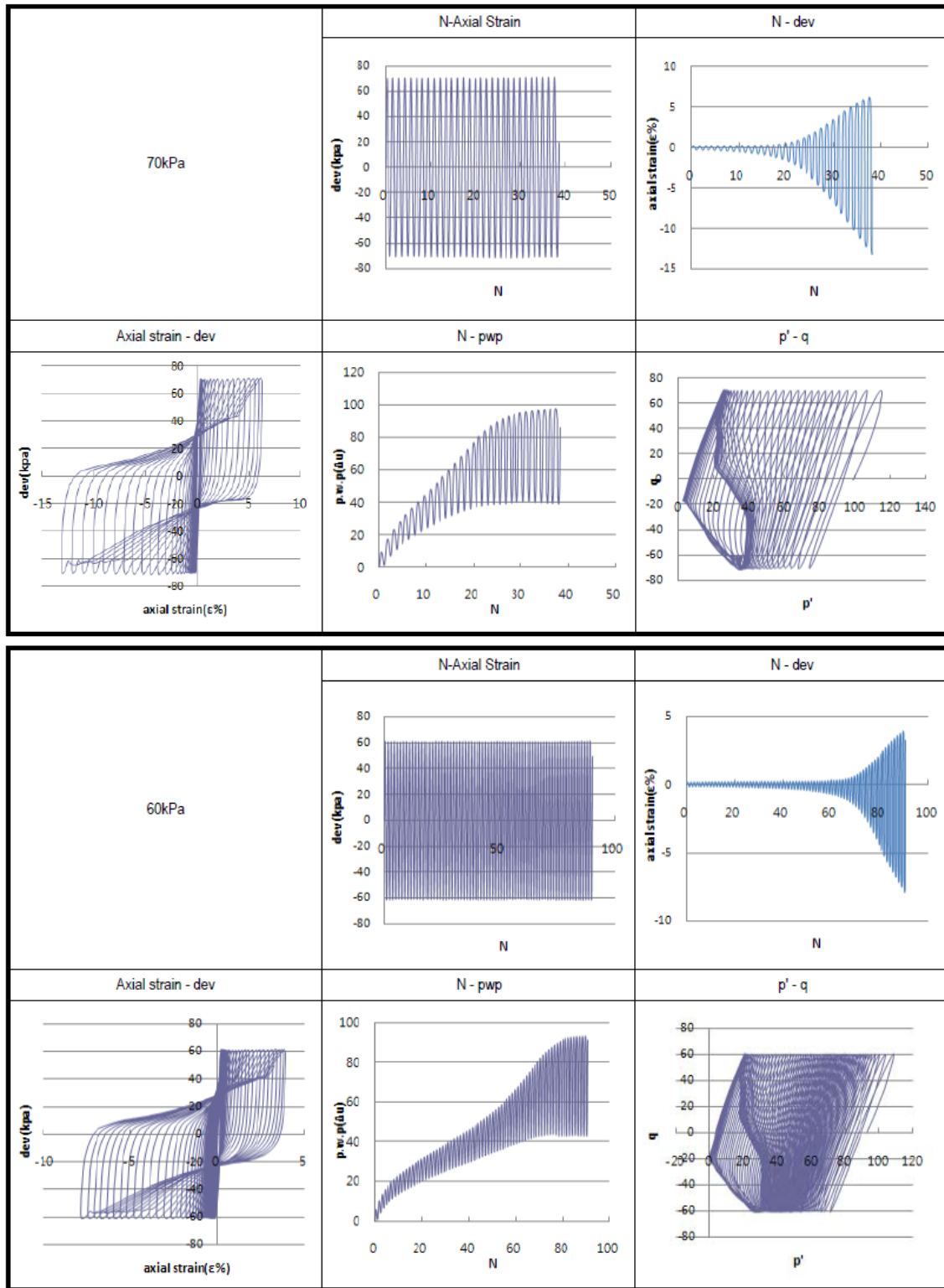


Figure 6: Cyclic response of sand (silty sand DR-80) under Cyclic loading in DjenDjen port: (a): axial strain vs N. (b) axial strain; and (c) stress- strain curve. (d) excess pore-water pressure; (e) effective stress path.

The relative density of the original soil is on average 30% below  $N_{SPT}$  10, and 50% above  $N_{SPT}$  10. We have therefore carried out a test on the relative density of the original soil, and an additional test on the relative density of 80% to evaluate the stability of the liquefaction after soil improvement. Table (5) shows the results of the repetitive and triaxial compression test. As the shear stress ratio increases, the number of charges for repetitive charge required for liquefaction decreases.

**Table 5:** Summary of cyclic triaxial test.

Dr (%)	D .A	$\sigma_{dev}$ (kPa)	CSR	N	Remarque
30 %	5 %	50	0.25	92	When N=15 CSR=0.293
		60	0.30	8	
		70	0.35	3	
50 %	5 %	60	0.30	35	When N=15 CSR=0.343
		70	0.35	15	
		80	0.40	5	
80 %	5 %	60	0.30	78	When N=15 CSR=0.372
		70	0.35	26	
		80	0.40	3	

Figure (7) shows the relationship of repetitive shear stress ratio to relative density. This ratio is a value 15 of the number of repetition of vibration corresponding to the magnitude of earthquake 7.5. As the relative density increases, the ratio of repetitive shear stress increases. These results can be applied to the assessment of liquefaction taking into account the relative density.

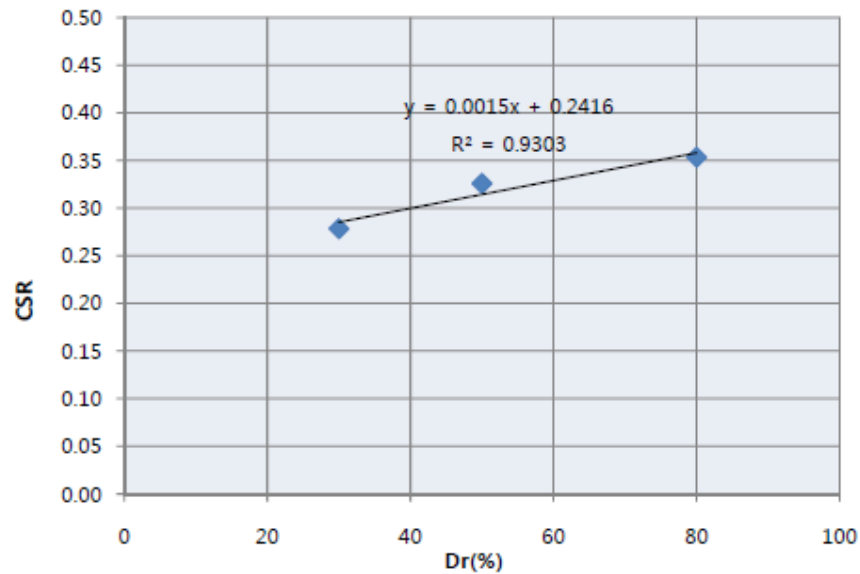


**Figure 7:** CSR versus relative density.



#### 4. Vibroflotation technique (VF):

Vibroflotation is a technique for in situ densification of thick layers of loose granular soil deposits. It consists in generating, with the help of a vibrator of depth (Vibroflot), horizontal vibrations in the ground soils in order to shear them and to provoke a localized liquefaction and an immediate settlement [13,17]. Treatment with this method generally achieves the following goals: increasing bearing capacity; reduction of settlement; acceleration of consolidation; eliminating the risk of liquefaction; no adverse effects have been reported on the environment [15,16,17].

In the caisson type VII; maximum settlements of 4.7 cm were observed, settlements up to 4.9 cm for type VIII, and a maximum settlement of 8.9 cm for type V; we can see a settlements behavior in a similar way, which explains why the three (03) graphs of the settlements is almost the same, only there is a difference in settlement values, caused by the few variation in the soil index properties. In conclusion; the results of the settlement (figure 8) are in excellent agreement with the forecasts, which reinforces our study. It is concluded that vibroflotation gives very satisfactory results in terms of soil improvement.

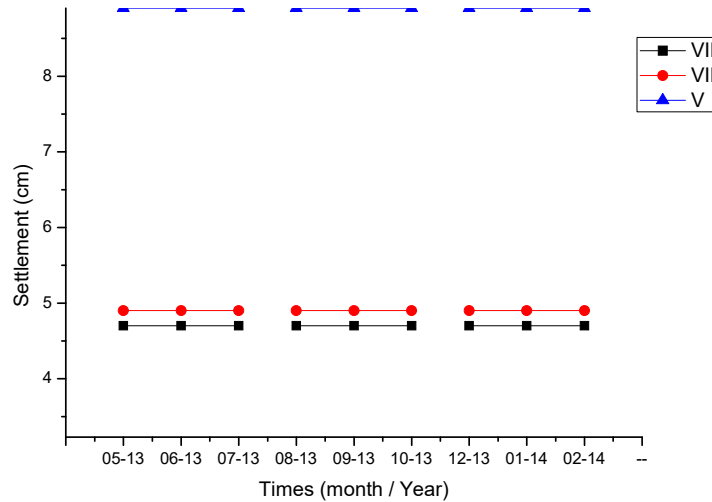




Figure 8: Comparison of settlement curves of in-situ measurements of three caissons as a function of time after soil improvement by vibroflotation.

#### **4.1 Assessment of potential liquefaction:**

The Numbers for soil design are calculated from the relational expression with the SPT N value, laboratory test results, the correlation between in-situ test results or between laboratory and in situ tests. Figure (9) and Table (6) are the results of the liquefaction test assumed after soil improvement; it takes more than 45% of the relative density improvement. If we convert it to SPT N. we get more than 15/30. So, the improved soil must be needed during 15/30.

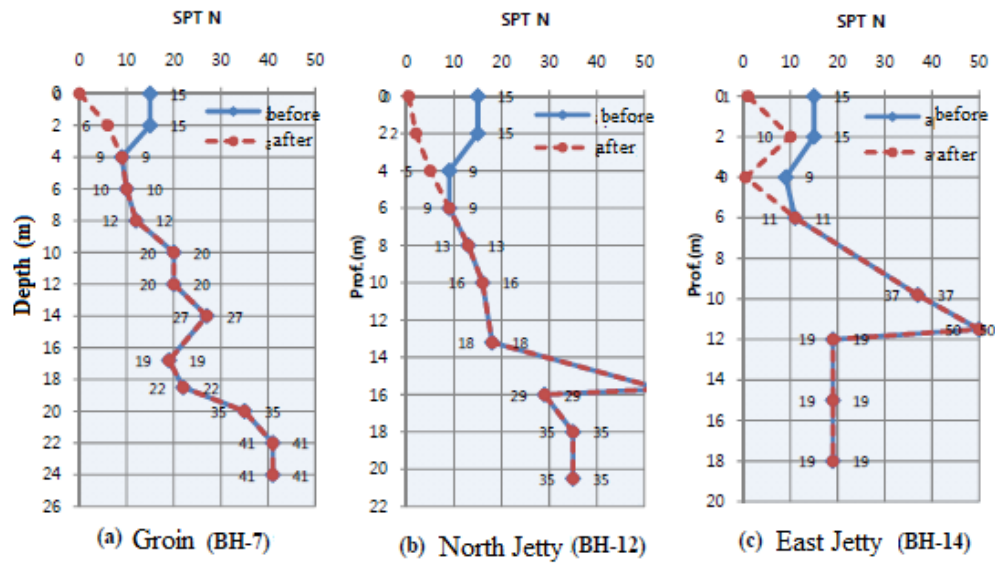


Figure 9: SPT tests before and after marine soil treatment by vibroflotation.

Table 6: Increase in relative density and decrease Liquefaction potential after treatment of seabed by vibroflotation.

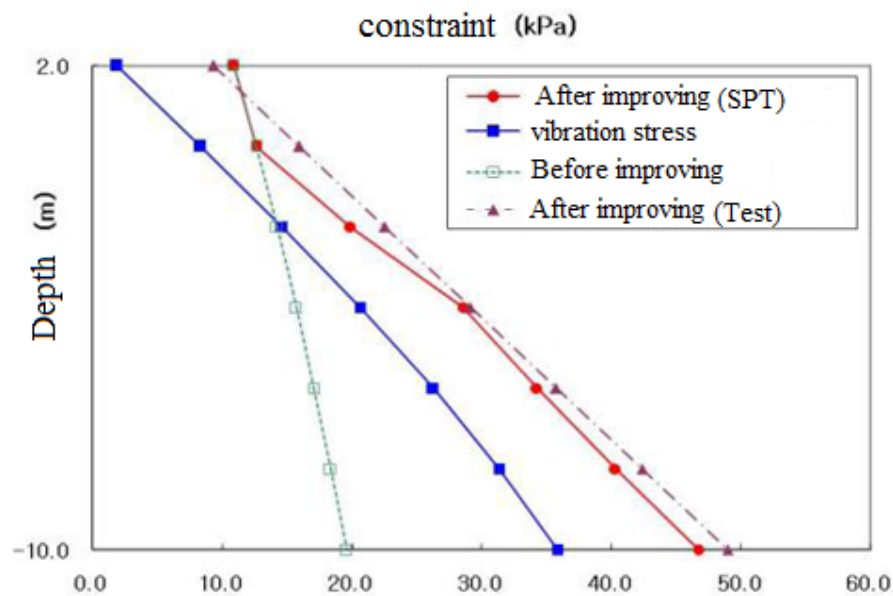
Soil Layer	Prof.		SPT N	Dr (%)	Liquefaction Potnetial
	GL- (m)	PWD (m)			
BH-7	-	-14.4	15	45	NO
silty Sand (N <10)	2.0	-16.4	15	45	NO
	4.0	-18.4	9	39	NO
	6.0	-20.4	10	40	NO
	6.0	-20.4	10	40	NO
BH-12	-	-19.7	15	45	NO
silty Sand (N <10)	2.0	-21.7	15	45	NO
	4.0	-23.7	9	39	NO
	6.0	-25.7	13	37	NO
	6.0	-25.7	13	37	NO
BH-14	-	-15.7	15	45	NO
silty Sand (N <10)	2.0	-17.7	15	45	NO
	4.0	-19.7	9	39	NO
	6.0	-21.7	11	41	NO
	6.0	-21.7	11	41	NO

## 5. Dynamic compaction technique (DC)

Land reclamation is generally defined as the process of creating new land by raising the elevation of a seabed, or other land at low altitude. It can be carried out by a movement of dry earth, also by hydraulic filling. Some possible failure modes in the embankment body and different failure modes need to be analyzed [18,19]. From the point of view of the foundation, this can pose a significant risk of partial or complete liquefaction and, consequently, reduction of soil resistance. Global Failure Stability Analysis provides suggestions for improvement methods to be performed.

Dynamic compaction (DC) is one of the techniques of soil improvement. It depends on the rearrangement of the soil particles using the dynamic energy produced by falling a weight (tamper) from a certain height. The concept of this technique is to improve the mechanical properties of the soil by transmitting high energy impacts on loose soils that initially have low load capacity and high compressibility potentials [20-23].

The feasibility of this technique ensure the stability of the workshop of caisson's manufacturing of the port of DjenDjen and minimize the risk of liquefaction during manufacturing. When the whole sequence of compaction has ended; the graphs of the safety factor (SF, standard and FS, on the ground from the SPT test) were presented to the liquefaction and stress distribution as a function of depth (figure 10) before and after compaction of the embankment. The results are perfectly satisfactory, which gives us the authorization to start the construction of a 1.75 m thick platform on the treated backfill, in order to install the sliding formwork and start the construction of the caissons. Since the construction of the first 1st caisson until the forty-fourth 44th; no soil settlement was noted and no geotechnical problems were encountered (Figure 11), which gives great reliability to this method of treating coastal hydraulic embankments.



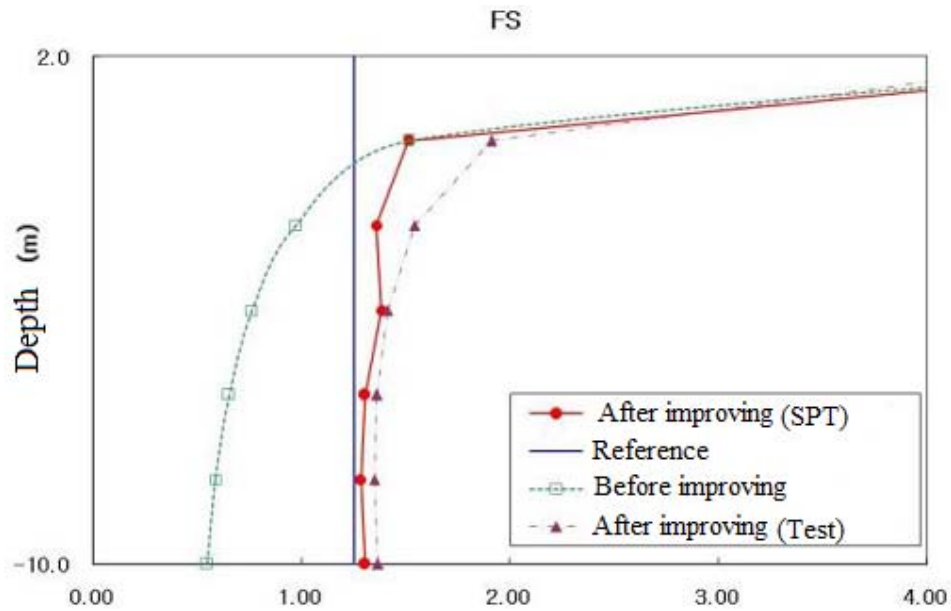


Figure 10: Safety factor (SPT) results for liquefaction and stress distribution before and after dynamic compaction.

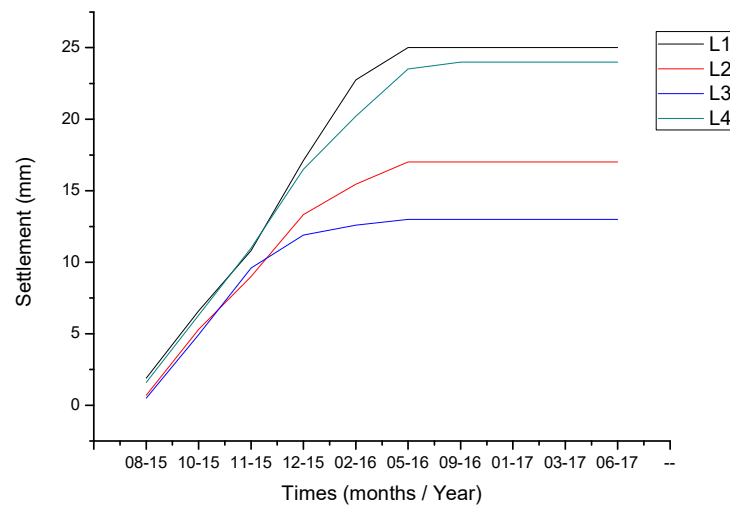


Figure 11: The results of the settlement of four (04) lines monitoring of caisson's workshop after platform implementation.



## 6. Pre-loading technique:

Pre-loading is a simple solution recommended for highly compressible saturated soils in order to partially accelerate their primary consolidation, which is accompanied by a reduction in settlement and as a result of an increase in undrained cohesion. When it comes to building on a saturated low lift and / or relatively compressible soil, pre-loading is the simplest technique to ensure short-term shear strength improvement [24-26].

The purpose of this study is to verify the stability of the caisson's quay walls and their foundation at the port of DjenDjen during the construction of a new container terminal. To ensure the stability and strength of the foundations of the structure and to determine the effect of the pre-loading method on the soil improvement of the foundations, the bearing capacity, the liquefaction, and settlement hazards for each profile of the foundations. Quay walls are evaluated after the completion of the work as shown in figures (12 and 13). On the basis of the AMBRASEY law and the Algerian anti-seismic standards, the examination was carried out in sections susceptible to liquefaction (sand above the layer of marly clay) in order to know if the results answer the safety factor of reference of 1.25. The results obtained according to the criteria

mentioned above confirm the liquefaction potential as a function of the depth given the weight of the quay wall, the zone where the sand layer remains corresponds to the safety factor of reference (1,25) (Figure 12).

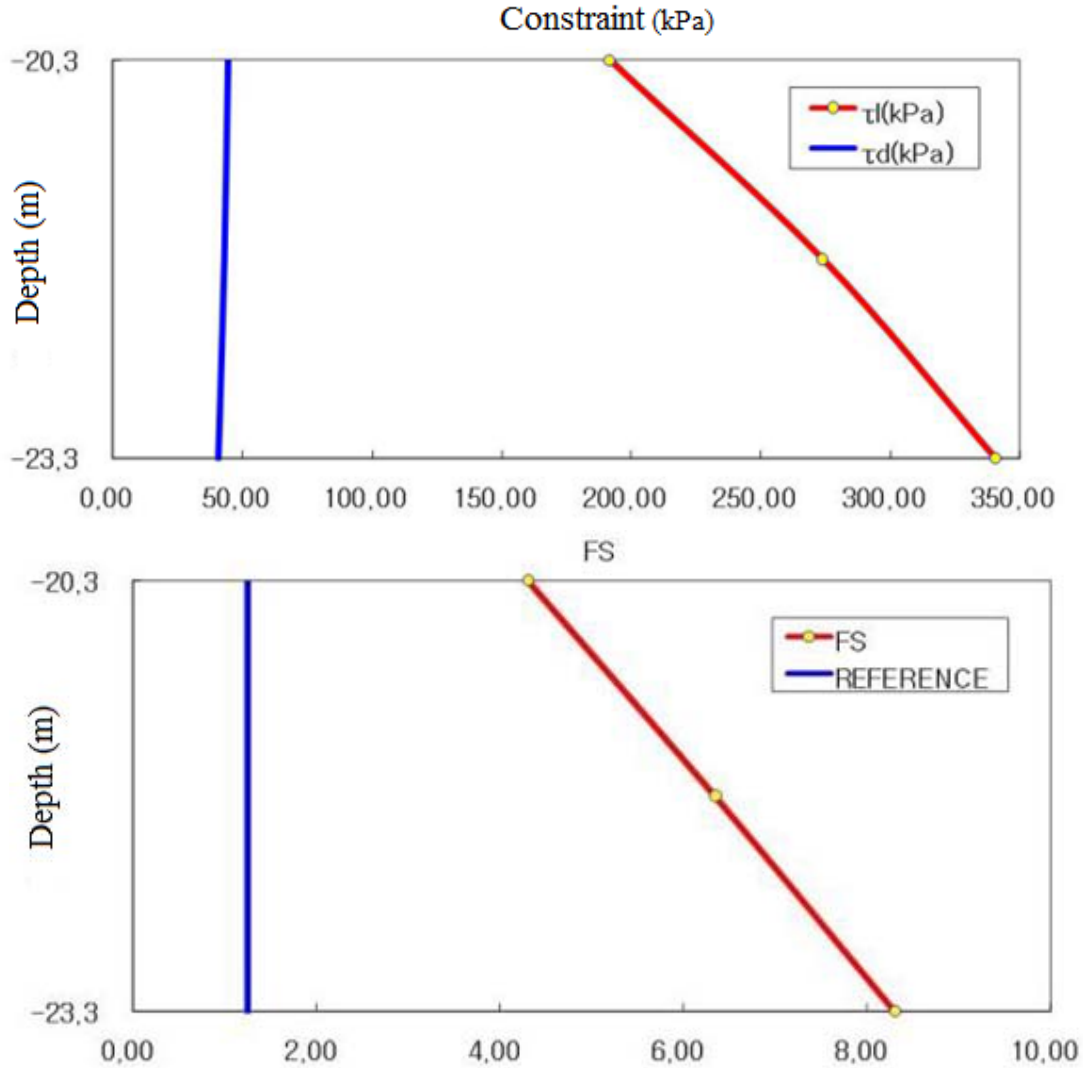


Figure 12: Safety factor (SPT) results for liquefaction and stress distribution before and after preloading.

The settlement expected during construction is 0.15 to 0.16m. A monthly settlement check of the caisson above our actual treated soil; found an average of 14.80 cm of settlement; illustrated in Figure (13). This difference in displacement is due to the effect of the soil treatment (Preloading), giving an increase in bearing capacity and an improvement of the compactness (density) of the soil which becomes denser and which has a great effect on the settlement and the deformation of the soil. Since the

removal of the preload blocks to the construction of the crown beam and its accessories (Figure 13), we have not noticed any settlement or geotechnical problems encountered, which gives the high reliability of this marine subsoil treatment method.

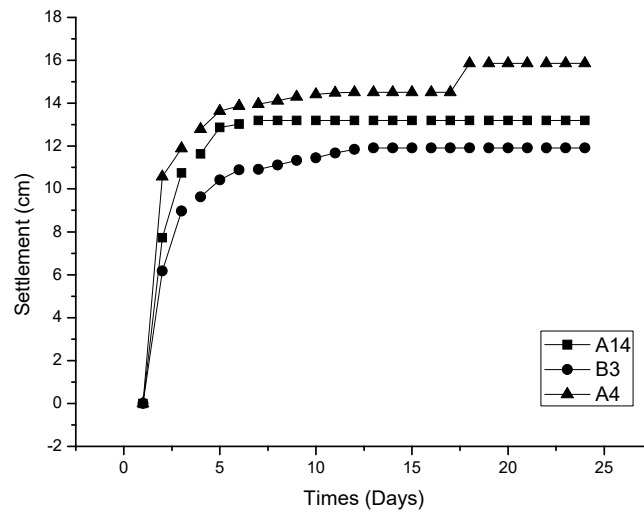


Fig. 13– Comparison of settlement curves of in-situ measurements of three caissons as a function of time during pre-loading.

## 7. Conclusion:

In the case where the foundation soil is particularly bad, it may be necessary to apply soil improvement measures (or other) to ensure that the structure is stable from a geotechnical perspective. Soil improvement methods should be determined only after development and analysis of the complete geotechnical companion. The three soil improvement methods used during the work of the port of DjenDjen (Algeria):



Vibroflotation, dynamic compaction and pre-loading give satisfactory results in terms of bearing capacity and reduction of the risk of liquefaction of settlements.

### **Acknowledgements:**

This work was supported by the K.E.C Laboratory, Department of Civil, Geotechnical & Coastal Engineering, under the project number (PN):  
KEC.LAB.DCGCE.M.DPED2016N001.

### **8. References**

- [1]- CIRIA – CUR – CETMEF. (2007). Therock manual. The use of rock in hydraulic engineering. 2nd edition, C683, CIRIA, London, 1304p.
- [2]- BRUUNP. (1985). Design and construction of mounds for breakwaters and coastal protection. Developments in Geotechnical Engineering, Vol. 37, 1st Edition Ed. Elsevier Science, 962 p.
- [3]- TERZAGHIK., PECKR.B., MESRIG. (1996). Soil mechanics in engineering practice. Ed. John Wiley & Sons, 3rd Edition, 565p.
- [4]- MOSELEY M.P., KIRSCH K. (2005). Ground improvement. Ed. Taylor & Francis e-Library, 431 p.
- [5]- Figueroa, J. L., A. S. Saada, L. Liang, and N. M. Dahisaria. 1994. Evaluation of soil liquefaction by energy principles. Journal of Geotechnical Engineering 120 (9):1554–69. doi:10.1061/(asce)0733–9410(1994)120:9(1554)
- [6]- Polito, C. P., R. A. Green, and J. Lee. 2008. Pore pressure generation models for sands and silty soils subjected to cyclic loading. Journal of Geotechnical and Geoenvironmental Engineering 134 (10):1490–500. doi:10.1061/(asce)1090–0241(2008)134:10(1490).
- [7]- Hyodo, M., H. Tanimizu, N. Yasufuku, and H. Murata. 1994. Undrained cyclic and monotonic triaxial behavior of saturated loose sand. Soils and Foundations 34 (1):19–32. doi:10.3208/sandf1972.34.19.
- [8]- Chiaro, G., J. Koseki, and T. Sato. 2012. Effects of initial static shear on liquefaction and large deformation properties of loose saturated Toyoura sand in undrained cyclic torsional shear tests. Soils and Foundations 52 (3):498–510. doi:10.1016/j.sandf.2012.05.008.
- [9]- Ishihara, K. 1996. Soil behavior in earthquake geotechnics. Oxford:Clarendon Press.
- [10]- Ishihara, K. 1993. Liquefaction and flow failure during earthquakes. Géotechnique 43 (3):351–415. doi:10.1680/geot.1993.43.3.351
- [11]- Seed HB, Lee KL. Liquefaction of saturated sands during cyclic loading. Journal of the Soil Mechanics and Foundations Division 1966; 92: 105–34.
- [12]- Matasovic N, Vucetic M. Cyclic characterization of liquefiable sands. Journal of Geotechnical and Geoenvironmental Engineering 1993; 119: 1805–22.

- [13]- MECSIJ., GÖKALPA., DÜZCEERR. (2005). Densification of hydraulic fills by vibroflotation technique. Proceedings of the 16th International Conference on Soil Mechanics and Geotechnical Engineering, PécsUniversity, Hungary, pp 1521-1524.
- [14]- GÖKALPA., DÜZCEER R. (2003). Vibratory deep compaction of hydraulic fills. Proceeding of The XIIIth European Conference on Soil Mechanics and Geotechnical Engineering, ISSMGE, Prague, Czech Republic, pp 635-638.
- [15]- KELLER. (1974). Amélioration des sols (vibroflottation) Ménard. Document technique Keller, Cnam, Paris, Brochure 11-01F.
- [16]- JEFFERIES M., BEEN K. (2015). Soil liquefaction, a critical state approach. CRC Press Book, 690p.
- [17]- AUSSILLOUS P., COLLARTD., POULIQUENO. (2007). Liquéfaction des sols sous vagues. Proceedingdu 18ème Congrès Français de Mécanique Grenoble, 27-31 août 2007, CFM2007-0359.URL :<http://hdl.handle.net/2042/16240>.
- [18]- VAN'T HOFF J., VAN DER KOLFF A.N. (2012). Hydraulic Fill Manual: For Dredging and Reclamation Works. Ed. CRC Press and Ed. Taylor & Francis e-Library, 672p.
- [19]- USACE (2015). Dredging and dredged material management. EM 1110-2-5025, Engineering and Design, Department of the Army,U.S. Army Corps of Engineers, Washington, DC 20314-1000, USA.
- [20]- HAMIDI B., NIKRAZ H., VARAKSIN S. (2009).A review on impact oriented ground improvement techniques. Australian Geomechanics Journal, Vol. 44(2), pp 17-24.
- [21] K. Chow, D. M. Yong, K. Y. Yong, and S. L. Lee, “DYNAMIC COMPACTION ANALYSIS”, Journal of Geotechnical Engineering. (1992) 118: 1141-1157.
- [22] DimitriosZekkos, Mohammad Kabalan, and Michael Flanagan, “Lessons Learned from Case Histories of Dynamic Compaction at Municipal Solid Waste Sites”, JOURNAL OF GEOTECHNICAL AND GEO-ENVIRONMENTAL ENGINEERING © ASCE / MAY 2013, DOI: 10.1061/(ASCE)GT.1943-5606.0000804.
- [23] Shi-Jin Feng; Wei-HouShui; Ke Tan; Li-YaGao; and Li-Jun He, “Field Evaluation of Dynamic Compaction on Granular Deposits”, JOURNAL OF PERFORMANCE OF CONSTRUCTED FACILITIES © ASCE / MAY/JUNE 2011, DOI: 10.1061/(ASCE)CF.1943-5509.0000160.
- [24]- BOUASSIDA M. (2015). Amélioration des sols en place. Introduction à la géotechnique. Université Tunis El Manar, Ecole Nationale d'Ingénieurs de Tunis, Tunisie, pp 139–163.
- [25]- Ramli Mohamad, PRECOMPRESSION OF SOFT SOILS BY SURCHARGE PRELOADING—SOME COMMON PITFALLS AND MISUNDERSTOOD FUNDAMENTALS, Kuala Lumpur, April 2008.
- [26] - Rika Deni Susanti, Maulana and Aazokhi Waruwu; BEARING CAPACITY IMPROVEMENT OF PEAT SOIL BY PRELOADING, ARPN Journal of Engineering and Applied Sciences, VOL. 12, NO. 1, JANUARY 2017. pp 121-124.

# A Review Regarding the Heat Recovery from Wastewater

O revizuire cu privire la recuperarea căldurii din apele uzate

Amjed Albaiyati <sup>12</sup>

<sup>1</sup> CAMBI Research Center, Technical University of Civil Engineering Bucharest  
021414 Bucharest, Romania  
E-mail: nume.autor@email.autor

<sup>2</sup> Kut Technical Institute, Middle Technical University  
Iraq

DOI: 10.37789/rjce.2021.12.4.5

**Abstract.** *One of the main challenges in the world today is reducing energy consumption and CO2 footprint in existing buildings without major construction work. Many of these buildings represent heritage buildings and the intervention constraints on the original building are much more restrictive for these particular cases. The building sector is one of the world's largest energy consumers, so it is important to seek out and use recovery energies for individual consumers. The main component of energy consumption in buildings is heating, but the demand for the domestic hot water is also very high, especially when daily consumption is high and especially for specific applications (hotels or laundries for example) This is why the implementation of technologies using renewable energy and recovery sources for water heating[1] has become very important and one of these technologies involves the recovery of the thermal energy from wastewater. Usually, heat recovery from wastewater is designed to recover residual energy from the hot drainage water and this recovered energy is used to preheat incoming cold water or to heat pumps.*

**Key words:** wastewater, energy recovering, heat exchanger

## 1. Introduction

The European Union (European Commission [1]) decided to reduce its greenhouse gas emissions by 40% and to improve its energy efficiency by 27% until 2030. With a total of 3441 TWh, 26.8% of the EU28 final energy consumption in 2013 originated from the household sector, coming only second to transport (31.6%) (European Commission [2]). Residential domestic hot water (DHW) consumption represented, with 442 TWh, approximately 16% of the EU household heating demand (Enerdata [3]), energy that is currently lost to the environment with its transfer to the sewers. With the improvement of the building envelope, DHW will have an increasingly important role in energy consumption, with a contribution to total heating demand between 20 and 32% in high efficiency single family buildings and between

35 to almost 50% in multifamily buildings (Meggers and Leibundgut[4] , Alnahhal and Spremberg [5], Bertrand et al. [6]).

Much of the heat goes through the drain without recovery, this means that year after year we flush down several kWh of heat straight to the sewer system. By installing a heat exchanger that recovers heat from the wastewater, it is possible to save energy. Greywater is a term used to define water from showers, bath tubs, sinks, dishwashers and washing machines. The focus on recovering energy from greywater has been a priority when it comes to energy savings in buildings.

Globally the domestic sector consumes a significant proportion of the total energy budget. In the UK this consumption is estimated to account for 23% of total consumption [7], in Hong Kong it is reported to be 17%. Within domestic energy consumption a significant proportion of energy use is associated with water heating activities [8] i.e. for washing, water related appliances and cooking. In the UK, 26% of domestic energy consumption is associated with water heating activities [9].

In order to determine the heat recovery potential of grey water streams for residential DHW end-uses heating, mass flow, duration and frequency of use per capita must be characterized to calculate their thermal load. It is also important to define typical temperature levels and to geographically allocate the various end-uses.

In this paper we have tried to complete a literature review for this subject, and we have considered especially theoretical studies to see how the energy can be recovered from wastewater, experimental studies and numerical studies. At the end of the paper we focused on some directions to be followed.

## **2. State of the art**

### **Experimental studies**

Shower water heat recovery in high-rise residential buildings of Hong Kong by using a full-scale experimental setup was used to calculate the deficiency of the effectiveness  $\epsilon$  of a single-pass counter-flow heat exchanger.

The horizontally installed heat exchanger is a 1 m long cold water PVC pipe (0.1 m in diameter) with a hot water copper pipe (40 mm in diameter) passing through it. The hot water copper pipe which simulates a slope drainage pipe is partially filled with hot water. The results indicated that annual energy savings of 4–15% from shower water heat could be achieved through a 1.5 m long single-pass counter-flow heat exchanger for a drainage pipe of diameter 50 mm[10].

Investigating the efficiency of a vertical inline drain water heat recovery heat exchanger in a system boosted with a heat pump where The facility consists of a 1100 mm vertical copper pipe with an inside diameter of 70 mm, this gives the heat exchanger an inside heat transfer area of 0.20 m<sup>2</sup>.

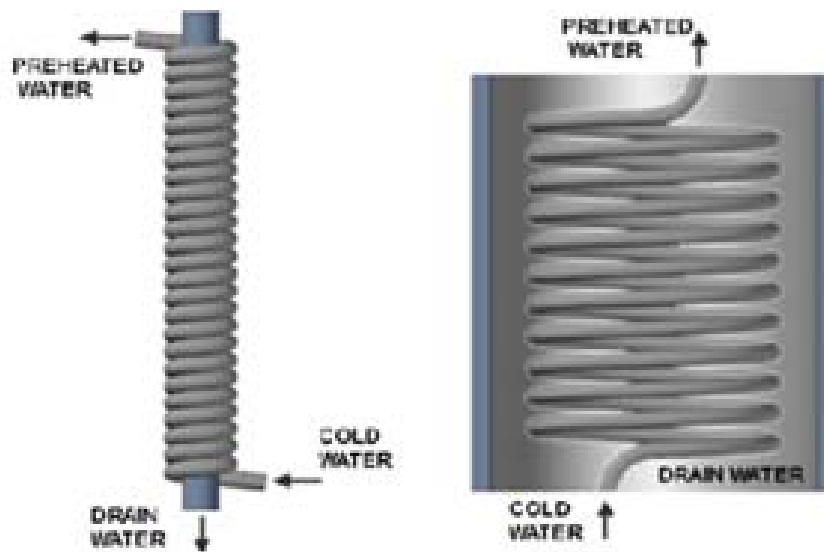


Fig. 1

Around the inner copper pipe a second copper pipe is wound to create the heat exchanger, the outside coil consists of 25 m copper pipe giving the heat exchanger a 0.57 m<sup>2</sup> heat transfer area of the coil. The results refer the heat recovery ratio ranges between 32 and 50%, the ratio is dependent on the flow rate of the drain water. The heat recovery ratio decreases when the flow rate increases, even though the heat flux increases. Higher flow rates lead to higher exiting temperature of the drain water, this in turn leads to a larger temperature difference between the wall and the average drain water temperature[11].

Efficient drain water heat recovery in horizontal domestic shower drains. The vertical, grey-water will flow around the entire boundary of the pipe wall as a film flow, while in the horizontal, grey water will flow in the bottom of the pipe. It is clear that film flow is conducive to high efficiency heat exchange occurring across the entire drainage pipe wall. However in the horizontal, heat exchange only occurs along a fraction of the pipe wall, resulting in the lower DWHR device efficiencies found in previous investigations. Therefore modifications to existing designs are required to overcome these efficiency problems in the horizontal, proposed a new design to improve heat transfer efficiency in the horizontal. The proposed design comprised a common 40 mm diameter plastic waste pipe through which waste drainage water would be carried to as normal. The cold water inlet pipe was diverted to run inside the waste pipe a shown maximizing the contact between hot drainage water and incoming cold water. The cold water pipe would consist of copper or any other suitable conductive material to promote heat exchange. In conclusion this study demonstrates that it is theoretically possible to design a DWHR system to operate to a satisfactory level of efficiency in a horizontal orientation. While certain practicalities need to be addressed for horizontal DWHR to be implemented, the economic analysis of this device shows that it could be a viable investment. The results of the investigation show that it is possible to recover energy from horizontal shower drains using a drain water

heat recovery device at a satisfactory level of efficiency. The results also demonstrate that such a system may be economically viable depending on a number of external factors. Implementation of this technology on a national level was shown to have the potential to bring about significant reductions in energy usage and CO<sub>2</sub> emissions[12].



Fig. 2.

Drain water heat recovery storage-type unit for residential housing. The unit provides reliable measurements of their thermal-hydraulic performance. The experimental unit is thus designed to supply hot and cold water to a DWHR storage device (test section), and to study its performance accumulating and delivering energy.

Besides the DWHR storage device, the experimental unit is made up of two water tanks, two thermal baths, a water pump, a flow meter, a differential pressure sensor, several temperature sensors, valves and pipes. The water tanks are used to pump hot or cold water into the test section. Each water tank temperature is controlled by a thermal bath by means of a coiled pipe. These tanks are linked to the test section through valves and pipes. The water mass flow rate is measured by a Coriolis mass flow meter with an accuracy of  $\pm 0.041\%$  of the actual flow rate within the operating range. The in-tube water inlet and outlet temperatures are measured with K-type thermocouples with an accuracy of  $\pm 0.3\text{ }^{\circ}\text{C}$ . The water pressure drop is obtained from a differential pressure transducer with an accuracy of  $\pm 0.04\%$  F.S. The experiments were performed in a climatic chamber in order to control the environmental conditions: the temperature of the chamber was kept constant during the experiments. In addition, all the elements of the experimental facility such as tanks and pipes have been fully insulated to reduce heat losses. A commercial insulation has been used (25 mm insulation thickness) for this purpose. Finally, the stored energy is extracted in the discharging process by cold water pumped through the accumulator coiled pipe. At this point, all the operational steps are completed. The authors conclude from this study the experimental unit provides reliable measurements of the temperatures at different locations (in-tank and in-tube) and the flow rate, to study the storage capacity and the delivering energy process of the DWHR storage device a 50% reduction in stored energy is observed at 24 h, which reveals its limitations for long-term storage applicability. The objective of these devices is the recovery of the waste heat from domestic warm drain water and transferring it to cold water entering the house. From the results, it can be concluded that the objective has been reached with the proposed design[13].

Heat exchanger development Of Waste water heat recovery. Description of experiment of this study prototype heat exchanger with a single "Heatsheet" panel was designed and made. It consists of separated hot and cold water flow systems, a heat exchanger, Single Panel Heat Exchanger; a thermosyphon 'Heat Sheet' was chosen as the key element of the proposed heat exchanger. The performance characteristics were required to be determined. The "Heatsheet" consisted of two plates seam welded together around the edges to form an envelope that has been evacuated and then load with a small amount of heat transfer fluid and hermetically sealed. Both sheets were punched with a dimple pattern for small pools of the working fluid to accumulate. The material of the sheet plates and supply water tube was stainless steel out of concern for the effects of possible fouling on the heat transfer surface by grease and other contaminants in the waste water. All pipes, hot water bath and hot water storage tank were well insulated to reduce heat loss in the system. They were for measuring water inlet and outlet temperature on both hot and cold water sides. Measurements of hot water usage and waste water temperature and flow rates were obtained for a potential application of the proposed exchanger (the dishwasher for the kitchen in the University Halls of Residence). A model of a multi-panel thermosyphon heat exchanger was also developed to predict the energy savings that would be expected if such a heat exchanger was used in this situation. The result indicated that an overall electricity of 7500 kWh could be saved annually from the dishwasher system by employing a four-panel thermosyphon heat exchanger[14].

Decentralized Drain Water Heat Recovery: Interaction between Wastewater and Heating Flows on a Single Residence Scale. System Set-Up The proposed system recovers the drain water and raw sewage in a collection tank, allowing for this tank to serve as a buffer to attenuate potential mismatches between the heat consumption by the heat pump and the flow of drain water. The heat contained in this holding tank is recovered through a heat exchanger, heating the primary fluid of a heat pump, which serves as the low temperature heat source for this heat pump. The heat pump is primarily used for space heating, but in case excess heat is available, it is used to heat up the feed water from the water supply to the desired temperature. The hot water is stored in the domestic hot water storage tank (DHWST), this way the heat pump can be operated continuously over a given time period, improving the performance of the heat pump, and increasing its profitability [15]. The consumed DHW is then pumped from the DHWST to match DHW demand. In case there's not enough heat available in the holding tank to provide all the space heating and DHW demand, a backup system is provided. When using a drain water heat recovery system, a back-up heating system remains necessary. It is generally used right after the consumption peaks, when the accumulated recovered heat is depleted to meet the peak in demand. The share of heat demand that can be met by the DWHR system varies between 8% and 42%. Due to a mismatch between the availability of waste water heat and the heat demand, recovered heat could be wasted. In order to avoid this hot water reservoir can be used to store the recovered heat. Using a hot water reservoir of 300 mm can reduce the amount of recovered heat that is unused from 25% without a reservoir to 99%, with a reservoir. This shows a mismatch between heat demand and the availability of heat in the



wastewater. Using the DWHR system greenhouse gas emissions related to domestic hot water- and space heating can be reduced by 7.6% to 22%. However, this increases heating costs by a factor ranging from 120% to 130%. At current traditional heating prices, the DWHR system for a single residence is not financially competitive with traditional systems, due to its important capital investment. Combining waste water streams from different residences would provide a larger flow, and potentially a high recoverable energy volume. However, heat would be lost between the residence and the collection point, reducing the energy density of the waste water. In turn this could lead to an increased GHG intensity of the recovered heat. An optimal collection point should be found, considering the trade-off between increased energy volume and reduced energy density[16].

COP and Economic Analysis of the Heat Recovery from Waste Water using Heat Pumps. The heat recovery system is composed of the following components: Two 40 meter deep wells as the source of clean water, Two centrifugal pumps for forwarding and pumping the clean water from the well, Plate heat exchanger, Heat pump for low temperatures, Heat pump for high temperatures, Tank for hot clean water, Washing machines, Tank for hot waste water, Two centrifugal pumps for pumping and transporting the waste water, Sewer system for waste water draining, System for automatic control, System of measuring instruments. Concluded from this study the recovery system described in this study is quite efficient both in energetic and economic terms. the system's total coefficient of performance is very high: COP is from 6 to 6.5, the component's partial COPs are the following: 3.19 for the heat plate exchanger, 1.95 for the heat pump1, 1.35 for the heat pump2, the total energy savings expressed in percentages: Minimally (1-1/6)  $100\% = 83.3\%$  or Maximally (1-1/6,5)  $100\% = 85\%$ , The energy savings of the components in percentages: Plate heat exchanger 49%, low temperature heat pump 30%, high temperature heat pump 21%, The payback period of the investment is relatively short, about 2 years. In addition to energy and economic advantages this solution is also very favorable in terms of environment protection. The recovery system protects the environment on direct and indirect way. Directly: The waste water does not enter in the sewer while it is still hot, the waste water is cleaned by filtration before getting out of the recovery system[17].

### Theoretical studies

Heat recovery from untreated wastewater A case study of heat recovery from sewer line to district heating network. The heat exchanging could be performed either within the sewer or by withdrawing water from the sewer and perform external heat exchanging outside the tunnels. Results showed that during a majority of the year approximately 4 MW of heat could be extracted while staying within conservative limits in regards to a minimum influent temperature as well as a maximum upstream temperature decrease. During wet season however, no or very limited heat could be recovered as the influent temperatures are already in a rather sensitive range in regards to the biological treatment process[18].



Heat exchanger applications in wastewater source heat pumps for buildings. WWHEXs can be classified under two main categories: (i) utilization of WWHEX and (ii) construction of WWHEX. The classification diagram Utilization of WWHEXs; can be used in three different locations to recover heat from WW. Mainly, the WWHEX may be inside the building to recover waste heat from domestic hot water, which is called domestic utilization. WWHEX can also be located inside or outside the sewage channel, which provides a larger excess heat from WW to provide heating/cooling for multiple buildings. Apart from these two locations, WWHEX can be installed downstream of a wastewater treatment plant (WWTP) to efficiently utilize the energy in the treated WW in larger scale. The heat recovery at the sewage treatment plant is technically easier since energy from the treated wastewater can be extracted more efficiently. WWHEXs Construction of HEX can be classified in two categories: (i) material used in construction and (ii) the commercial type of HEXs. These two are very important in selection and installation of WWHEXs to WWSHP system. This study concludes was WWSHP systems are relatively recent, but rapidly growing and developing technology. To achieve a more sustainable world, one of the most important phenomena is energy recovery from otherwise wasted sources.

The key findings of this study and some directions for future research can be summarized as follows: Most commercial applications and academic studies employ special design and shell-and-tube HEXs, Limited number of studies on CFD analysis of WWHEXs is reported in the literature, Rigorous methods for performance improvement of WWHEX should be pursued, Prevention of bio-fouling in WWHEXs is a potentially important area that needs further attention[19].

Heat recovery from municipal wastewater: evaluation and proposals. Methodology in this study is the Conceptual model of Heat Recovery An evaluation of the feasibility of a Sewage Heat Recovery System (SHRS), that is, a system able to recover thermal energy from wastewater (Heat Offer) and to supply it to the potential users (Heat Demand), should take place from the evaluation of a conceptual model, referred to a specific local reality, composed by several elements. A heat recovery system requires three main components: the first one is the heat exchanger, which is responsible for heat transfer from the heat source to transport medium. The second part is the heat pump, which is the tool able to increase the temperature of the recovered heat. The last part is the heat supply system, which is in charge of the transport of the thermal energy to the users, and it has as a main goal the minimization of heat dissipation. To design a specific SHRS model, first of all wastewater characteristics should be considered, then SHRS' components and its position in the sewer (the last issue is determined by nature and location of potential users of the recovered thermal energy) should be defined, together with the potential users, and finally the various implications of the SHRS on the local reality should be discussed. Sewers actually represent the main source of heat loss in buildings[12]. Wastewater as a thermal energy source Municipal wastewater may be considered as an important energy source. In fact, besides the traditional technical solutions devoted to the recovery of the chemical energy contained in sludges by means of anaerobic digestion processes, a relevant amount of thermal energy should be valorized from the sewer system[20].

## Numerical studies

The authors also studied numerical analysis to efficient drain water heat recovery in horizontal domestic shower drains. The commercial computational fluid dynamic software package CFX was used to develop a numerical model of the experimental prototype DWHR device. This model was subsequently calibrated against the measured flow and temperature data obtained during the experimental assessments of effectiveness. Following calibration the numerical model was then modified to optimise the energy recovery potential of the device. A 3D model of the prototype device was constructed and meshed using ANSYS Model Builder. A tetrahedral mesh was constructed comprising a 12.7 mm diameter cold water pipe, with a wall thickness ( $d$ ) of 1.58 mm and a 40 mm diameter outer waste pipe. The model consisted of three domains: a hot fluid domain contained the hot drain-water flowing by gravity in a partially full pipe with air; a cold fluid domain contained the cold water mains flowing under pressure in a copper pipe full of water; and a solid domain representing the 1.58 mm thick copper pipe, the medium through which heat transfer would take place between the two fluids. the differences between the numerical model predictions and measured data were acceptably small and the model was deemed to be calibrated[12].

The authors also studied numerical analysis to Drain water heat recovery storage-type unit for residential housing, A numerical simulation platform has been adapted for the prediction of the DWHR storage system, providing additional and more detailed information. The in-tank water natural convection flow and its local temperature evolution are described by a 3D transient CFD analysis. Extraction process tests were conducted to determine the effect of flow rate and temperature in the heat recovery performance of the DWHR storage device. For the DWHR storage built in this work, the maximum heat recovered is reached at the lowest flow rates (3 l/min) for the two different in-tank temperatures. The DWHR storage had the capacity to recover from 34% to 60% of the energy available in the drain water for the investigated flow rates. In these tests a comparison between the numerical and experimental results has been carried out. Different results of the DWHR storage device are shown, such as the evolution of the non-dimensional temperature over time of the water in-tank and in-tube and the energy recovery ratio, where the numerical results were shown a trend similar to the experimental data for the different tests. A heat losses test was also conducted. There were no significant temperature gradients in the radial direction[13].

Analysis of Grey-water Heat Recovery System in Residential Buildings, Two different simulation programs have been used, Energy Plus and SIMIEN to find what impact the energy reduction would have on the building and to see if the simulations would correspond to the theoretical estimates done in this study. The theoretical estimates based on equations for heat recovery and measured data for energy use in the case building gave a little bit better results than the simulated results for the same case building. Although there is a difference both gave a positive indication that a heat

recovery unit would not only reduce the energy consumption but also reduce the annual operating cost of a building[21].

### 3. Conclusions and Perspectives

One of the main challenges in the world today is reducing energy consumption and CO<sub>2</sub> footprint in existing buildings without major construction work. Many of these buildings represent heritage buildings and the intervention constraints on the original building are much more restrictive for these particular cases. The building sector is one of the world's largest energy consumers, so it is important to seek out and use recovery energies for individual consumers. The main component of energy consumption in buildings is heating, but the demand for the domestic hot water is also very high, especially when daily consumption is high and especially for specific applications (hotels or laundries for example). This is why the implementation of technologies using renewable energy and recovery sources for water heating[1] has become very important and one of these technologies involves the recovery of the thermal energy from wastewater. Usually, heat recovery from wastewater is designed to recover residual energy from the hot drainage water and this recovered energy is used to preheat incoming cold water or to heat pumps.

Wastewater heat recovery applications are becoming widespread in energy saving applications. This interesting technology is an efficient and inexpensive way to recover thermal energy for reuse also in facilities systems in buildings, such as the production of sanitary hot water or heating. It is known that a sustainable and low emissions operation in air conditioning and heating processes is achieved by harvesting the otherwise wasted energy in wastewater through specially designed heat exchangers, lying at the core of heat pumps. This combined system is called wastewater source heat pump.

### References

1. Efficiency, E., *its contribution to energy security and the 2030 Framework for climate and energy policy*. Communication from the Commission to the European Parliament and the Council, COM, (2014). **520**.
2. Commission, E. *Statistical Pocketbook* (2015); Available from: <http://dx.doi.org/10.2833/77358,URL;2015>.
3. Enerdata. (2006) 8/2/2016; Available from: ODYSSEE database on energy efficiency data & indicators.
4. Meggers, F. and H. Leibundgut, *The potential of wastewater heat and exergy: Decentralized high-temperature recovery with a heat pump*. Energy and Buildings, (2011). **43**(4): p. 879-886.
5. Alnahhal, S. and E. Spremberg, *Contribution to exemplary in-house wastewater heat recovery in Berlin, Germany*. Procedia Cirp, (2016). **40**: p. 35-40.
6. Bertrand, A., et al., *Characterisation of domestic hot water end-uses for integrated urban thermal energy assessment and optimisation*. Applied energy, (2017). **186**: p. 152-166.
7. Johnson, *Domestic Energy End Use and Sustainability*. (2005).

8. Prado, R.T. and O.M. Gonçalves, *Water heating through electric shower and energy demand*. Energy and buildings, (1998). **29**(1): p. 77-82.
9. Swan, L.G. and V.I. Ugursal, *Modeling of end-use energy consumption in the residential sector: A review of modeling techniques*. Renewable and sustainable energy reviews, (2009). **13**(8): p. 1819-1835.
10. Wong, L., K. Mui, and Y. Guan, *Shower water heat recovery in high-rise residential buildings of Hong Kong*. Applied Energy, (2010). **87**(2): p. 703-709.
11. Wallin, J. and J. Claesson, *Investigating the efficiency of a vertical inline drain water heat recovery heat exchanger in a system boosted with a heat pump*. Energy and Buildings, 2014. **80**: p. 7-16.
12. McNabola, A. and K. Shields, *Efficient drain water heat recovery in horizontal domestic shower drains*. Energy and Buildings, (2013). **59**: p. 44-49.
13. Torras, S., et al., *Drain water heat recovery storage-type unit for residential housing*. Applied Thermal Engineering, (2016). **103**: p. 670-683.
14. Hua, L., *Heat exchanger development for waste water heat recovery*. (2005).
15. Spriet, J. and P. Hendrick, *Wastewater as a Heat Source for Individual Residence Heating: A Techno-economic Feasibility Study in the Brussels Capital Region*. Journal of Sustainable Development of Energy, Water and Environment Systems, (2017). **5**(3): p. 289-308.
16. Spriet, J. and A. McNabola. *Decentralized Drain Water Heat Recovery: Interaction between Wastewater and Heating Flows on a Single Residence Scale*. in *Multidisciplinary Digital Publishing Institute Proceedings*. (2018).
17. Nyers, J., *COP and economic analysis of the heat recovery from waste water using heat pumps*. Acta Polytechnica Hungarica, (2016). **13**(5): p. 135-154.
18. Vestberg, O., *Heat recovery from untreated wastewater: A case study of heat recovery from sewerline to district heating network*. (2017).
19. Culha, O., et al., *Heat exchanger applications in wastewater source heat pumps for buildings: A key review*. Energy and Buildings, (2015). **104**: p. 215-232.
20. Fiore, S. and G. Genon, *Heat recovery from municipal wastewater: evaluation and proposals*. Environmental Engineering & Management Journal (EEMJ), (2014). **13**(7).
21. Kleven, M.H., *Analysis of Grey-water Heat Recovery System in Residential Buildings*. (2012), Institutt for energi-og prosesssteknikk.

## Software programs used in designing of low voltage electrical distribution panels

Programe software utilizate în proiectarea tablourilor electrice de distribuție de joasă tensiune

Cristina Gabriela Sărăcin<sup>1</sup>, Diana Paraipan<sup>1</sup>

<sup>1</sup>Universitatea Politehnica din București

Splaiul Independenței Nr.313

E-mail: [cristina.saracin@upb.ro](mailto:cristina.saracin@upb.ro), [dianaparaipan98@gmail.com](mailto:dianaparaipan98@gmail.com)

DOI: 10.37789/rjce.2021.12.4.6

**Abstract.**– This paper presents the ABB Doc and Schrack Design programs used in the design of voltage electrical distribution panels. The consumers' power supply depends on the correct choice of the protection and switching equipment and the correct size of the distribution panel. Therefore, the paper exemplifies and compares these software applications used successfully in the size of distribution cabinets. Therefore, the paper exemplifies and compares these software applications used successfully in the size of distribution cabinets. Dimensions of the switchboard are obtained by choosing and correctly positioning the electrical equipment in the switchboard. Schrack Design program allows the manufacturing of electrical panels without calculating the necessary parameters choices of protection and switching equipment. The choice of electrical equipment and electrical distribution panels is made exclusively by the user. It can make component selections from the manufacturer's database or add electrical equipment from other companies to this database. Once the options have been selected, the program generates the single-wire or multi-wire circuit diagram. The validation of the chosen solutions involves the thermal calculation of the electrical distribution panels which is done with the help of the Schrack Design program.

**Keywords:** electrical distribution panels, ABB Doc program, Schrack Design program

### 1. Introduction

The electrical distribution panel has the role of powering the electrical receivers offering protection against overloads and short circuits. The panel is a component of the distribution system that branches the power supply on circuits that are safeguarded by protection and switching equipment [1].

When manufacturing and designing electrical distribution panels, each company specialized in the field of low and medium voltage electrical installations, must comply with the following rules:

- the electrical distribution panel must be mounted in such a way that the distance to the floor is not higher than 2,2 m;
- the electrical distribution panel must be provided with switches that allow the power supply to be stopped in case of breakdowns;

- the temperature of the room, where the panel it is supposed to be mounted, must be within the range of 0-40°C;
- the installation of circuit breakers must allow to stop all phases simultaneously in the event of fault in the supply circuits;
- fuses must not be mounted on the work/protection nulls;
- for currents higher than 100 A, the connections in the panel must be made with distribution bars;
- the colour code must be observed as follows: null (white, light blue, gray), protective conductors (green-yellow), phases (dark blue, black).

The electrical distribution panels are subject to operational risks and, for this reason, their constant maintenance is necessary. Software programs dedicated to the design and sizing of electrical equipment are used to create electrical distribution panels. In this paper, we will present two programs, ABB Doc and Schrack Design used to design low voltage electrical distribution panel.

## **2. The ABB Doc software used in designing of electrical distribution panel**

The ABB Doc is a program used in the design of electrical diagrams and calculates the necessary protection and switching elements electrical distribution panels. ABB Doc has numerous key features such as [2]:

- drawing the single-line electric diagram;
- drawing the key diagram of the auxiliary circuits;
- calculation of line current and voltage drops;
- calculation of short-circuit currents;
- dimensioning low- and medium-voltage cables;
- dimensioning switching- and protection devices;
- switchboard configuration;
- setting and coordination of protection devices;
- verifying cable protection;
- printing the single-line diagram and project documentation.

To make a project with the help of the ABB DOC program, four power supply options can be chosen, one medium voltage (MV) and three low voltage (LV) power supplies. In the case of power supplies on low voltage, we can have three possibilities, namely: “LV distribution”, “Trafo MV-LV” and “Generator”.

In the case of power supply - “LV distribution”,  $I_{cc}$  is defined as the short-circuit current calculated according to the following parameters:

- apparent short-circuit power;
- short-circuit impedance of the supply line;
- power factor in case of short circuit;
- the ratio between the short-circuit current per phase and line current.

In the second case of power supply through a transformer - “Trafo MV-LV”, the followings must be configured:

- apparent power of the transformer;
- transformer short circuit voltage.

Finally, the third case of power supply through generator - "Generator", it involves only the supply voltage parameter.

In addition, the choosing of voltage but also the power supply, the ABB DOC software offers the possibility to configure the following parameters [3]:

- distributed phases (three-phase with neutral conductor LLLN, three-phase without neutral conductor LLL and single-phase L2L3, L1L3, L1L2, L1N, L2N, L3N);
- distribution systems (TN-S, TN-C, TT, TI);
- parameters regarding the calculation methods;
- parameters for sizing conductive elements according to standards (IEC 60092[4], IEC 60364 [5], UNE 20460-7-740 [6], DIN VDE 298 [7]);
- the parameters regarding the ambient temperature and the working temperature of the installation.

For example, it is proposed the designing of a low voltage industrial electrical panel that must supply the following groups of receivers:

- a) 3 single-phase resistive electrical receivers with nominal power  $P_n = 5\text{kW}$ ,  $\cos\phi_n = 0,9$ ;
- b) 4 three-phase resistive electrical receivers with nominal power  $P_n = 5\text{kW}$ ,  $\cos\phi_n = 0,9$ ;
- c) 3 three-phase electric motors having  $P_n = 5,5\text{kW}$ ,  $\cos\phi_n = 0,88$ ,  $\eta = 0,88$ ,  $I_p/I_n=7$ .

The first step consists in making the single line diagram (figure 1). To start, we choose "Generic Load" corresponding to the resistive load type from the Objects menu and then complete  $V_n$ ,  $P_n$  and  $\cos\phi_n$  and evenly distribute the receivers in group (a) on the three phases (L1N, L2N, L3N). We make the same choice regarding the type of load for the three-phase resistive receivers from group (b) but, the circuit is three-phase (LLLN). The third group (c) of receivers is the motor from the "Objects" menu; select "Motor" and then fill in the parameters  $V_n$ ,  $P_n$ ,  $\cos\phi_n$ ,  $\eta$ .

In the second stage, the cables necessary to power the receivers are dimensioned. In order for the conductive element to be calculated by the program, the fields circuit length, cable laying mode and maximum permissible voltage drop across the circuit are completed. The criteria on the basis of which the cables are determined are the followings:

- the criterion of the maximum admissible heating of the conductors;
- the criterion of the maximum allowable voltage drop in the network;
- the criterion of short-term thermal stability when starting the engines.

The third step aims to choose the switching and protection equipment. From the Object menu of the ABB-DOC program, we choose "Circuit-breaker with overload and short circuit protection + RCB". The IEC 60364-4-43 standard "Electrical installation of buildings - Protection against overload current" specifies the coordination between the conductive elements and the protective equipment. The relationships, used by the program, comply with IEC 60898 [8] based on formulas  $I_b \leq I_n \leq I_z$  și  $I_2 \leq 1,45 \cdot I_z$

where:  $I_b$  is the current required by the circuit;

$I_z$  - the maximum allowed current of the conductive element;

$I_n$  - rated current of the protective equipment;

$I_2$  - operating current of the protection device.

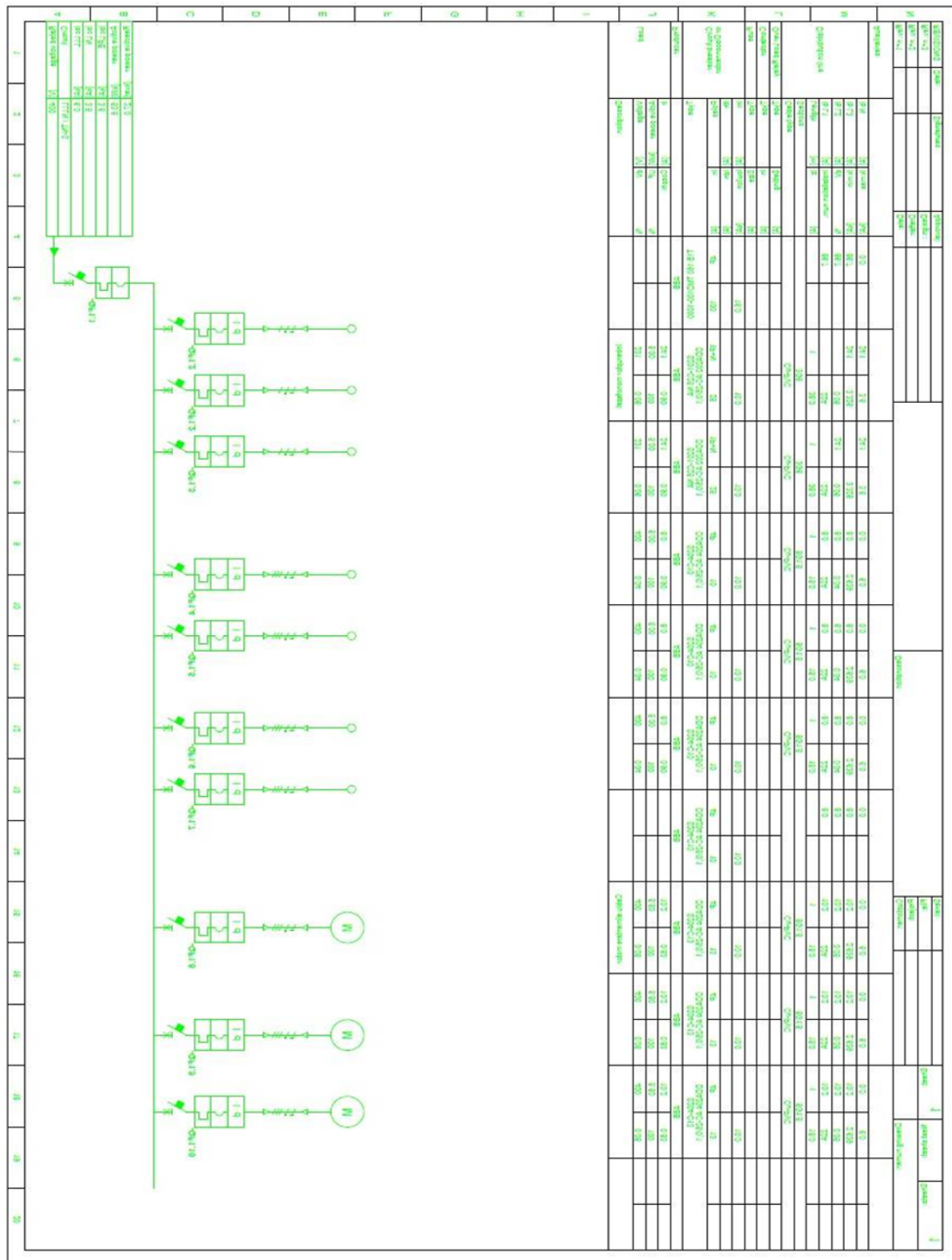


Fig. 1. Single-wire diagram of the electrical distribution panel

Based on the single line diagram, the ABB Doc program proposed the electrical distribution panel from fig. 2 (front and top view).



Software programs used in designing of low voltage electrical distribution panels

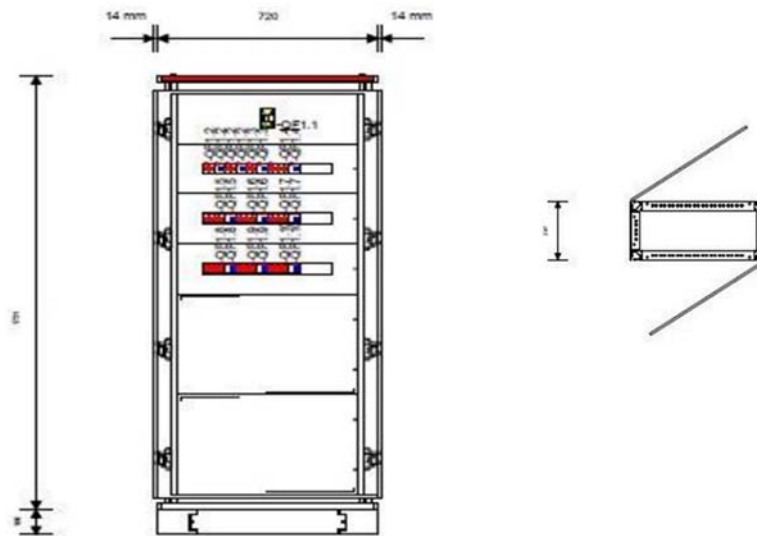


Fig. 2. Diagram of the electrical distribution panel

### 3. The Schrack Design software used in designing of electrical distribution panel

The Schrack Design program is a software offered free of charge by Schrack Technik to their customers. With the help of this program it is possible to design the distribution boards using components made by Schrack Technik or other manufacturers. The new created equipment can also be saved in the database of the Schrack Design program. The design of electrical panels is performed according to the EN 61439 [9] and IEC 60890 [10] standards.

The Schrack Design program has the following main functionalities [11]:

- selection of the desired switching and protection equipment;
- inserting components using the "drag and drop" function;
- adding external images to the drawing;
- adding standard symbols for consumers;
- activating the Copy/Paste function;
- marking change and simultaneous numbering for multiple products;
- the possibility to create favourite product groups;
- realization of electrical assembly schemes;
- adding links between the pages of single-wire and multi-wire schemes;
- insertion of "csv" articles;
- performing the thermal calculation;
- integration of electrical distribution panels horizontally and vertically;
- combination of two or more electrical panels in one.

The Schrack Design program allows the realization of electrical panels without calculating the parameters necessary for the choice of protection and switching equipment. Thus, this software allows to obtain single line and multi-wire schemes following the user's choice of protective equipment. In case of incorrect choice of the dimensions of the electrical distribution panel (from the Schrack database) or, of the

electrical switching and protection equipment, the program will determine that they were not chosen correctly (the panel heats up) and generate an error (fig. 3).



Fig. 3. Error generated by Schrack Designer program

Given that the allowable temperature limit is exceeded due to the small size of the electrical distribution panel (cabinet), this software also provides information on solving this design error (fig.4).

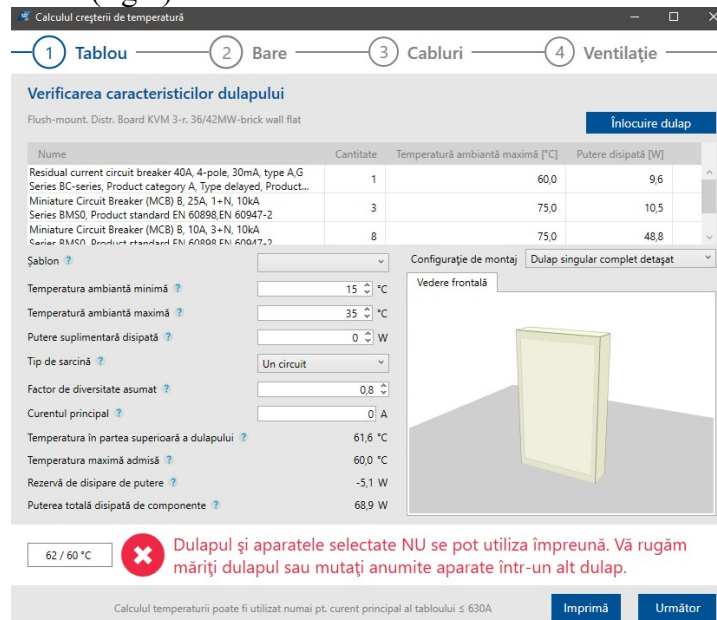


Fig. 4. Error display when choosing the electrical distribution panel

After choosing the electrical distribution panel and its components, the program allows you to read an informative guide on temperature balancing, namely:

- the application requires a check on the chosen cabinet; thus, the positions of the components in the cabinet can be changed and, if they do not lead to an improvement in temperature, it is proposed to replace the electric cabinet with a larger one;
- check the distribution bars;
- it is required to specify the cables used (including conductive material, insulation, cross section, number of conductive elements, number of circuits, length, maximum current and dissipated power);
- ventilation can be added to the chosen electric panel.

When choosing the correct size of the electrical distribution panel, the program displays the information presented in fig. 5.

Protocol de calcul al creșterii de temperatură	
Tip de dulap	IL172218AS
Dimensiuni dulap	
Lățime	590 mm
Înălțime	915 mm
Adâncime	250 mm
Temperatura ambiantă minimă	15 °C
Temperatura ambiantă maximă	35 °C
Temperatura în partea superioară a dulapului	47,2 °C
Creșterea temperaturii în partea superioară a dulapului	12,2 K
Configurație de montaj	Dulap singular complet detașat
Factor de diversitate asumat	0.800
Curentul principal	0 A
Puterea totală disipată de componente	62.8 W
Rezervă de disipare de putere	90.6 W
Putere suplimentară disipată	0.0 W
Normative	
Evaluare	
<p><b>Dulapul și aparatele selectate pot fi utilizate în configurația dată conform cu IEC TR 60890</b></p> <p>Calculul temperaturii poate fi utilizat numai pt. curent principal al tabloului ≤ 630A</p>	

Fig. 5. Nominal data of the electrical distribution panel

After the completion of the project, a report is presented stating whether the cabinet together with the chosen appliances can be used in the respective installation configuration according to the standards in force. Schrack Design helps to easily design electrical distribution panel and also guarantees their compliance with current standards.

#### 4. Comparison of ABB Doc versus Schrack Design software

ABB Doc allows the realization of the diagrams of primary circuits and auxiliary circuits, calculation of line current and voltage drops, calculation of short-circuit currents, sizing of cables, sizing of switching and protection devices, setting and coordination of protection devices.

Following the completion of the single line diagram, the ABB Doc program is run, which verifies the correctness of the designed single line diagram. If errors occur on the circuits they are shown in red by the program. If the scheme is correct (the single-wire representation in fig.1) the colour is green and the program calculates the nominal currents on each circuit and dimensions the elements necessary to supply and protect consumers. ABB Doc balances the consumption on the phases of the electricity network; thus, the program applies an algorithm to move single-phase tasks from one phase to another, so that consumers are evenly distributed over the three phases.

The Schrack Design software does not perform the calculations presented above, but it comes to complete the shortcomings of the ABB Doc program, namely that of the study of heating the switchboards for currents not exceeding 630A.

In addition, the Schrack database contains for each product the value of dissipated power and thus, the total active power can be observed including on the distribution bars. Also, the Schrack Design program allows the realization of the distribution board, the verification of the load on the distribution bars, the specification of the used cables and the addition of a ventilation system for the distribution board.

Schrack Design monitors the temperature in the panel in real time and displays messages if the temperature exceeds the maximum allowed limit for the chosen configuration. This real-time thermal calculation is repeated each time an equipment is selected from a database. The wrong choice of the size of the paintings can lead to the increase of temperatures above the maximum allowed limit and this aspect can be visualized in the program by messages written in red (fig. 3, fig. 4).

## 5. Conclusions

In this paper were presented the ABB Doc and Schrack Design software that can be used by engineers who carry out electrical installation projects. Both programs offer to the user the possibility to design medium and the low voltage electrical distribution panel according to established requirements. These programs allow the sizing of the supply circuits necessary for consumers and the realization of electrical distribution panels.

From the study we can say that, for the size of the cables and switching and protection equipment necessary for consumers, the ABB Doc program can be used successfully. However, if you want the thermal calculation of a distribution board, Schrack Design program allows us to do this in real time at the time of design.

In conclusion, for an optimal result regarding the dimensioning of the electrical distribution panels, it is recommended to use both programs, these being harmoniously complemented by scientifically covering the design stages necessary for low voltage electrical installations.

## References

- [1] C. G. Sărăcin, „Instalații electrice”, Editura Matrix ROM, 2009.
- [2] <https://new.abb.com/low-voltage/solutions/selectivity/tools-support/doc>
- [3] [https://library.e.abb.com/public/a7a540898e0685bdc1257e1a0048b3ef/DOC\\_UserManual\\_EN\\_SLD.pdf](https://library.e.abb.com/public/a7a540898e0685bdc1257e1a0048b3ef/DOC_UserManual_EN_SLD.pdf)
- [4] <https://www.elandcables.com/electrical-cable-and-accessories/cables-by-standard/iec60092-cable>
- [5] [https://webstore.iec.ch/preview/info\\_iec60364-1%7Bed5.0%7Den\\_d.pdf](https://webstore.iec.ch/preview/info_iec60364-1%7Bed5.0%7Den_d.pdf)
- [6] <https://www.en-standard.eu/une-20460-7-740-2007-11m-2017-electrical-installations-of-buildings-part-7-740-requirements-for-special-installations-or-locations-temporary-electrical-installations-for-structures-amusement-devices-and-booths-at-fairgrounds-amusement-parks-and-circuses/>
- [7] [https://www.vde-verlag.de/buecher/leseprobe/9783800746910\\_PROBE\\_01.pdf](https://www.vde-verlag.de/buecher/leseprobe/9783800746910_PROBE_01.pdf)
- [8] <https://webstore.iec.ch/searchform&q=IEC%2060898-1>
- [9] [https://www.hensel-electric.de/media-61439/docs/EN/leitfaden\\_IEC\\_EN61439\\_en.pdf](https://www.hensel-electric.de/media-61439/docs/EN/leitfaden_IEC_EN61439_en.pdf)
- [10] <https://webstore.iec.ch/publication/3820>
- [11] <https://www.schrack.ro/tools/schrack-design-software/alte-versiuni-schrack-design>
- [12] P. D. Parincu, G. M. Atanasiu, „Regenerative Concepts of Design for Residential Buildings Development” Romanian Journal of Civil Engineering, nr.1/2016, volume 7.
- [13] N. Postavaru „Standardization of education and strategy for 2030” Romanian Journal of Civil Engineering, nr.3/2014, volume 5.
- [14] E. Cazacu, “Instalații electrice moderne. Baze teoretice, elemente de calcul și proiectare” Editura Matrix ROM, 2015.

# Modeling the Drying Shrinkage of Structural Concretes

Modelarea contracției prin uscare a betoanelor structurale

Abderraouf Kebir<sup>1</sup>, Abdelmalek Brahma<sup>2</sup>

<sup>1</sup> Dept. of Civil Engineering, Saad Dahleb University.  
Blida 09000, Algeria  
E-mail: [kebirgc@gmail.com](mailto:kebirgc@gmail.com)

<sup>2</sup> Dept. of Civil Engineering, Saad Dahleb University.  
Blida 09000, Algeria  
E-mail: [a.brahma@hotmail.com](mailto:a.brahma@hotmail.com)

DOI: 10.37789/rjce.2021.12.4.7

**Abstract.** *Shrinkage in hydraulic materials is a complex time-dependent process. For standard concretes, one of the most significant parts of shrinkage is drying shrinkage. In fact, to predict deformations of concrete due to shrinkage, various predictive models have been developed; most of them use many numbers of factors that can affect shrinkage such as concrete strength, concrete age at loading, curing conditions type, ambient conditions, type of cement and aggregates, water to cement ratio, concrete mix, member shape and size, loading duration and type. A such number of parameters increases the complexity of using these models lead to some prediction imperfections; thence a new simplified model is needed. The main target of the current paper is to formulate a novel and simplified model with a minimum of factors that affect drying shrinkage behaviour as like as relative humidity and volume to area ratio of the concrete element (V/S). To achieve this goal, we had developed a prediction model based on probability density function and a small number of parameters that influence shrinkage like relative humidity and volume to surface ratio of the element. A huge database has been used to calibrate our model's parameters using the most recent studies and researches to validate the model.*

**Key words:** hydraulic materials, drying shrinkage, modelling, prediction, concrete deformation, structural concrete.

## 1. Introduction

To predict concrete shrinkage behavior, diverse analytical models have been elaborated and some of them are approved by diverse codes and recommended by famous researchers [1].

Shrinkage is affected by multiple variables as well as concrete strength, concrete loading time, cement type, type of curing conditions, ambient conditions, water to cement ratio, concrete mix, member size and shape, aggregates type, duration and type of loading, etc.[2]. This large number of parameters affecting shrinkage increases the

complexity of utilizing these models and can lead to imperfections in shrinkage predictions. It can also reduce databases exploitable results due to the lack of one or more of these parameters. Thence, a new simplified prediction model containing fewer parameters that affect shrinkage phenomena is necessary. The quality of a shrinkage predictive model depends on the contribution of each parameter which conducts the phenomena [3]. In its report 209.1R-2 [4], the American Concrete Institute (ACI) defines shrinking as the deformation measured on a load-free concrete sample. ACI states that shrinkage excludes changes in length due to variations in temperature, but it depends on the environment, configuration, and size of the specimen.

Researchers must often describe and analyze phenomena in diverse areas of research, with actions understood only from laboratory observations. For this reason, the synthesis of a mathematical model with similar behavior to the actual phenomenon is of interest. In particular cases, with the understanding of the model parameters and the experience requirement of the phenomenon, we are able to suggest a mathematical model named a deterministic model. The exact mechanisms of the phenomenon, though, are generally unknown. We might, therefore, formulate a mathematical model on which we determine the parameters of measurements from samples.

The drying shrinkage in concretes is the most significant part of shrinkage deformations [5]; it results from the reduction of pores' relative humidity which increases directly the capillary tension of pores occupied the water and in the solid surface tension at pore walls. The data from experimental results show that the measured ultimate values of concrete drying shrinkage of many specimens had a nonlinear function of the ambient relative humidity [6].

This study aims to develop a representative prediction model of drying shrinkage of hydraulic materials with fewer affecting factors and more predictive accuracy. This manuscript is structured in the following way: First, we expose the relation between drying shrinkage development and the probability density function. In Section 2, 3, and 4, we present step by step the demonstration that leads from mathematical density function to a model that can describe the evolution of drying shrinkage; these model parameters were estimated by using large experimental results gathered in different databases then simplified to reduce the number of parameters. In Section 5, we present a comparison of our developed model and various American and European prediction models that existed in the literature. Finally, section 6 summarizes the main conclusions.

## **2. Experimental Investigation**

The present research is based on a vast range of experimental results obtained in various American and European laboratories by internationally renowned researchers [7] and [8].

The experimental results analyzed are those that include the most parameters influencing the drying shrinkage.

### 3. Analytical Investigation

The current study is founded on a statistical study of experimental results given and summarized by Bazant [8]. The analysis of these results presents the dominant values between [300-600  $\mu\text{m/m}$ ] that most frequently present shrinkage deformation value.

### 4. Modeling

In our case, the drying shrinkage evolution is described by a curvature that starts by exponential shape then it advances towards an asymptotic limit, as shown in Fig.1. In statistics, this form of shapes matches whit the curve of the density probability function  $F(t, t_0)$  obtained with direct integration of the density probability function  $F(t, t_0)$  in function of time (t), as seen in Fig. 2.

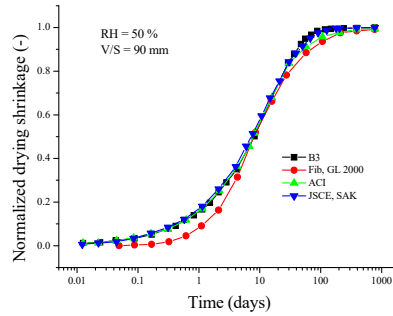


Fig. 1. Normalized drying shrinkage evolution [9].

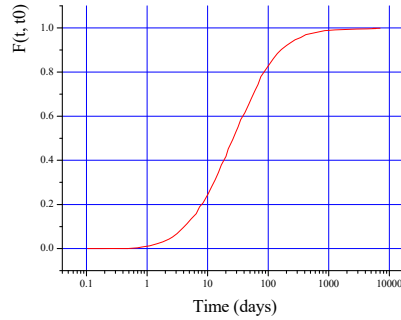


Fig. 2. Probability density function  $F(t, t_0)$  [7].

For this case of study, the probability density function  $f(t, t_0)$  given in Eq.(1) is two parameters Weibull function [10]:

$$f(t, t_0) = \frac{c}{t - t_0} \times \left( \frac{t - t_0}{t - t_0} \right)^{C-1} \times \exp \left\{ \left( \frac{t - t_0}{t - t_0} \right)^C \right\} \quad (1)$$

Such that  $t-t_0 > 0$ ,  
where  $t_0$  is the time of loading, and  $f(t, t_0)$  is a probability density function.

For the resolution of this equation, let:

$$b = (t-t_0)^{-C} \Rightarrow b = \frac{1}{(t-t_0)^C}$$

and  $y = t - t_0$

Hence, Eq. (1) becomes as follows:

$$f(t, t_0) = \frac{c}{(t-t_0)} \times \frac{(t-t_0)^{C-1}}{(t-t_0)^{C-1}} \times \exp\left\{\frac{(t-t_0)^C}{(t-t_0)^C}\right\} \Rightarrow f(t, t_0) = c \times \frac{(t-t_0)^{C-1}}{(t-t_0)^C} \times \exp\left\{\frac{(t-t_0)^C}{(t-t_0)^C}\right\} \quad (2)$$

Therefore;

$$f(t, t_0) = c \times b \times y^{C-1} \times \exp(-b \times y^C) \quad (3)$$

$$\text{The probability density function is given by: } F(t, t_0) = \int f(t, t_0) dt \quad (4)$$

Proceed to the development of Eq. (4)

$$\text{Such as } F(t, t_0) = \int_{-\infty}^0 f(t, t_0) dt + \int_0^t f(t, t_0) dt \quad (5)$$

$$\int_{-\infty}^0 f(t, t_0) dt = 0 \quad (6)$$

Replace the function  $f(t, t_0)$  by the equation in the integral as follows:

$$F(t, t_0) = \int_0^t \left( c \times b \times (t-t_0)^{(C-1)} \times \exp(-b \times (t-t_0)^C) \right) dt \quad (7)$$

Let:

$$v = b \times (t-t_0)^C \Rightarrow v' = c \times b \times (t-t_0)^{C-1} \quad (8)$$

by replacing  $v$  and  $v'$  in Eq. (5), we obtain

$$\int v' \times e^{-v} = -e^{-v}$$

Where:

$$F(t, t_0) = -e^{-b(t-t_0)^C} \Big|_0^t = 1 - e^{-b(t-t_0)^C} \quad (9)$$

To consider the development of the density probability function  $F(t, t_0)$  to reach an asymptotic limit, we multiply the Eq. (9) by a non-zero positive number " $a$ " which yields to the final form:



$$F(t, t_0) = a \times (1 - e^{-b(t-t_0)^c}) \quad (10)$$

In our case, the function  $F(t, t_0)$  represents the degree of progress of drying shrinkage  $\varphi(t, t_0)$  where:

$$\varphi(t, t_0) = a \times (1 - e^{-b(t-t_0)^c}) \quad (11)$$

#### 4.1 Estimation of the Model Parameters

To identify the model parameters, we used the results of the tests given by Bazant [7]. These test series involve 35 cylindrical samples of diameter 160 mm and 36 cylindrical samples of diameter 83 mm. also besides; three cylindrical samples of 300 mm diameter are also measured. The length of all cylinders is double their diameter.

The most appropriate and simplest method for estimating the parameters of linear models is the least-squares method [11]. This method consists of minimizing the differences between the regression line and the explained variable "y"; in other words, it reduces the sum of the squares also called the "sum of the squares of the residues" denoted "SCR".

$$SCR = \sum_{i=1}^N \varepsilon_i^2 \quad (12)$$

With,  $\varepsilon_i = y_i - \hat{y}_i$ ; error at the point  $t$  between the measured and calculated value. The  $\hat{\beta}$  estimation is the value of  $\beta$  which renders the expression (12) minimal

$$y_i = \hat{\beta}_0 + \hat{\beta}_1 x_{1i} + \hat{\beta}_2 x_{2i} + \dots + \hat{\beta}_k x_{ki} + \varepsilon_i \quad (13)$$

The matrix form of this expression is:

$$y_N = X_{Nk} \cdot \hat{\beta}_k + \varepsilon_N \quad (14)$$

The system (14) resolution allows the determination of the  $\hat{\beta}$  estimator.

$$\hat{\beta} = (X' \cdot X)^{-1} X' \cdot Y \quad (15)$$

The degree of validity of a regression model is based on the following conditions [11]:

- The  $\bar{R}^2$  must be as high as possible.
- Student's and Fisher's tests must provide acceptable results.
- The standard deviations of the coefficients must be the lowest on the estimated values of the coefficients.

From the set of observations on the variables of the model selected during our study, we have proposed several expressions by multiple regressions giving the parameters of the model Eq. (11); the expressions retained are given by the relations (16), (17), and (18).

With:  $V/S$ =volume area ratio, in (mm), and  $RH$ =relative humidity in (%).

The test's parameters of model coefficients  $a$ ,  $b$  and  $c$  are given in Table 1, Table 2, and Table 3.

$$a = \beta_1 + \beta_2.(RH)^2 + \beta_3\left(\frac{V/S}{RH}\right) \quad (16)$$

$$b = \beta_4 + \beta_5.(V/S) + \frac{\beta_6}{RH} \quad (17)$$

$$c = \beta_7 + \beta_8((V/S)^2.(RH)) \quad (18)$$

Model Coefficients		Standard Deviation	Student's test		Fisher's test		Correlation coefficient	
			$T_{Student}$	$P(S)^*$	$T_{Fisher}$	$P(F)^{**}$	$R^2$	$\bar{R}^2$
$\beta_1$	1.25004	0.0155	80.640	0.00	682.51	0.0000	0.9572	0.9558
$\beta_2$	-0.8423	0.0267	-30.82	0.00	682.51	0.0000	0.9572	0.9558
$\beta_3$	-0.0012	0.0001	-9.607	0.00	682.51	0.0000	0.9572	0.9558

Table 1.

**Test « a » parameter's tests**

Model Coefficients		standard deviation	Student's test		Fisher's test		Correlation coefficient	
			$T_{Student}$	$P(S)^*$	$T_{Fisher}$	$P(F)^{**}$	$R^2$	$\bar{R}^2$
$\beta_4$	0.236297	0.0027	85.8150	0.00	1071.38	0.0000	0.9723	0.9714
$\beta_5$	-0.00400	8.7E-05	-45.890	0.00	1071.38	0.0000	0.9723	0.9714
$\beta_6$	0.002927	0.0004	6.0662	0.00	1071.38	0.0000	0.9723	0.9714

Table 2.

**Test « b » parameter's tests**

Model Coefficients		standard deviation	Student's test		Fisher's test		Correlation coefficient	
			$T_{Student}$	$P(S)^*$	$T_{Fisher}$	$P(F)^{**}$	$R^2$	$\bar{R}^2$
$\beta_7$	0.540896	0.0037	144.6832	0.0000	682.517	0.0000	0.7901	0.7202

$\beta_8$	3.13E-05	8.9E-06	3.5082	0.0127	682.517	0.0000	0.7901	0.7202
-----------	----------	---------	--------	--------	---------	--------	--------	--------

Table 3.

#### Test « c » parameter's tests

$P(S)^*$  : Probability of significance of each estimated coefficient.

$P(F)^{**}$ : Probability of significance associated with  $T_{Fisher}$  value.

## 4.2 Improvement of the Model

### 4.2.1 Adjusting the Parameter « a »

The parameter "a" represents the limit value of drying shrinkage; this parameter « a » is influenced by the relative humidity conditions  $RH$  and the  $V/S$  ratio of the element [3]. The relative humidity is one among the most essential factors affecting the final shrinking of concrete.

Fig. 3 [3] shows a reduction of the shrinkage for 14 and 28 days when the relative humidity tends to increase. By comparison, the shrinkage initially increases significantly for higher ages and then decreases.

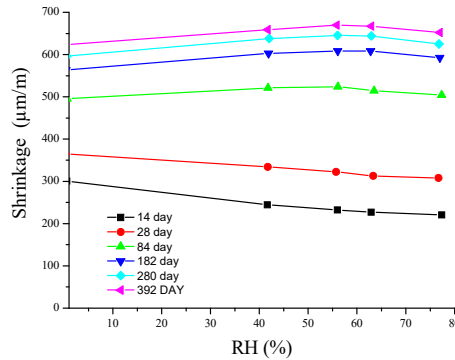


Fig. 3. Relative humidity  $RH$  effect on the shrinkage of concrete at different ages [3].

Figure 4 discusses the influence of the  $V / S$  ratio on the shrinkage measured for various concrete ages. The higher the  $V / S$  ratio, the lower the shrinkage.

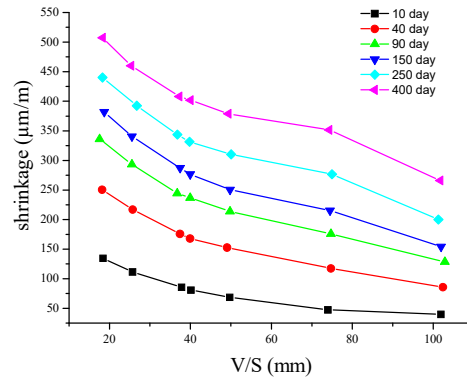


Fig. 4. V/S ratio effect on the shrinkage of concrete at different ages [3].

A statistical analysis founded on experimental results given by [8] shows that the values of the parameter "a" are mostly between [300-600 μm/m] as illustrated in Fig. 5.

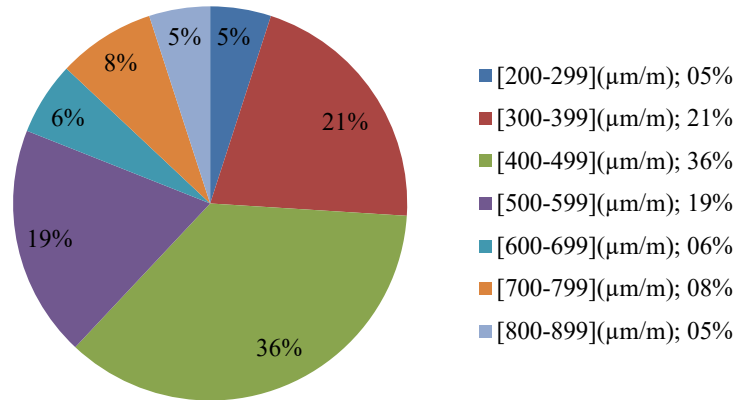


Fig. 5. Proposal of the values by interval of the parameter (a) (μm/m).

#### 4.2.2 Adjusting the Parameter « c »

The variation of the parameter « c » is a function of the relative humidity *RH* and V/S ratio as reported in Table 4.

Table 4.

« c » coefficient values predicted in our model

V/S	RH	c	V/S	RH	c	V/S	RH	c
76 mm	20%	0.59	102 mm	20%	0.536	152 mm	20%	0.599
76 mm	50%	0.44	102 mm	50%	0.508	152 mm	50%	0.576
76 mm	75%	0.51	102 mm	75%	0.525	152 mm	75%	0.653

Note that the " $c$ " parameter values vary little and is close to 0.5.

Adopting  $c = 0.5$ , the equation yielding the progression of the drying shrinkage is reduced to an expression with two parameters:

$$\varphi(t, t_0) = a \times (1 - e^{-b(t-t_0)^{0.5}}) \quad (19)$$

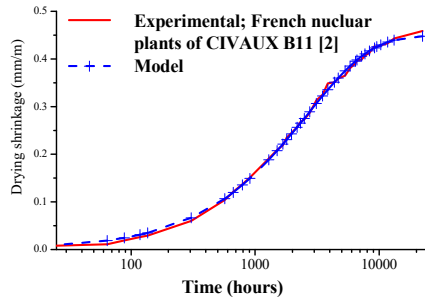
## 5. Validation of the Model

To validate our model, we first compare the model predictions with experimental results for high-performance and normal concrete given by [12] and [13] and then with most common American and European models such as the ACI, Sakata, B3, B4, B4S, CEB 99, GL2000, Idiart, SANS 10100, Wits, Fib and EC2 model.

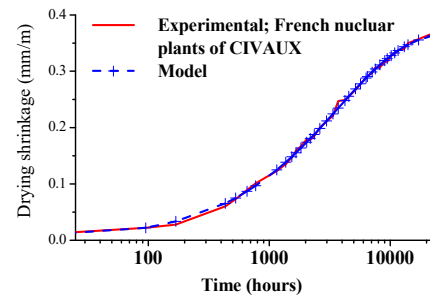
### 5.1 Confronting Drying Shrinkage Model Evolution of High-Performance Concrete With Experimental Results of Granger [12].

The high-performance concrete constitutes a new concrete with novel characteristics. It is useful to compare the developed model prediction with the experimental results obtained by Granger [12].

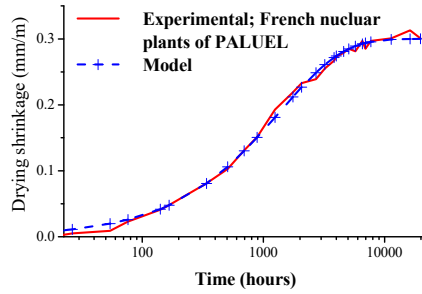
The results are grouped by model and experimental results in Fig. 6 (experimental results obtained by Granger [12] for French nuclear plants of CIVAUX, PALUEL, and CHOOZ). Our predictive model tends to align well with the development of high-performance concrete drying shrinkage.



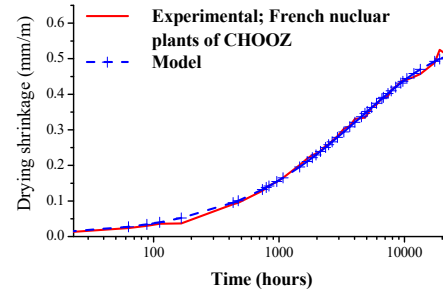
6.a.



6.b.



6.c.

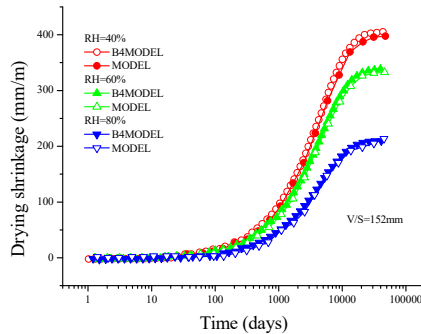


6.d.

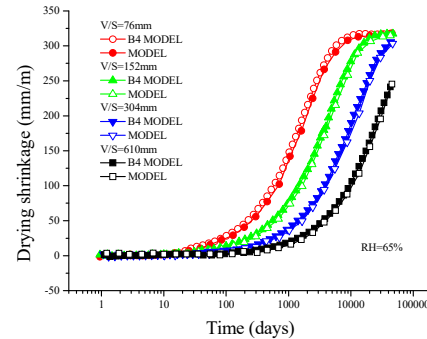
Fig. 6. Confronting drying shrinkage model evolution of high-performance concrete with experimental values obtained by [12] for French nuclear plants of CIVAUX, PALUEL, and CHOOZ.

## 5.2 Comparison of Model Predictions With Experimental Values of Bazant and al [13]

Figure 7.(a) shows the contribution of the drying shrinkage for a constant volume to surface ratio  $V/S=152$  mm and variable environmental relative humidity  $RH$  (40%, 60%, 80%), as well as constant environmental relative humidity of  $RH=65\%$  and variable  $V/S$  ratio (76; 152; 304; 610 mm) in Fig. 7.(b).



7.a.



7.b.

Fig. 7. Predictions of drying shrinkage curves as a function of varying  $V/S$  ratio and humidity, and B4 model [13].

In the curves of Fig. 7, we provide a comparison between our model prediction and normal concrete drying shrinkage with different  $RH$  and  $V/S$  ratio.

Curves in Fig. 7.(a) shows the influence of relative humidity ( $RH$ ) for constant  $V/S$  ratio. This influence is less nuanced at younger ages (the first days), but it clearly appears at advanced ages. We observe on the curves of Fig. 7.(a) that the amplitude of the drying

shrinkage increases inversely with the decrease of the relative humidity  $RH$ .

The curves in Fig. 7.(b) illustrate the influence of the size of concrete element ( $V/S$  ratio). It is clearly appears that the effect of the dimension of the elements ( $V/S$  ratio) is more marked. We observe on these curves that the drying shrinkage decreases with increasing  $V/S$  ratio of specimens.

### 5.3 Confrontation of Developed Model Predictions With Most Common Models, Recent Research and Various Databases

#### 5.3.1 Confrontation With Goel and al [2]

Figure 8 presents the prediction of drying shrinkage deformations obtained from six analytical models: ACI 209 model[4], the B3 model [9], the CEB-FIP model [14], GL2000 model [15], Muller model [16], and our prediction model.

To compare these varied prediction models, results predicted by these models are to be compared with experimental results. therefore, the experimental results of Russell and Larson [17] and the RILEM data bank [9] have been selected.

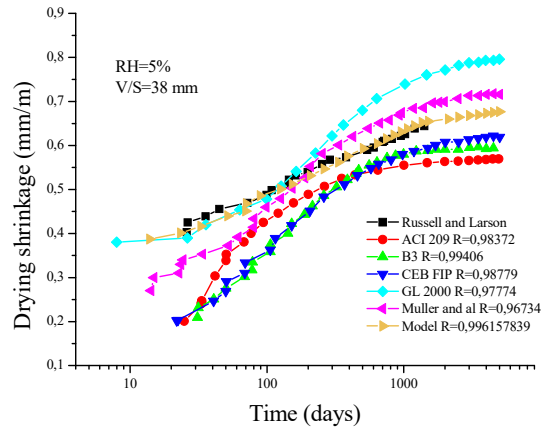


Fig. 8. Drying shrinkage predictions in concrete with  $V/S=38$  mm and  $RH=5\%$ .

From Fig. 8, in the GL2000 model it is observed an underestimation of experimental concrete shrinkage up to around 160 days of age and overestimates it after this age. Also, the Muller model presents an overestimation of experimental shrinkage after about 180 days. The B3 model and ACI model underestimates the experimental results. Our prediction model underestimates experimental shrinkage to the age of about 100 days then fit perfectly with it, these underestimations may be caused by other factors influencing shrinkage desiccation such as the concrete age at loading, cement type, aggregates, water-cement ratio, concrete mix, loading type, loading duration, etc.

### 5.3.2 Confrontation With Idiart and al [18]

In the curves of Fig. 9, we provide a comparison between predictions of the developed model and three simulation models (parabolic, linear and constant shrinkage coefficient) given by [18].

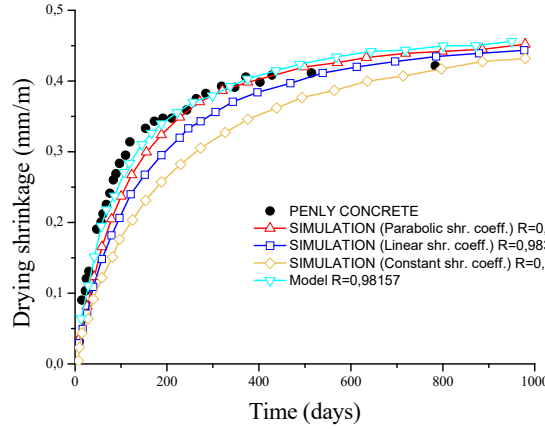


Fig. 9. Comparison of the developed and Idiart [18].

From Fig. 9, it is observed that all three simulations have the same beginning and ending rate of drying shrinkage but linear and constant shr coef underestimate experimental results at middle ages. Parabolic shr coef and our model fit perfectly and predict well the evolution of drying shrinkage of PENLY concrete.

### 5.3.3 Confrontation With Gaylard and al [19]

The most detailed model comparisons in the published literature are focused on the RILEM database, a compilation of 490 concrete shrinkage profiles primarily from study groups in North America and Europe [8].

In Fig. 10, we present concrete drying shrinkage predictions for structural use on the basis of historical data for South African concrete shrinkage [19].

We used eight published models as comparisons with our model developed in this study: ACI 209 [4], RILEM B3 model [9], CEB MC90-99 [14], GL2000 model [15], SANS 10100 model [20], Eurocode 2 [21], Fib model [22], WITS model [19]

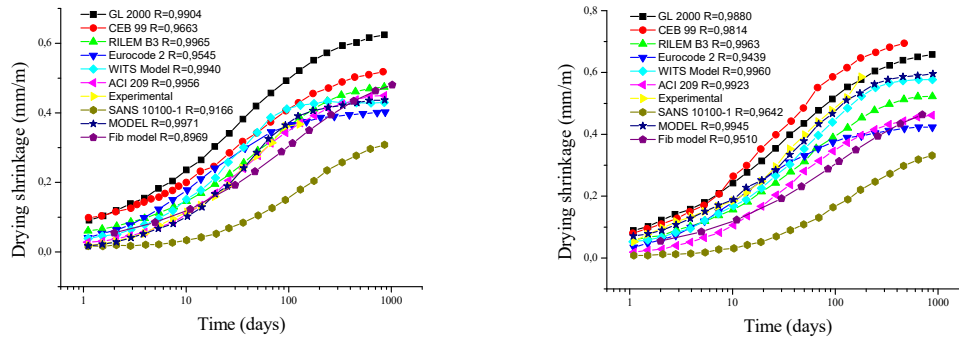


Fig. 10. Eight models predictions and experimental results [19] compared to our model.



It is obvious from Fig. 10 that the model developed was performing well, as expected. The models SANS 10100-1 [20] and GL2000 [12] appeared to underpredict and overpredict, respectively. No specific tendency concerning the performance of the other models is directly apparent from early and advanced age examination of the results.

### 5.3.4 Confrontation With Al-Saleh [1]

In Figure 11 we provide a comparison of experimental results measurements of drying shrinkage and theoretical drying shrinkage predictions applying the next five models: ACI 209 [4], CEB-FIP [14], B3 [9], Sakata [23], and GL2000 [15]. Measures on samples were taken with  $V/S=125$  mm and various relative humidities  $RH=50\%$  and  $RH=5\%$ .

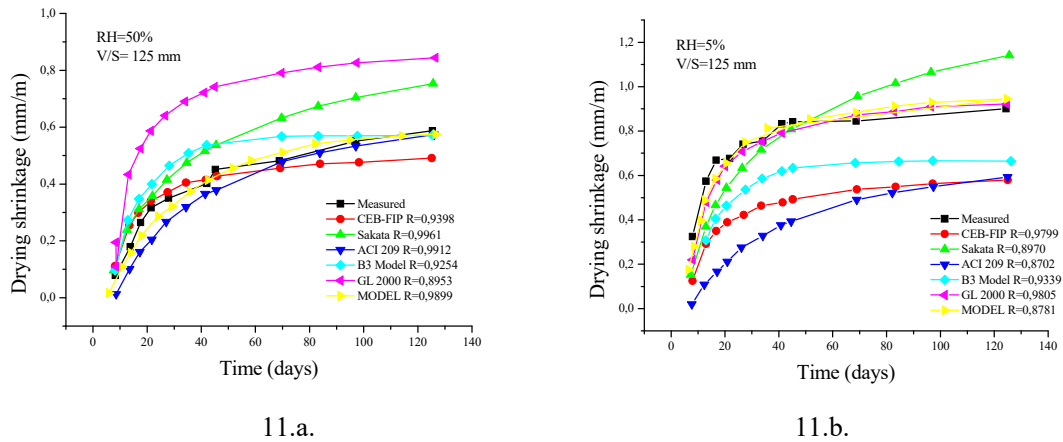


Fig. 11. Models prediction and drying shrinkage experimental measures [1].

Figure 11.(a) illustrates that ACI 209 and B3 models are the nearest theoretical drying shrinkage in  $RH=50\%$ , particularly when approaching ultimate drying shrinkage. At the start of the drying-time, it is found that the ACI 209 model under predicts experimental drying shrinkage whilst the B3 model slightly over predicts experimental results. It can be noted from Fig. 11.(a) that CEB-FIP model at the beginning of the drying period is closed to the experimental drying shrinkage values. However, the model's predicted deformations start to deviate as time goes towards ultimate shrinkage from experimental drying shrinkage strains. The expected drying shrinkage using Sakata model is close to the experimental deformations after 40 days of drying time, subsequently, the values obtained increased with a fast rate as the drying time goes towards the ultimate. It is noticed that GL 2000 model has the worst prediction from early age until the end of the drying period. Our model predicts well the development of drying shrinkage compared to the results of experiments.

In Figure 11.(b) we observe an augmentation of the final experimental drying shrinkage rate due to very low relative humidity  $RH=5\%$ . Our model and GL 2000 model describe well the evolution of experimental drying shrinkage. A rather large difference is observed at early and later ages for the rest of the models compared to

experimental results. These imperfections are due to the presence of several parameters in these models.

### 5.3.5 Confrontation With Vinkler [24]

Three experimental specimens of  $V/S=200$  mm (mentioned as ST1),  $V/S=400$  mm (mentioned as ST2) and  $V/S=800$  mm (mentioned as ST3) and standard cylinders of  $V/S=75$ mm were used. Cylinders were separated into two sets of two samples and retained under diverse environmental conditions: the initial group (mentioned as V1-V2) was maintained with the same ambient conditions as the specimens with 40% relative humidity, second group (mentioned as V3-V4) was maintained in controlled conditions with 65 % relative humidity. Different curing conditions allow for the determination of drying shrinkage and for comparison of drying shrinkage measured in cylinders (V1-V2, V3-V4) and in large concrete elements (ST1, ST2, and ST3).

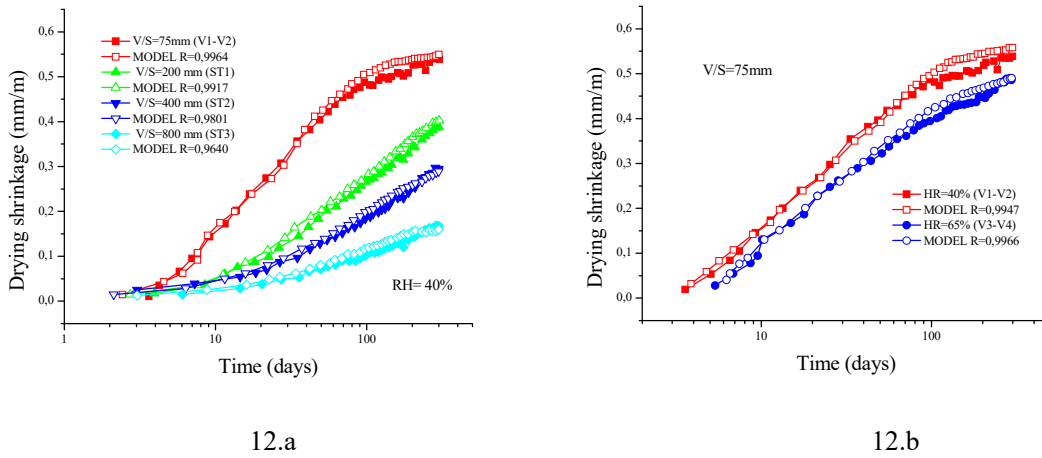


Fig. 12. Predictions of drying shrinkage curves as a function of varying V/S ratio and humidity.

The thicker specimen shrinks less as intended due to the slower drying process. The strains in (ST1, ST2 and ST3) are smaller compared with the shrinkage of cylinders.

The far more interesting remarks from previous experimental data and model predictions are as follows:

1. The size impact has been illustrated quite clearly in Fig. 12.(a). The higher is volume-surface ratio, a slower shrinkage deformation was observed. The cause is obvious: thicker elements dry more slowly because the moisture moves and travels over a longer distance in the element and so the drying shrinkage acts consistently. This result is in correlation with [9] and [25].

2. Relative humidity variation affects directly the rate of drying shrinkage. We observe that the shrinkage rate increase with lower relative humidity condition as it is shown in Fig. 12.(b).

In Figure 13 we present a comparison to predict drying shrinkage of concrete and the most common models which are: Fib model [22], EC 2 [21], B4, B4S [13], and ACI 209 [4].

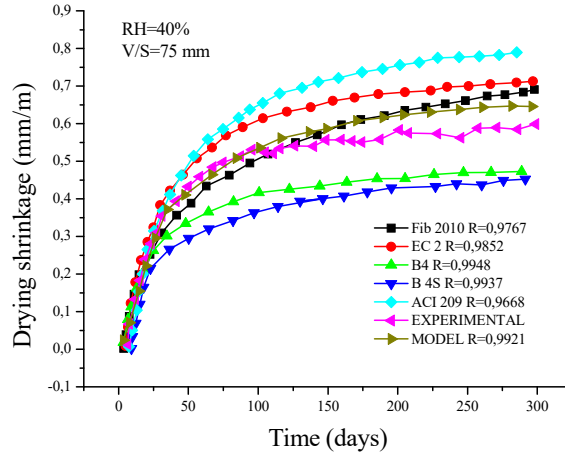


Fig. 13. Different models predictions with RH=40% and V/S=75 mm and [24] experimental results.

From Fig. 13, we note that drying shrinkage shows that the models exhibit a fast increase of strains at early age while the measured strain development is slower.

After a while, the rate of strains in forecasting models is reduced. ACI and EC2 models overestimate the evolution of drying shrinkage while B4 and B4S models underestimate it. Our model and Fib's model fit perfectly with experimental measurements at early ages and overestimate the evolution at later ages.

The analysis of these curves clearly shows the concordance behaviour that exists between the experimental results (of different researchers in different laboratories) and those predicted by our model. However, a slight difference is observed only on a few curves at the early age, and sometimes at later ages compared to experimental results.

The developed model well describes the evolution of concrete's drying shrinkage. Additionally, it presents better precision compared with the most common models.

## 6. Conclusion

The principal objective of this research was to develop a simplified predictive model with fewer affecting factors for drying shrinkage of structural concretes, namely for normal and high-performance concrete in order to predict the deformation rate during hardening. The main variables in the model are the volume-area ratio (V/S) and the relative humidity (RH). To reach this objective, we had based on a large number of experimental results obtained from various American and European laboratories and some current and important codes of practice. This step leads us to summarize four essential points:

1. The developed model is well adapted to represent and describe the evolution of drying shrinkage of high-performance concrete, and it has been validated by comparison with real experimental results.
2. The final developed model is very simple and easy to use and it presents the advantage of containing only two parameters in comparison with the necessary parameters of the other models.
3. The developed model can easily describe deferred deformations of concrete structures with more precision since the shrinkage strongly depends on desiccation.
4. It is a general model that applies particularly well to the range of conventional concretes such as ordinary concretes and high performance concretes and to concretes with similar characteristics to those of the latter. Extreme cases require the introduction of corrective factors.

## References

- [1] S. A. Al-Saleh, „Comparison of theoretical and experimental shrinkage in concrete” ,Constr. Build. Mater. ,vol. 72, no. 01, 2014 ,pp. 326–332.
- [2] R. Goel, R. Kumar, D. K. Paul, „Comparative study of various creep and shrinkage prediction models for concrete” ,J. Mater. Civ. Eng. ,vol. 19, no. 3, 2007 ,pp. 249–260.
- [3] L. Bal, F. Buyle-Bodin, „Artificial neural network for predicting drying shrinkage of concrete” ,Constr. Build. Mater. ,vol. 38, no. 01, 2013 ,pp. 248–254.
- [4] A. A. Al-Manaseer, M. A. Chiorino, M. A. Issa, K. A. Rieder, Z. P. Bazant, M. A. Daye, H. Marzouk, I. Robertson, J. J. Brooks, W. H. Dilger, „Report on Factors Affecting Shrinkage and Creep of Hardened Concrete” ,Concr. Int. ,vol. 01, no. 01, 2005 ,pp. 21–22.
- [5] P. Havlásek, M. Jirásek, „Multiscale modeling of drying shrinkage and creep of concrete” ,Cem. Concr. Res. ,vol. 85, no. 01, 2016 ,pp. 55–74.
- [6] Z. P. Bažant, P. Havlasek, M. Jirásek, „Microprestress-solidification theory: Modeling of size effect on drying creep” ,Comput. Model. Concr. Struct. - Proc. EURO-C 2014 ,vol. 2, no. 01, Jan. 2014 ,pp. 749–758.
- [7] Z. P. Bazant, F. H. Wittmann, J. K. Kim, F. Alou, „Statistical Extrapolation of Shrinkage Data-Part I: Regression” ,Aci Mater. J. ,vol. 84, no. 84, 1987 ,pp. 20–34.
- [8] Z. P. Bazant, G.-H. Li, „Unbiased statistical comparison of creep and shrinkage prediction models” ,ACI Mater. J. ,vol. 105, no. 6, 2008 ,pp. 610–621.
- [9] Z. P. Bazant, S. Baweja, „Creep and shrinkage prediction model for analysis and design of concrete structures: Model B3” ,ACI Spec. Publ. ,vol. 194, no. 01, 2000 ,pp. 1–84.
- [10] F. Scholz, B. P. Works, „Weibull reliability analysis” ,Dep. Stat. Univ. Washingt. ,vol. 5, no. 01, 2002 ,pp. 21–23.
- [11] G. Saporta, Probabilités, analyse des données et statistique, no. 2006. Editions Technip, 2006.
- [12] L. Granger, „Comportement différé du béton dans les enceintes de centrales nucléaires: analyse et modélisation” ,vol. 4, no. 1, 1995 ,pp. 45–56.
- [13] Z. P. Bazant, Mi. Jirásek, M. H. Hubler, I. Carol, „RILEM draft recommendation: TC-242-MDC multi-decade creep and shrinkage of concrete: material model and structural analysis. model B4 for creep, drying shrinkage and autogenous shrinkage of normal and high-strength concretes with multi-decade applicabilit” ,Mater. Struct. ,vol. 48, no. 4, 2015 ,pp. 753–770.

- [14] M. Wicke, E. Siviero, H. Hilsdorf, H. S. Müller, J. Walraven, „Structural concrete. Textbook on behaviour, design and performance. Updated knowledge of the CEB/FIP Model Code 1990. Volume 1: Introduction-Design process-Materials” ,Bulletin-FIB ,vol. 1, no. 1, 1999 ,pp. 18–43.
- [15] N. J. Gardner, M. J. Lockman, „Design provisions for drying shrinkage and creep of normal-strength concrete” ,Mater. J. ,vol. 98, no. 2, 2001 ,pp. 159–167.
- [16] H. S. Müller, C. H. Küttner, V. Kvitsel, „Creep and shrinkage models of normal and high-performance concrete: concept for a unified code-type approach” ,Rev. française génie Civ. ,vol. 3, no. 3–4, 1999 ,pp. 113–132.
- [17] H. G. Russel, S. C. Larson, „Thirteen years of deformations in water tower place” ,Struct. J. ,vol. 86, no. 2, 1989 ,pp. 182–191.
- [18] A. Idiart, C. M. López, I. Carol, „Modeling of drying shrinkage of concrete specimens at the meso-level” ,Mater. Struct. ,vol. 44, no. 1, Mar. 2011 ,pp. 415–435.
- [19] P. C. Gaylard, Y. Ballim, L. P. Fatti, „A model for the drying shrinkage of South African concretes” ,J. South African Inst. Civ. Eng. ,vol. 55, no. 1, 2013 ,pp. 45–59.
- [20] South African Bureau of Standards, „SANS 10100-1: The Structural Use of Concrete. Part 1: Design” ,South African Bur. Stand. ,vol. 4, no. 1, 2000 ,pp. 1–16.
- [21] European Committee for Standardization, „EN 1992-1-1: Eurocode 2: Design of Concrete Structures – Part 1: General Rules and Rules for Buildings.” ,vol. 4, no. 1, 2003 ,pp. 124–132.
- [22] International Federation for Structural Concrete (fib), „Model Code 2010–final draft, vols. 1 and 2, fédération internationale du béton” ,Bulletins ,vol. 65, no. 4, 2012 ,p. 350–374.
- [23] K. Sakata, „Prediction of concrete creep and shrinkage” ,Creep Shrinkage Concr. ,vol. 2, no. 4, 2004 ,pp. 55–74.
- [24] M. Vinkler, J. L. Viték, „Drying shrinkage of concrete elements” ,Struct. Concr. ,vol. 18, no. 1, 2017 ,pp. 92–103.
- [25] Z. P. Bažant, „Prediction of concrete creep and shrinkage: past, present and future” ,Nucl. Eng. Des. ,vol. 203, no. 1, 2001 ,pp. 27–38.

## Analiza implementării măsurilor de apărare împotriva incendiilor în clădiri civile

Analysis of the implementation of fire protection measures in civil buildings

Conf.univ.dr.ing. Aurel Trofin<sup>1</sup>

Drd.ing. Mihai Ciprian Mitrea<sup>2</sup>

<sup>1</sup>Academia de Poliție “Alexandru Ioan Cuza”, Facultatea de Pompieri  
Șoseaua Morarilor nr. 3, Sector 2, București

E-mail: [aureltrofin@gmail.com](mailto:aureltrofin@gmail.com)

<sup>2</sup>Inspectoratul pentru Situații de Urgență „Petrodava” al Județului Neamț  
Str. Cuiejdii, nr. 34, Piatra Neamț, județul Neamț

E-mail: [mitreamihai@gmail.com](mailto:mitreamihai@gmail.com)

DOI: 10.37789/rjce.2021.12.4.8

**Rezumat.** Implementarea măsurilor de apărare împotriva incendiilor în contextul legislației actuale, presupune identificarea unui set de măsuri legislative și norme tehnice specifice domeniului de activitate și implementarea standardizată în toate etapele de proiectare, execuție, punere în funcțiune și exploatare a clădirilor civile. Totodată, factorii de decizie pentru fiecare etapă enumerată anterior răspund de modul de implementare a normelor tehnice și a măsurilor necesare asigurării securității la incendiu a tuturor lucrătorilor și utilizatorilor din construcțiile civile.

**Cuvinte cheie:** lucrător, loc de muncă, incendiu, măsuri specifice, intervenție.

**Abstract.** Implementing the fire protection measures in the context of current legislation, involves the identification of a set of legislative measures and technical rules specific to the field of activity and standardized implementation in all stages of design, execution, commissioning and operation of civil buildings. At the same time, the decision makers for each stage listed above are responsible for the implementation of technical rules and measures necessary to ensure fire safety of all workers and users of civil buildings.

**Key words:** worker, job, fire, specific measures, intervention.

### 1. Introducere – analiza prevederilor legislative

Clădirile civile (publice) sunt construcții supraterane (cu sau fără subsoluri ori demisoluri) sau subterane, având următoarele destinații și funcțiuni: de locuit, administrație, comerț, sănătate, cultură, învățământ, sport, turism, etc<sup>1</sup>.

---

<sup>1</sup> Normativul de siguranță la foc a construcțiilor - Indicativ P 118-99

Măsurile de apărare împotriva incendiilor trebuie adoptate în documentațiile tehnice de proiectare pentru îndeplinirea cerinței esențiale securitate la incendiu a construcțiilor, instalațiilor și altor amenajări și sunt verificate de specialiștii inspectoratelor pentru situații de urgență în conformitate cu prevederile reglementărilor tehnice în vigoare, iar în baza documentațiilor specifice întocmite conform OMAI 129 din 2016 se emit *avize de securitate la incendiu*.

Conform legii nr. 307 din 12 iulie 2006 privind apărarea împotriva incendiilor, republicată în Monitorul Oficial nr. 297 din 17 aprilie 2019, *autorizația de securitate la incendiu* este actul administrativ emis de inspectoratul pentru situații de urgență județean sau al municipiului București, prin care se certifică, în urma verificărilor în teren și a documentelor *îndeplinirea cerinței esențiale securitate la incendiu* la construcții, instalații tehnologice și alte amenajări și realizarea măsurilor de apărare împotriva incendiilor.

Autorizația de securitate la incendiu conferă proprietarilor clădirilor civile dreptul de a le edifica, de a le pune în funcțiune și de a le exploata din punct de vedere al îndeplinirii cerinței esențiale *securitate la incendiu*.

Avizele și autorizațiile de securitate la incendiu se emit pentru construcții noi sau la efectuarea unor lucrări de modernizare sau extindere a celor existente. Având în vedere faptul că legislația dispune pentru viitor, pot să apară situații în care un obiectiv asupra căruia nu se fac lucrări de extindere sau modernizare să funcționeze fără a fi necesară autorizația de securitate la incendiu deși, pentru categoria de obiective din care el face parte, acest document este necesar. Astfel, două obiective de același tip se pot regăsi în situația în care unul să dețină autorizație de securitate la incendiu și să fie construit și echipat cu instalații de limitare și stingere a incendiilor conform normativelor în vigoare, în timp ce celălalt să nu corespundă acestor normative dar să funcționeze legal din punct de vedere al securității la incendiu. În acest ultim caz pentru a menține un risc la incendiu acceptabil pentru utilizatorii construcției administratorul trebuie să asigure respectarea cu strictețe a măsurilor organizatorice privind apărarea împotriva incendiilor.

La terminarea lucrărilor de construcții aferente clădirilor civile cu săli aglomerate, înalte, foarte înalte, din categoria de importanță excepțională sau deosebită, de producție și/sau depozitare cu suprafețe desfășurate de peste 5.000 mp și risc mare sau foarte mare de incendiu, centrelor comerciale cu suprafața desfășurată de peste 2.500 mp, parcajelor cu mai mult de 100 de locuri de parcare pentru autoturisme, clădirilor de turism având capacitatea mai mare de 50 de locuri de cazare, spitalelor, căminelor pentru copii și bătrâni sau altor clădiri destinate persoanelor ce nu se pot evacua singure se face recepția, iar investitorii sunt obligați să solicite în scris și să includă în comisia de recepție, în calitate de membru, o persoană desemnată de inspecțiile de prevenire din cadrul inspectoratelor pentru situații de urgență<sup>2</sup>.

Procesul-verbal de recepție va consemna realizarea măsurilor de securitate la incendiu prevăzute în documentația de execuție fără de care recepția nu este acceptată.

---

<sup>2</sup> Conform art. 31, alin (1) din Legea nr. 307 din 12 iulie 2006 privind apărarea împotriva incendiilor, republicată în Monitorul Oficial nr. 297 din 17 aprilie 2019

Măsurile în domeniul apărării împotriva incendiilor stabilite prin scenariul de securitate la incendiu trebuie să se reflecte în piesele desenate ale documentațiilor de proiectare și execuție, iar măsurile organizatorice trebuie să se regăsească în actele de autoritate privind apărarea împotriva incendiilor<sup>3</sup>.

Scenariile de securitate la incendiu se includ în documentațiile tehnice ale construcțiilor și se păstrează de către utilizatori (investitori, proprietari, beneficiari, administratori etc.) pe toată durata de existență a construcțiilor și amenajărilor, iar în baza lor se întocmesc de către administrator, persoane autorizate, servicii de specialitate, SVSU sau SPSU *documentele de autoritate*.

Persoanele fizice și juridice răspund, potrivit legii, de stabilirea și aplicarea măsurilor de apărare împotriva incendiilor, precum și de consecințele producerii incendiilor și sunt obligate să respecte reglementările tehnice și dispozițiile de apărare împotriva incendiilor și să nu primejduiască, prin deciziile și faptele lor, viața, bunurile și mediul înconjurător.

Organizarea intervenției în caz de incendiu cuprinde totalitatea măsurilor tehnico-organizatorice necesare stabilirii forțelor, responsabilităților, sarcinilor, mijloacelor, metodelor și procedeele ce pot fi utilizate pentru evacuarea și salvarea persoanelor și animalelor, protecția bunurilor și vecinătăților, precum și pentru stingerea incendiilor.

Organizarea intervenției în caz de incendiu cuprinde organizarea intervenției pe locurile de muncă, organizarea intervenției de către SVSU și SPSU și nu în ultimul rând, organizarea intervenției echipajelor ISU, conform prevederilor legale.

Orice persoană care observă un incendiu are obligația conform legii apărării împotriva incendiilor să anunțe prin orice mijloc serviciile de urgență, primarul sau poliția și să ia măsuri, după posibilitățile sale, pentru limitarea și stingerea acestuia.

## 2. Analiza riscului de incendiu

Riscul de incendiu reprezintă probabilitatea izbucnirii incendiilor în spații, încăperi, construcții sau compartimente de incendiu ori instalații și este identificat și evaluat în Scenariul de securitate la incendiu. Structura cadru a Scenariului de securitate la incendiu se regăsește la anexa nr. 1 din Normele metodologice privind avizarea și autorizarea de securitate la incendiu și protecție civilă, aprobate cu OMAI nr. 129/2016.

La clădirile civile (publice) riscul de incendiu este determinat în funcție destinația clădirii respective și de densitatea sarcinii termice ( $q$ ) stabilită prin calcul, conform SR 10903-2:2016, și poate fi<sup>4</sup>:

- mare:  $q_i = \text{peste } 840 \text{ MJ/m}^2$ ;
- mijlociu:  $q_i = 420 \div 840 \text{ MJ/m}^2$ ;
- mic:  $q_i = \text{sub } 420 \text{ MJ/m}^2$ .

<sup>3</sup> Aurel TROFIN, Optimizarea salvării persoanelor în caz de incendiu, din construcții, prin modelarea competențelor specifice - Revista Română de Inginerie Civilă, Volumul 10 (2019), Nr. 2, Editura MatrixRom, pag. 148-159, <http://www.rric.ro/revista.php?id=28>

<sup>4</sup> Normativ de siguranță la foc a construcțiilor - Indicativ P 118-99



În funcție de destinație (funcțiune), unele spații și încăperi din clădirile civile (publice) se încadrează în următoarele riscuri de incendiu:

- mare: în care se utilizează, sau depozitează materiale sau substanțe combustibile (arhive, biblioteci, birouri, parcaje etc.);
- mijlociu: în care se utilizează foc deschis (bucătării, centrale termice, oficii cu preparări calde etc.);
- mic: celelalte încăperi și spații.

În încăperile și spațiile echipate cu instalații automate de stingere a incendiilor, riscurile mari de incendiu pot fi considerate mijlocii, iar riscurile mijlocii pot fi considerate mici. Pentru întregul compartiment de incendiu sau clădire, riscul de incendiu considerat va fi cel mai mare care reprezintă minimum 30% din volumul acestora.

### 3. Metoda de analiză 5 De ce (5 Why)?

Etapele pentru aplicarea Metodei de analiză 5 De ce (5 Why)? la implementarea măsurilor de apărare împotriva incendiilor sunt următoarele<sup>5</sup>:

1. Observarea și analiza problemei – efecte, mod de manifestare, sarcină de muncă prea vagă sau prea complexă pentru a fi ușor și rapid înțeleasă;
2. Clarificarea problemei;
3. Definirea problemei;
4. Identificarea cauzelor posibile;
5. Aplicarea metodei 5 De ce<sup>6</sup>?
  - De ce? – motivul;
  - De ce? – cauza aparentă;
  - De ce? – cauza cauzei anterioare;
  - De ce? – cauză succesivă;
  - De ce? – cauza de bază.
6. Identificarea soluțiilor posibile
7. Selectarea soluțiilor cele mai probabile.



#### 3.1. Evaluarea implementării cerințelor de securitate

Pentru fiecare clădire civilă nou construită sau existentă, se va evalua nivelul de implementare a cerințelor de securitate:

- Stabilirea (evaluarea) nivelului calitativ al investiției în funcție de bugetul disponibil și comanda socială – *Cartea tehnică a construcției* – implementarea cerințelor fundamentale aplicabile conform Legii nr. 10 din 18 ianuarie 1995, republicată privind calitatea în construcții, implementarea prevederilor Legii 50/1991, republicată și actualizată 2021, privind autorizarea executării lucrărilor de construcții, obținerea acordurilor și a

<sup>5</sup> <http://www.leanblog.ro/wp/instrumente-lean/instrumente-lean/instrumente-de-analiza/metoda-5-de-ce/>

<sup>6</sup> <https://www.bulsuk.com/2009/07/5-why-analysis-using-table.html>

avizelor, efectuarea recepției la terminarea lucrărilor de construcții, precum și a recepției finale la expirarea perioadei de garanție.

- Protecția pasivă la incendiu – implementarea prevederilor normativelor care se materializează printr-o protecție structurală stabilită de proiectant în faza de proiectare a unei clădiri/ construcții cu o anumită destinație, în funcție de: tipul construcției, suprafața construită, gradul de rezistență la foc, numărul de utilizatori și se materializează prin: compartimente de incendiu cu pereți rezistenți la foc/ antifoc; elemente de protecție a golurilor; utilizarea unor materiale incombustibile; limitarea clasei de combustibilitate a materialelor de construcție prin ignifugarea materialelor combustibile/ termoprotecția structurilor metalice; asigurarea căilor de evacuare, etc.; verificarea proiectelor prin diriginți de specialitate sau operatori economici de consultanță specializați.
- Protecția activă la incendiu – instalații automate de protecție / semnalizare care intră în funcțiune fără intervenția factorului uman, iar aceste instalații sunt: instalații automate de semnalizare, instalații automate de stins incendii, clapete antifoc montate pe tubulaturi de ventilație/ exhaustare, trape pentru evacuarea fumului și gazelor fierbinți, uși antifoc etc.; verificarea proiectelor prin specialiști verifikatori de proiecte atestați.
- Nivelul de satisfacere a cerințelor de securitate – Scenariul de securitate la incendiu prin care arhitectul trebuie să stabilească elementele specifice asigurării protecției active și pasive a clădirii civile și nivelul calitativ al construcției (investiției).
- Soluții care reduc efectele evenimentelor negative – organizarea apărării împotriva incendiilor conform documentelor de autoritate și instrucțiunilor proprii emise și implementarea măsurilor de apărare împotriva incendiilor, obiectivelor SMART și soluțiilor practice.

### ***3.2. Analiza obligațiilor privind apărarea împotriva incendiilor***

Legea nr. 307 din 12 iulie 2006 privind apărarea împotriva incendiilor, republicată în Monitorul Oficial nr. 297 din 17 aprilie 2019 stabilește o serie de obligații privind apărarea împotriva incendiilor, astfel:

–Prefectul (art. 16):

- instituie, în condițiile legii, măsuri obligatorii în domeniul apărării împotriva incendiilor.

–Consiliul local (art. 13):

- analizează, semestrial și ori de câte ori este nevoie, capacitatea de apărare împotriva incendiilor a unității administrativ-teritoriale pe care o reprezintă și informează inspectoratul cu privire la măsurile stabilite pentru optimizarea acesteia;
- instituie reguli și măsuri specifice corelate cu nivelul și natura riscurilor locale.

–Primarul (art. 14):

- asigură controlul respectării măsurilor de apărare împotriva incendiilor pe timpul adunărilor sau al manifestărilor publice;
  - asigură controlul respectării măsurilor de apărare împotriva incendiilor la construcțiile și instalațiile tehnologice aparținând domeniului public și privat al unității administrativ-teritoriale, precum și la instituțiile publice;
  - dispune verificarea îndeplinirii măsurilor stabilite prin avizele, autorizațiile și acordurile pe care le emite.
- Proiectanții de construcții civile (art. 23):
- elaborează scenarii de securitate la incendiu pentru construcțiile civile pe baza criteriilor emise de IGSU și evaluează riscurile de incendiu, pe baza metodologiei emise de IGSU;
  - includerea în documentațiile pe care le întocmesc măsurile de apărare împotriva incendiilor, specifice naturii riscurilor pe care le conțin construcțiile proiectate;
  - prevederea în documentațiile tehnice de proiectare, potrivit reglementărilor specifice, mijloacele tehnice pentru apărarea împotriva incendiilor și echipamentele de protecție specifice;
  - includerea în proiecte și predarea beneficiarilor schemele și instrucțiunile de funcționare a mijloacelor de apărare împotriva incendiilor pe care le-au prevăzut în documentații, precum și regulile necesare de verificare și întreținere în exploatare a acestora, întocmite de producători;
  - asigurarea asistenței tehnice necesară realizării măsurilor de apărare împotriva incendiilor, cuprinse în documentații, până la punerea în funcțiune.
- Executanții lucrărilor de construcții (art. 24):
- realizarea integrală și la timp a măsurilor de apărare împotriva incendiilor, cuprinse în proiecte, cu respectarea prevederilor legale aplicabile acestora;
  - asigurarea măsurilor de apărare împotriva incendiilor pe timpul executării lucrărilor, precum și la organizările de șantier;
  - asigurarea funcționării mijloacelor de apărare împotriva incendiilor prevăzute în documentațiile de execuție la parametrii proiectați, înainte de punerea în funcțiune.
- Cadrele tehnice/personalul de specialitate cu atribuții în domeniul apărării împotriva incendiilor (art. 27):
- participă la elaborarea și aplicarea concepției de apărare împotriva incendiilor la nivelul instituției sau operatorului economic;
  - controlează aplicarea normelor de apărare împotriva incendiilor în domeniul specific;
  - propun includerea în bugetele proprii a fondurilor necesare organizării activității de apărare împotriva incendiilor, dotării cu mijloace tehnice pentru apărarea împotriva incendiilor și echipamente de protecție specifice;
  - îndrumă și controlează activitatea de apărare împotriva incendiilor și analizează respectarea încadrării în criteriile de constituire a serviciilor de

urgență voluntare sau private, după caz, în unitățile și instituțiile din care fac parte;

- prezintă conducerii, semestrial sau ori de câte ori situația impune, raportul de evaluare a capacității de apărare împotriva incendiilor;
- răspund de pregătirea serviciului de urgență voluntar sau privat, după caz, precum și de participarea acestuia la concursurile profesionale;
- acordă sprijin și asistență tehnică de specialitate centrelor operative pentru situații de urgență în îndeplinirea atribuțiilor.

–Administratorul sau conducătorul instituției (art. 19):

- solicită și obține avizele și autorizațiile de securitate la incendiu, dacă clădirea sau unele spații își schimbă destinația;
- asigură identificarea, evaluarea și implementarea măsurilor de apărare împotriva incendiilor conform criteriilor stabilite prin ordine ale miniștrilor sau inspectorului general al IGSU;
- stabilește, prin dispoziții scrise, responsabilitățile și modul de organizare pentru apărarea împotriva incendiilor în unitatea sa, le actualizează ori de câte ori apar modificări și le aduce la cunoștință salariaților, utilizatorilor și oricăror persoane cu care colaborează;
- elaborează instrucțiunile de apărare împotriva incendiilor și stabilește atribuțiile ce le revin salariaților la locurile de muncă;
- asigură întocmirea și actualizarea planurilor de intervenție și condițiile pentru aplicarea acestora în orice moment;
- asigură utilizarea, verificarea, întreținerea și repararea mijloacelor de apărare împotriva incendiilor cu personal atestat, conform instrucțiunilor furnizate de proiectant;
- stabilește și transmite către transportatorii, distribuitorii și utilizatorii produselor sale regulile și măsurile de apărare împotriva incendiilor, specifice acestora, corelate cu riscurile la utilizarea, manipularea, transportul și depozitarea produselor respective;
- verifică dacă salariații cunosc și respectă instrucțiunile necesare privind măsurile de apărare împotriva incendiilor și verifică respectarea acestor măsuri semnalate corespunzător prin indicatoare de avertizare de către persoanele din exterior care au acces în unitatea sa.

–Persoanele fizice, asociațiile familiale sau persoanele juridice care dețin părți din același imobil (art. 20):

- trebuie să colaboreze pentru îndeplinirea obligațiilor ce le revin din legea apărării împotriva incendiilor, în vederea asigurării măsurilor de apărare împotriva incendiilor pentru întregul imobil.

–Utilizatorul (art. 21):

- respectă normele de apărare împotriva incendiilor, specifice activităților pe care le organizează sau le desfășoară;
- cunoaște și respectă măsurile de apărare împotriva incendiilor, stabilite prin actele de autoritate și instrucțiuni proprii;

- întreține și folosește, în scopul pentru care au fost realizate, dotările pentru apărarea împotriva incendiilor;
  - aduce la cunoștința administratorului, conducătorului instituției sau proprietarului, după caz, orice defecțiune tehnică ori altă situație care constituie pericol de incendiu.
- Fiecare salariat la locul de muncă (art. 22):
- respectă regulile și măsurile de apărare împotriva incendiilor, stabilite prin actele de autoritate și instrucțiuni proprii;
  - utilizează substanțele periculoase, instalațiile, utilajele, mașinile, aparatura și echipamentele, potrivit instrucțiunilor tehnice, precum și celor date de administrator sau de conducătorul instituției, după caz;
  - nu efectuează manevre nepermise sau modificări neautorizate ale sistemelor și instalațiilor de apărare împotriva incendiilor;
  - comunică, imediat după constatare, conducătorului locului de muncă orice încălcare a normelor de apărare împotriva incendiilor sau a oricărei situații stabilite de acesta ca fiind un pericol de incendiu, precum și orice defecțiune sesizată la sistemele și instalațiile de apărare împotriva incendiilor;
  - cooperează cu salariații desemnați de administrator, după caz, respectiv cu cadrul tehnic specializat, care are atribuții în domeniul apărării împotriva incendiilor, în vederea realizării măsurilor de apărare împotriva incendiilor;
  - acționează în conformitate cu procedurile stabilite la locul de muncă, în cazul apariției oricărui pericol iminent de incendiu;
  - furnizează persoanelor abilitate toate datele și informațiile de care are cunoștință, referitoare la producerea incendiilor.

### 3.3. Evaluarea răspunderii juridice

Încălcarea dispozițiilor Legii nr. 307 din 12 iulie 2006 privind apărarea împotriva incendiilor atrage răspunderea disciplinară, contravențională, materială, civilă sau penală, după caz, astfel<sup>7</sup>:

*Tabelul 1*

#### **Sanționarea nerespectării și neimplementării măsurilor de apărare împotriva incendiilor**

<b>Contravenție, amendă (valoare)</b>	<b>Fapte care se sancționează</b>	<b>Articolul din lege vizat</b>
de la 500 lei la 1.000 lei	- necooperarea persoanelor fizice sau juridice care dețin părți din același imobil în vederea asigurării măsurilor de apărare împotriva incendiilor.	- art. 9; art. 20
de la 1.001 lei la 2.500 lei	- neanunțarea, prin orice mijloc, a serviciilor de urgență, a primarului sau a poliției de către persoana care observă un incendiu și, după caz, neluarea măsurilor, după posibilitățile sale, pentru limitarea și stingerea incendiului;	- art. 6, pct. 2

<sup>7</sup> Legea nr. 307 din 12 iulie 2006 privind apărarea împotriva incendiilor, republicată în Monitorul Oficial nr. 297 din 17 aprilie 2019

#### Analiza implementării măsurilor de apărare împotriva incendiilor în clădiri civile

	- nerespectarea de către primar, administrator sau conducătorul instituției a obligațiilor de încadrare a serviciului de urgență voluntar sau privat cu personal atestat în condițiile legii, de pregătire profesională și antrenare a acestuia pentru intervenție.	- art. 14, lit. b; art. 19, lit. i și lit. n; art. 33, pct. 3
de la 2.501 lei la 5.000 lei	- necunoașterea și nerespectarea de către utilizator a măsurilor de apărare împotriva incendiilor, stabilite de administrator, proprietar, producător sau importator, după caz.	- art. 21, lit. a
de la 5.001 lei la 10.000 lei	- neinclusiunea măsurilor de apărare împotriva incendiilor, cuprinse în proiecte, cu respectarea condițiilor de calitate prevăzute de lege.	- art. 23, lit. b
de la 20.000 lei la 50.000 lei	- începerea lucrărilor de execuție la construcții și amenajări noi, de modificare a celor existente și/sau schimbarea destinației acestora, fără obținerea avizului de securitate la incendiu; - punerea în funcțiune a construcțiilor și amenajărilor noi ori a celor existente la care s-au executat lucrări de modificare și/sau s-a schimbat destinația acestora, fără obținerea autorizației de securitate la incendiu; - funcționarea serviciilor de urgență private după anularea avizului de înființare și/sau avizului pentru sectorul de competență.	- art. 30, pct. 1 - art. 30, pct. 2 - art. 33, pct. 6
de la 30.000 lei la 100.000 lei și oprirea funcționării ori utilizării construcțiilor sau amenajărilor*	- încălcarea gravă a cerinței de securitate la incendiu în ceea ce privește periclitarea vieții ocupanților și forțelor de intervenție, neasigurarea stabilității elementelor portante, respectiv a limitării propagării focului și fumului în interiorul edificiului și la vecinătăți, potrivit criteriilor stabilite prin HGR nr. 915/2015 <sup>8</sup>	- art. 30, pct. 13

\* - sancțiune contravențională complementară

Contravenientul poate achita, în termen de cel mult 15 zile de la data înmânării sau comunicării procesului-verbal de contravenție, jumătate din cuantumul amenzii aplicate de agentul constatator, conform prevederilor art. 28, pct. 1 din Ordonanța nr. 2 din 12 iulie 2001 privind regimul juridic al contravențiilor, cu modificările și actualizările ulterioare.

#### 3.4. Analiza organizării apărării împotriva incendiilor la locul de muncă

Organizarea apărării împotriva incendiilor la locul de muncă, conform Normelor generale de apărare împotriva incendiilor aprobate prin OMAI nr. 163 din 28 februarie, constă în:

- prevenirea incendiilor, prin luarea în evidență a materialelor și dotărilor tehnologice care prezintă pericol de incendiu, a surselor posibile de aprindere ce

<sup>8</sup> a se vedea prevederile Hotărârii Guvernului nr. 915/2015 privind stabilirea criteriilor pentru oprirea funcționării ori utilizării construcțiilor sau amenajărilor, publicată în Monitorul Oficial al României, Partea I, nr. 824 din 4 noiembrie 2015.

pot apărea și a mijloacelor care le pot genera, precum și prin stabilirea și aplicarea măsurilor specifice de prevenire a incendiilor:

- *materiale combustibile* – densitatea de sarcină termică – riscul de incendiu – Scenariul de securitate la incendiu/Evaluare de risc de incendiu;
- *dotările tehnologice* – tensiuni de lucru (supraîncărcarea circuitelor electrice) – pozarea conductorilor electrici – tablouri electrice – siguranțe fuzibile, zone cu pericol de explozie (instalații de gaze și consumatori) – verificări periodice și măsuri suplimentare specifice;
- *surse probabile de aprindere*, conform statisticilor cele mai frecvente cauze de incendiu sunt de natură electrică, iar în perioada rece datorită surselor de încălzire;
- *mijloacele care pot genera incendii* – verificare la terminarea programului de muncă – verificare periodică – asigurarea mentenanței;
- *cerințe minime de securitate* – Hotărârea nr. 1.091 din 16 august 2006 privind cerințele minime de securitate și sănătate pentru locul de muncă<sup>9</sup>;
- *stabilirea și aplicarea măsurilor specifice de prevenire a incendiilor* – dispoziții implementate – verificare – evaluare – control.
- organizarea intervenției de stingere a incendiilor:
  - stabilirea atribuțiilor salariaților pe locurile de muncă definite în *legea apărării împotriva incendiilor*, astfel încât în cazul unui incendiu să pună în aplicare procedurile specifice de intervenție în caz de incendiu;
  - verificarea periodică a mijloacelor tehnice pentru prima intervenție – stingătoare de incendiu - hidranți interiori - pătură antifoc - ball fire etc.;
  - Planul de evacuare – afișare - verificarea atribuțiilor la exercițiile organizate;
  - Planul de intervenție – simularea periodică a unor scenarii complexe (evacuarea persoanelor și bunurilor de valoare, stingerea unor incendii în fază incipientă, acordarea primului ajutor medical de urgență).
- afișarea instrucțiunilor de apărare împotriva incendiilor și atribuțiilor salariaților la locurile de muncă:
  - actele de autoritate privind apărarea împotriva incendiilor emise de administratorul operatorului economic/conducătorul instituției și semnarea într-un tabel a tuturor salariaților de luare la cunoștință;
  - afișarea instrucțiunilor și planurilor de evacuare în locuri vizibile pentru locurile de muncă definite conform legii apărării împotriva incendiilor.
- organizarea salvării utilizatorilor și a evacuării bunurilor, prin întocmirea și afișarea planurilor de protecție specifice și prin menținerea condițiilor de evacuare pe traseele stabilite:
  - studiu individual și documentarea pe platforme digitale (facebook, youtube, bloguri de specialitate, site-uri ISUJ, IGSU, DSU etc.);

<sup>9</sup> <https://www.inspectiamuncii.ro/-/legislatie-s-1>

#### Analiza implementării măsurilor de apărare împotriva incendiilor în clădiri civile

- antrenamente pentru evacuarea de urgență, evacuarea accidentaților și evacuarea tuturor utilizatorilor în caz de incendiu;
- traseele de evacuare, marcaje, pictograme, lămpi de evacuare.
- elaborarea documentelor specifice de instruire la locul de muncă, desfășurarea propriu-zisă și verificarea efectuării acestora:
  - instrucțiuni specifice de apărare împotriva incendiilor;
  - tematica stabilită pentru instruirea în domeniu;
  - studiu individual, prezentări de filmulețe etc
  - teste anuale de specialitate.
- marcarea pericolului de incendiu prin montarea indicatoarelor de securitate sau a altor inscripții ori mijloace de atenționare:
  - marcarea prizelor cu tensiuni 230V / 400V;
  - indicatoare de securitate conform HGR nr. 971 din 26 iulie 2006 privind cerințele minime pentru semnalizarea de securitate și/sau de sănătate la locul de muncă.

Cadrele tehnice sau personalul de specialitate cu atribuții în domeniul apărării împotriva incendiilor vor prezenta conducerii, semestrial sau ori de câte ori situația impune, raportul de evaluare a capacității de apărare împotriva incendiilor, iar acesta trebuie să cuprindă cel puțin următoarele probleme analizate: implementarea noilor prevederi legislative, stadiul îndeplinirii măsurilor stabilite la controalele interne sau ISU, deficiențele ce se manifestă în domeniul apărării împotriva incendiilor, concluziile rezultate din activitatea de instruire și pregătire a personalului, relațiile cu terții privind apărarea împotriva incendiilor, asigurarea dotării, calitatea și funcționarea mijloacelor tehnice de apărare împotriva incendiilor, eficiența activităților desfășurate de structurile cu atribuții în domeniul apărării împotriva incendiilor și măsurile propuse pentru îmbunătățirea activității.

### 3.5. Analiza și aplicarea Metodei 5 De ce (5 Why)?

Tabelul 2

Aplicarea Metodei de analiză 5 De ce?

Întrebare primară	Întrebare secundară se aplică metoda "5 De ce (Why)"
Ce (What) activități sunt necesare pentru implementarea măsurilor de apărare împotriva incendiilor?	<b>De ce</b> sunt necesare toate activitățile? - instruirea în domeniul securității și sănătății în muncă și situațiilor de urgență: <ul style="list-style-type: none"> <li>○ tematica stabilită conform caracteristicilor tehnice ale construcțiilor și tehnologiilor existente;</li> <li>○ instrucțiunile specifice de apărare împotriva incendiilor;</li> <li>○ vizionarea de filmulețe pentru acordarea primului ajutor (manualul de prim ajutor în format video) și de stingere a incendiilor în fază incipientă (utilizând stingătoare și hidranții interiori de incendiu);</li> <li>○ teste de specialitate;</li> </ul>
Evaluare	- procedura specifică la terminarea programului de lucru; - evidența registrelor instalațiilor de detectare/semnalizare/stingere a incendiilor și a registrului pentru evidența permiselor de lucru cu



	<p>focul;</p> <ul style="list-style-type: none"> <li>- graficele de întreținere și verificare pentru diferite categorii de utilaje, instalații și sisteme care pot genera incendii sau care se utilizează în caz de incendiu;</li> <li>- executarea exercițiilor de stingere și evacuare în caz de incendiu, conform procedurilor;</li> <li>- executarea unor exerciții de acordare a primului ajutor medical de urgență fără echipamente sau cu ajutorul materialelor sanitare din trusa de prim ajutor;</li> <li>- rapoartele întocmite în urma controalelor preventive proprii sau ale ISU – planul de măsuri propuse;</li> <li>- raportul anual de evaluare a nivelului de apărare împotriva incendiilor.</li> </ul>
<b>Unde</b> (Where) sunt organizate?	<p><b>De ce</b> sunt organizate în acele locuri?</p> <ul style="list-style-type: none"> <li>- organizarea activităților de instruire, exercițiilor de acordare a primului ajutor medical de urgență și evacuare în caz de incendiu la sediul operatorului economic sau instituției publice;</li> <li>- organizarea unor exerciții de stingere a incendiilor în fază incipientă într-un centru de formare al SVSU, SPSU sau ISU.</li> </ul>
<b>Când</b> (When) se face?	<p><b>De ce</b> este făcută în acel moment?</p> <ul style="list-style-type: none"> <li>- conform Dispozițiilor generale privind instruirea salariaților în domeniul situațiilor de urgență, aprobate cu OMAI nr. 712 din 2005, modificate și completate cu OMAI 786 din 2005;</li> <li>- dispoziții interne (acte de autoritate, conform Legii 307 din 2006 cu actualizările și completările ulterioare și conform OMAI 163/2007).</li> </ul>
<b>Cine</b> (Who) o face?	<p><b>De ce</b> este făcută de acea persoană?</p> <ul style="list-style-type: none"> <li>- formarea unui specialist din cadrul obiectivului și organizarea activităților la sediu;</li> <li>- colaborarea cu un specialist și organizarea activităților la sediu*;</li> <li>- contractarea unui serviciu de specialitate și organizarea activităților la sediul acestuia și/sau sediul solicitantului;</li> <li>- realizarea unui protocol cu un SVSU, SPSU, ISU și organizarea unor activități periodice.</li> </ul>
<b>Cum</b> (How) este făcută? Este bine așa?	<p><b>De ce</b> este făcută în acel mod?</p> <ul style="list-style-type: none"> <li>- de frica sancționării de către inspectorii ISU prin aplicarea unor amenzi conform legii apărării împotriva incendiilor;</li> <li>- evaluarea materialelor, instrucțiunilor, procedurilor, accesoriilor, echipamentelor și a posibilităților de lucru;</li> <li>- administratorul sau conducătorul instituției răspunde de organizarea tuturor activităților de organizare și implementare a măsurilor de apărare împotriva incendiilor;</li> <li>- utilizatorul și fiecare salariat sunt obligați să cunoască și să respecte măsurile de apărare împotriva incendiilor;</li> <li>- salariatul trebuie să acționeze, în conformitate cu procedurile stabilite la locul de muncă, în cazul apariției oricărui pericol iminent de incendiu.</li> </ul>

\* - de verificat prevederile Criteriilor de stabilire a consiliilor locale și operatorilor economici care au obligația de a angaja cel puțin un cadru tehnic sau personal de specialitate cu atribuții în domeniul apărării împotriva incendiilor, aprobate cu OMAI nr. 106/2007.

Modelul de analiză prezentat în tabelul de mai sus ”5 De ce? corelat cu analiza 5 W” prezintă în tablou ușor de vizualizat și de monitorizat, iar elementele cheie

identificate trebuie să fie reevaluate periodic și să fie identificate soluții practice de implementat, astfel încât, obiectivele SMART stabilite la implementarea măsurilor de apărare împotriva incendiilor să fie realizate și cuantificate.

#### 4. Securitatea locului de muncă

Conform Hotărârii Guvernului nr. 1.091 din 16 august 2006 au fost stabilite cerințe minime de securitate și sănătate pentru locurile de muncă, astfel:

- instalațiile electrice, termice, sanitare și de ventilare trebuie să fie proiectate și realizate astfel încât să nu prezinte pericol de incendiu sau explozie;
- zonele periculoase trebuie marcate clar cu indicatoare conform Hotărârii nr. 971 din 26 iulie 2006;
- ușile de ieșire în caz de urgență trebuie să fie semnalizate corespunzător, să se deschidă spre exterior și nu trebuie să fie încuiate;
- căile și ieșirile de urgență care necesită iluminare trebuie prevăzute cu iluminat de siguranță de intensitate suficientă, în cazul în care se întrerupe alimentarea cu energie electrică;
- căile și ieșirile de urgență trebuie să rămână în permanență libere și să conducă în mod cât mai direct posibil în aer liber sau în spații sigure;
- în caz de pericol, trebuie să fie posibilă evacuarea rapidă și în condiții cât mai sigure a lucrătorilor de la toate posturile de lucru;
- în funcție de dimensiunile și destinația clădirilor, de echipamentele pe care acestea le conțin, de proprietățile fizice și chimice ale substanțelor prezente și de numărul maxim potențial de persoane prezente, locurile de muncă trebuie prevăzute cu dispozitive corespunzătoare pentru stingerea incendiilor și, dacă este cazul, cu detectoare de incendii și sisteme de alertare;
- angajatorul va numi prin decizie o persoană cu atribuții concrete care să supravegheze lucrătorii care lucrează în condiții de izolare;
- pentru a se putea interveni în timp util în caz de accident sau avarie la locurile de muncă în condiții de izolare, acestea vor fi dotate cu mijloace tehnice care permit legătura cu persoana care asigură supravegherea:
  - constant automat (centrale de supraveghere, dispozitive de alarmare prin unde radio);
  - periodic automat (radio-telefon, telefon);
  - periodic prin intermediul unei persoane (apeluri telefonice, radio-telefon, cameră de luat vederi și monitor).
- locurile de muncă trebuie dotate cu echipamente de prim ajutor, iar acestea trebuie să fie marcate corespunzător și să fie ușor accesibile;
- conform legii nr. 349 din 2002, cu modificările și completările ulterioare, pentru prevenirea incendiilor se interzice fumatul în toate spațiile publice închise și spațiile închise de la locul de muncă. Fumatul este permis numai în camere special amenajate care servesc exclusiv fumului, nu sunt spații de trecere sau de acces în spații publice închise, sunt dotate cu sisteme de ventilație

cu presiune negativă, ce asigură evacuarea fumului de tutun, dispun de scrumiere și stingătoare, sunt amenajate în conformitate cu prevederile legale în vigoare privind prevenirea și stingerea incendiilor și marcate la loc vizibil cu indicatoare: ”Cameră pentru fumat” sau ”Loc pentru fumat”.

#### 4.1. Analiza și aplicarea Metodei 5 S



Aplicarea principiilor 5S pentru locurile de muncă și asigurarea securității la incendiu (a sorta – *sort*, a ordona – *set in order*, a da strălucire – *shine*, a standardiza – *standardize* și a susține – *sustain*)<sup>10</sup> presupune evaluarea următoarelor probleme.

Tabelul 3

Aplicarea Metodei de analiză 5 S

5S + SIGURANȚA	
	<b>SORTARE</b> <ul style="list-style-type: none"> <li>- legislație, normative, proceduri;</li> <li>- cele mai bune practici de apărare împotriva incendiilor;</li> <li>- cele mai bune măsuri de apărare împotriva incendiilor implementate;</li> <li>- evaluarea și implementarea procedeele de lucru la punerea în funcțiune a unor instalații, la manipularea unor substanțe chimice periculoase, la terminarea programului de lucru;</li> <li>- antrenamente specifice de evacuare a persoanelor și a unor substanțe periculoase, de stingere a incendiilor în fază incipientă, de acordare a primului ajutor medical de urgență.</li> </ul>
	<b>SISTEMATIZARE</b> <ul style="list-style-type: none"> <li>- prevederea unui buget pentru apărarea împotriva incendiilor;</li> <li>- angajarea unui cadru tehnic, specializarea unui angajat ori contractarea unui serviciu specializat;</li> <li>- analizarea actelor de autoritate și a instrucțiunilor proprii de apărare împotriva incendiilor;</li> <li>- evaluarea parametrilor tehnologici în limitele normate, pe timpul exploatării diferitelor instalații, echipamente și utilaje tehnologice;</li> <li>- implementarea unor soluții tehnice pentru reducerea riscului de incendiu;</li> <li>- evaluarea Planului de intervenție, a Planurilor de evacuare și a responsabililor cu asigurarea, protejarea și evacuarea persoanelor și bunurilor în caz de incendiu;</li> <li>- diseminarea rapoartelor întocmite în urma controalelor preventive proprii sau ale ISU – planul de măsuri propuse;</li> <li>- diseminarea raportului anual de evaluare a nivelului de apărare împotriva incendiilor;</li> <li>- evidența registrelor instalațiilor de detectare/semnalizare/stingere a incendiilor și a registrului pentru evidența permiselor de lucru cu focul;</li> <li>- graficele de întreținere și verificare pentru diferite categorii de utilaje, instalații și sisteme care pot genera incendii sau care se utilizează în caz de incendiu;</li> <li>- instruirea personalului într-un mod organizat – șefii locurilor de muncă;</li> <li>- executarea exercițiilor cu sprijinul SPSU, SVSU sau ISU.</li> </ul>
	<b>STRĂLUCIRE</b> <ul style="list-style-type: none"> <li>- responsabilizarea persoanelor pe locurile de muncă;</li> <li>- evaluarea și stabilirea de sarcini și măsuri de implementat;</li> <li>- afișarea instrucțiunilor, planurilor de evacuare, marcarea căilor de evacuare cu</li> </ul>

<sup>10</sup> [https://trilogiq.ro/app/uploads/2017/07/TR\\_RO\\_5S-Safety\\_Poster-01.pdf](https://trilogiq.ro/app/uploads/2017/07/TR_RO_5S-Safety_Poster-01.pdf)

	indicatoare de securitate.
	<b>STANDARDIZARE</b> <ul style="list-style-type: none"> <li>- implementarea procedurilor și reevaluarea periodică;</li> <li>- Planul de intervenție și Planurile de evacuare;</li> <li>- raportul anual de evaluare a nivelului de apărare împotriva incendiilor;</li> <li>- planul de măsuri propuse în urma controalelor preventive proprii sau ale ISU.</li> </ul>
	<b>SUSȚINEREA SCHIMBĂRII</b> <ul style="list-style-type: none"> <li>- ghidare după maxima ”mai bine previi decât să intervii”;</li> <li>- lucrătorul de la locul de muncă este ”un membru al familiei locului de muncă”, este o persoană importantă și trebuie să își asigure protecția și să asigure securitatea locului de muncă;</li> <li>- reevaluarea și actualizarea documentelor specifice de apărare împotriva incendiilor;</li> <li>- verificarea, reevaluarea și actualizarea atribuțiilor stabilite în documentații;</li> <li>- asigurarea continuității instructajelor și antrenamentelor specifice și obținerea unui feedback din partea lucrătorilor;</li> <li>- debriefing după fiecare activitate.</li> </ul>

În procesul de management al schimbării fiecare etapă din sistemul ”5S” se bazează pe etapa anterioară și astfel se obțin cele mai bune rezultate, metoda fiind ciclică, iar avantajele implementării metodei vizează: creșterea eficienței, îmbunătățirea calității și a evaluării sistemelor, eficientizarea ergonomiei, motivarea personalului și reducerea costurilor<sup>11</sup>.

#### 4.2. Evaluarea culorilor de securitate

Conform Hotărârii nr. 971 din 26 iulie 2006 privind cerințele minime pentru semnalizarea de securitate și/sau de sănătate la locul de muncă, semnalizarea referitoare la o interdicție, un avertisment sau o obligație, precum și semnalizarea privind localizarea și identificarea mijloacelor de salvare ori prim ajutor trebuie să se realizeze prin utilizarea panourilor (indicatoare) permanente.

Astfel, culorile de securitate din tabelul de mai jos se aplică tuturor mijloacelor de semnalizare:

Tabelul 4

##### Aplicarea culorilor pentru semnalizarea de securitate și/sau de sănătate la locul de muncă

Culoare	Semnificație sau scop	Indicații și precizări
Roșu	Semnal de interdicție	Atitudini periculoase
	Pericol-alarma	Stop, oprire, dispozitiv de oprire de urgență Evacuare
	Materiale și echipamente de prevenire și stingere a incendiilor	Identificare și localizare
Galben sau galben-oranj	Semnal de avertizare	Atenție, precauție Verificare
Albastru	Semnal de obligație	Comportament sau acțiune specifică Obligația purtării echipamentului individual de protecție
Verde	Semnal de salvare sau de prim ajutor	Uși, ieșiri, căi de acces, echipamente, posturi, încăperi

<sup>11</sup> <https://www.intermanagement.eu/resurse/Principiile+metodei+japoneze+5+S>

Lucrătorilor trebuie să li se asigure o instruire corespunzătoare cu privire la semnalizarea de securitate ce va cuprinde semnificația semnalizării și comportamentul general și specific ce trebuie adoptat în caz de producerea unui eveniment negativ.

#### 4.3. Procedura de stingere a incendiilor la locul de muncă

Responsabilul cu modul de organizare a intervenției de stingere a incendiilor în cazul clădirilor civile este administratorul societății comerciale sau conducătorul instituției, iar etapele intervenției de stingere a incendiilor la locul de muncă sunt următoarele<sup>12</sup>:

Tabelul 5

Procedura de stingere a incendiilor la locul de muncă

Etaple intervenției de stingere a incendiilor la locul de muncă	
	<b>ALARMAREA PERSONALULUI</b> <ul style="list-style-type: none"> <li>- este alarmat imediat personalul de la locul de muncă prin mijloace specifice: <ul style="list-style-type: none"> <li>- instalația de detectare, semnalizare, alertare și alarmare;</li> <li>- sistem audio – mesaje preînregistrate;</li> <li>- sirenă.</li> </ul> </li> </ul>
	<b>ANUNȚAREA INCENDIULUI</b> <ul style="list-style-type: none"> <li>- anunțarea incendiului la 112 - forțele de intervenție ISU;</li> <li>- anunțarea la dispecerat SPSU, SVSU.</li> </ul>
	<b>SALVAREA PERSOANELOR</b> <ul style="list-style-type: none"> <li>- salvarea rapidă și în siguranță a personalului surprins de incendiu, conform planurilor de evacuare și a planului de intervenție;</li> <li>- verificarea numărului de lucrători prezenți;</li> <li>- evacuarea de urgență.</li> </ul>
	<b>ÎNTRERUPEREA ALIMENTĂRII UTILITĂȚILOR</b> <ul style="list-style-type: none"> <li>- întreruperea alimentării cu energie electrică, gaze și fluide combustibile a consumatorilor;</li> <li>- intervenții specifice la instalații și utilaje de către personalul desemnat pe locurile de muncă.</li> </ul>
	<b>ASIGURAREA PROTECȚIEI PERSONALULUI</b> <ul style="list-style-type: none"> <li>- asigurarea protecției personalului de intervenție împotriva efectelor negative al incendiului: temperatură, fum, gaze toxice etc.</li> </ul>
	<b>STINGEREA INCENDIULUI ÎN FAZĂ INCIPIENTĂ</b> <ul style="list-style-type: none"> <li>- se acționează asupra focarului de incendiu cu mijloacele tehnice de apărare împotriva incendiilor din dotare;</li> <li>- se verifică intrarea în funcțiune a instalațiilor și a sistemelor automate de detectare/semnalizare/stingere sau se acționează manual.</li> </ul>
	<b>EVACUAREA/PROTECȚIA BUNURILOR</b> <ul style="list-style-type: none"> <li>- se evacuează bunurile de valoare care pot fi afectate de incendiu;</li> <li>- se evacuează/se protejează substanțele chimice periculoase care pot contribui la dezvoltarea violentă a incendiului;</li> <li>- dacă se asigură protecția personalului de pe locul de muncă se protejează echipamentele care pot fi deteriorate în timpul intervenției.</li> </ul>

<sup>12</sup> <https://legislatiamuncii.manager.ro/a/20973/psi-organizarea-interventiei-de-stingere-a-incendiilor-la-locul-de-munca.html>



#### VERIFICAREA UNOR FOCARE ASCUNSE

- se verifică amănunțit locurile în care se poate propaga incendiul și unde pot apărea focare noi;
- se vor stinge focarele identificate sau se va răci zona afectată.

Procedura de stingere a incendiilor la locul de muncă propusă în tabelul nr. 5 poate fi afișată în proximitatea planului de evacuare în caz de incendiu. Pentru fiecare etapă a intervenției, se vor stabili persoane care răspund de modul de îndeplinire a atribuțiilor, procedura va fi verificată periodic pe timpul desfășurării unor exerciții de stingere a incendiilor și analizată în raportul de evaluare a capacității de apărare împotriva incendiilor.

## 5. Concluzii

Exercitarea autorității de stat în domeniul apărării împotriva incendiilor se realizează prin activități de reglementare, autorizare, avizare, atestare, recunoaștere, desemnare, supraveghere a pieței, control, organizarea stingerii incendiilor și tragerea la răspundere juridică a persoanelor vinovate.

Controlul de stat în domeniul apărării împotriva incendiilor se exercită, la nivel central, prin inspecția de prevenire și alte compartimente și unități din structura sau subordinea Inspectoratului General pentru Situații de Urgență, respectiv, la nivel local, prin inspecțiile de prevenire din cadrul inspectoratelor, în scopul aplicării unitare a prevederilor legale pe întregul teritoriu al României, potrivit competențelor.

O construcție care este autorizată din punct de vedere al securității la incendiu asigură un nivel de securitate la incendiu crescut pentru utilizatorii săi, iar implementarea măsurilor de apărare împotriva incendiilor prin actele de autoritate și instrucțiuni proprii sunt necesare pentru a evita apariția unor incendii atât pentru construcțiile autorizate cât și pentru cele neautorizate.

Planurile de protecție împotriva incendiilor, actele de autoritate și instrucțiunile de apărare împotriva incendiilor sunt emise în scopul reducerii riscului de incendiu, pentru a asigura astfel creșterea gradului de protecție a salariaților și utilizatorilor. Documentele menționate anterior trebuie să fie întocmite în conformitate cu prevederile legislative în vigoare, fiind ulterior analizate și evaluate periodic pentru a corespunde unor standarde de calitate, astfel încât, să poată fi implementate în timp util și eficient într-o situație critică.

Măsurile specifice de apărare împotriva incendiilor în clădiri civile se vor stabili în funcție de următorii factori determinanți ai probabilității declanșării unor incendii: categoriile de materialele și substanțe combustibile, modul de gestionare a deșeurilor combustibile, sursele specifice de aprindere, mijloacele tehnice de apărare împotriva incendiilor și activitățile desfășurate.

Analiza implementării măsurilor de apărare împotriva incendiilor prin metode standardizate va contribui la identificarea celor mai importante elemente care trebuie reevaluate periodic și pentru care trebuie identificate strategii speciale de rezolvare a cerințelor impuse prin măsurile organizatorice.

Atribuțiile stabilite prin legea apărării împotriva incendiilor trebuie să se regăsească în fișele de post, fișele de instructaj periodic trebuie completate numai după ce au fost prezentate instrucțiunile proprii și alte materiale specifice conform tematicii, debriefingul după fiecare exercițiu organizat trebuie să scoată în evidență aspectele pozitive și cele negative, iar prin măsurile organizatorice adoptate trebuie cultivată și dezvoltată o cultură a securității individuale și a locului de muncă, astfel încât, la apariția unui început de incendiu, personalul stabilit prin documentațiile specifice întocmite să intervină respectând procedeele și instrucțiunile exersate la antrenamente.

În toate fazele de cercetare, proiectare, execuție și pe întreaga lor durată de existență, construcțiile civile se supun unei examinări sistematice și calificate pentru identificarea, evaluarea și controlul riscurilor de incendiu, în condițiile prevăzute de reglementările și metodele de analiză specifice.

## 6. Bibliografie

- [1] Aurel TROFIN, Optimizarea salvării persoanelor în caz de incendiu, din construcții, prin modelarea competențelor specifice - Revista Română de Inginerie Civilă, Volumul 10 (2019), Nr. 2, Editura MatrixRom, pag. 148-159, <http://www.rric.ro/revista.php?id=28>
- [2] Legea nr. 307 din 12 iulie 2006 privind apărarea împotriva incendiilor, cu modificările și actualizările ulterioare.
- [3] Hotărârea Guvernului nr. 915/2015 privind stabilirea criteriilor pentru oprirea funcționării ori utilizării construcțiilor sau amenajărilor.
- [4] Hotărârea Guvernului nr. 971 din 26 iulie 2006 privind cerințele minime pentru semnalizarea de securitate și/sau de sănătate la locul de muncă
- [5] Hotărârea Guvernului nr. 1.091 din 16 august 2006 privind cerințele minime de securitate și sănătate pentru locul de muncă.
- [6] OMAI nr. 129/2016 pentru aprobarea Normelor metodologice privind avizarea și autorizarea de securitate la incendiu și protecție civilă.
- [7] OMAI nr. 712 din 23 iunie 2005 pentru aprobarea Dispozițiilor generale privind instruirea salariaților în domeniul situațiilor de urgență, actualizat și completat cu OMAI nr. 786 din 02.09.2005.
- [8] OMAI nr. 163 din 28 februarie 2007 pentru aprobarea Normelor generale de apărare împotriva incendiilor.
- [9] Normativul de siguranță la foc a construcțiilor - Indicativ P 118-99  
<http://www.leanblog.ro/wp/instrumente-lean/instrumente-lean/5s/>  
<https://www.intermanagement.eu/resurse/Principiile+metodei+japoneze+5+S>  
[https://en.wikipedia.org/wiki/5S\\_\(methodology\)](https://en.wikipedia.org/wiki/5S_(methodology))  
<https://www.bulsuk.com/2009/07/5-why-analysis-using-table.html>  
<https://www.inspectiamuncii.ro/-/legislatie-s-1>  
[https://trilogiq.ro/app/uploads/2017/07/TR\\_RO\\_5S-Safety\\_Poster-01.pdf](https://trilogiq.ro/app/uploads/2017/07/TR_RO_5S-Safety_Poster-01.pdf)  
<https://legislatiamuncii.manager.ro/>  
<https://eprof.ro/ssm/>

## Metodă eficientă de încălzire cu microunde pentru fabricarea spumei de sticlă din deșeu de sticlă

Effective microwave heating method for manufacturing glass foam from glass waste

Lucian Păunescu<sup>1</sup>, Sorin Mircea Axinte<sup>2</sup>, Marius Florin Drăgoescu<sup>3</sup>,  
Bogdan Valentin Păunescu<sup>4</sup>

<sup>1</sup>Daily Sourcing & Research SRL  
95-97 Calea Grivitei street, sector 1, Bucharest 010705, Romania  
E-mail: [lucianpaunescu16@gmail.com](mailto:lucianpaunescu16@gmail.com)

<sup>2</sup>Department of Applied Chemistry and Materials Science, University „Politehnica” of Bucharest  
1-7 Gh. Polizu street, sector 1, Bucharest 011061, Romania  
E-mail: [sorinaxinte@yahoo.com](mailto:sorinaxinte@yahoo.com)

<sup>3</sup>Department of Applied Chemistry and Materials Science, University „Politehnica” of Bucharest  
1-7 Gh. Polizu street, sector 1, Bucharest 011061, Romania  
E-mail: [mar\\_dmf@yahoo.com](mailto:mar_dmf@yahoo.com)

<sup>4</sup>Consitrans SA  
56 Polona street, sector 1, Bucharest 010504, Romania  
E-mail: [pnschogdan@yahoo.com](mailto:pnschogdan@yahoo.com)

DOI: 10.37789/rjce.2021.12.4.9

**Rezumat.** *In lucrare este prezentată o tehnică originală de fabricare a spumei de sticlă prin sinterizarea la temperatură înaltă a deșeului de sticlă datorită încălzirii cu microunde. Încălzirea materiei prime este realizată predominant direct și parțial indirect utilizând un tub ceramic din SiC cu o grosime optimă a peretelui de 2,5 mm. Această metodă contribuie la reducerea semnificativă a consumului specific de energie, a vitezei de încălzire și a duratei procesului comparativ cu tehnicile convenționale de încălzire. Caracteristicile spumei de sticlă sunt similare cu acelea ale spumelor fabricate conventional și pot fi utilizate ca înlocuitori ai materialelor de construcție existente.*

**Cuvinte cheie:** spumă de sticlă, microundă, încălzire predominant directă, agent de spumare, eficiență energetică

**Abstract.** An original technique for manufacturing glass foam by high temperature sintering of glass waste due to the microwave heating is presented in the paper. The heating of the raw material is performed predominantly direct and partially indirect by using a SiC ceramic tube with an optimal wall thickness of 2.5 mm. This method



contributes to the significant reduction of the specific energy consumption, the heating rate and the process duration compared to the conventional heating techniques. The characteristics of glass foam are similar to those of conventionally manufactured foams and can be used as replacements for existing building materials.

**Key words:** glass foam, microwave, predominantly direct heating, foaming agent, energy efficiency

## 1. Introducere

The manufacture of glass foam using recycled glass waste is a process that emerged and imposed in the last decades of the 20<sup>th</sup> century as an objective consequence of the need to reduce the amount of a waste with a very high annual generation rate, capable of causing major environmental damage. According to [1], in 2018 the container glass generation was 12.3 million tons in the United States representing 4.2 percent of all municipal solid waste generation. Also, in the same period, the global oil crisis [2] has produced a reorientation of the energy policy of the world's states by replacing traditional energy-intensive industrial products obtained by recycling waste incorporating much lower amounts of primary energy. This is also the case for building materials. It was found that the glass foam manufactured by sintering at 750-1150 °C the recycled powder glass waste has remarkable physical, thermal, mechanical and morphological characteristics better compared to those of thermal insulation building materials and the energy consumption is significantly lower. The glass foams are lightweight, with very good thermal insulation properties, resistance to fire and moisture, non-toxic, physical and chemical stability, resistance to attack of rodents, insects, bacteria, acids, etc. [3, 4]. Several companies in the world (Misapor, Pittsburgh Corning, Geocell, Glapor, etc.) began to industrially produce different varieties of glass foam. The manufacturing method is based exclusively on conventional heating techniques [4].

Unlike the method of manufacturing glass foam used in the industrial production, the team of researchers from the Romanian company Daily Sourcing & Research has performed in recent years several experimental tests applying the unconventional method of microwave heating. Although known since the 1930s and recognized in the literature [5] as a fast, economical and „clean” heating technique, it has been industrially used only in drying or low temperature heating processes. It has been experimentally found at the beginning of the new millennium that several types of materials are susceptible to efficient microwave heating (organics, ceramics, metals, glass, polymers, etc.) [5]. Despite this, the industrial application of microwaves is still in different experimental stages.

An explanation of the low interest shown by industrial manufacturers for the use of microwaves as an energy source in the process of making glass foam could be the theory presented in 1997 in the paper [6], which considers that the commercial glass (soda-lime glass), the main raw material, is poorly microwave susceptible at room temperature due to its high content of transparent microwave materials ( $\text{SiO}_2$ ,

$\text{Al}_2\text{O}_3$ ). The electrical conductivity of the glass and implicitly, the dielectric properties of this material, increase rapidly with increasing the temperature, so that at about 500 °C the microwave susceptibility reaches a high energy efficiency level [7-9]. The theory developed in the paper [6] was taken over in a market study [4], which concluded that the microwave application to the industrial glass foam furnaces would be interesting only for areas with temperatures above 500 °C, which would mean equipping the furnace with a conventional heating system in the temperature areas below 500 °C. Experimental results obtained by Daily Sourcing & Research [10] challenged the theory of the poor microwave susceptibility of soda-lime glass at low temperatures. Due to the presence in the composition of this glass of some inherent contaminants ( $\text{Fe}_2\text{O}_3$ ,  $\text{Cr}_2\text{O}_3$ , etc.) even in low weight proportions that absorb more efficiently the electromagnetic radiation at room temperature, the microwave heating process can occur with normal efficiency starting from ambient temperature [9-11].

In order to obtain a maximum energy efficiency of the glass powder heating process, the direct microwave heating is necessary. In the case of glass (generally, silicate materials) this desideratum could not be experimentally achieved, because the direct contact of the microwave field with the material subjected to irradiation caused the severe destruction of its internal structure at the foaming temperature [12]. The adopted solution was the placement between the material and the microwave emission source of a high microwave susceptible ceramic screen in the form of a crucible or cylindrical tube. The distribution of the waves that penetrated the screen coming in direct contact with the material and those that were absorbed in the wall of the screen was adjusted by the thickness of its wall. Experimentally, it was found a thickness of 2.5 mm ensures a predominantly direct heating and a partially indirect heating suitable for a very high energy efficiency, without affecting the structure of the glass foam [13].

Further, experimental results obtained in the manufacturing process of glass foam under the condition of using the predominantly direct and partially indirect microwave heating method are presented.

## 2. Methods and materials

Commonly, the manufacture of glass foam from recycled glass waste consists of the sintering at high temperature (750-1150 °C) of a pressed powder mixture containing glass waste, a foaming agent and, where appropriate, mineral additives to facilitate the foaming process. The foaming agent (solid or liquid) releases a gas or a gaseous compound at a temperature approximately similar to that of the softening point of the mixture containing the raw material. The gas bubbles penetrate the viscous mixture, but they cannot leave it being blocked in this space. Continuing the heating process, the material expands increasing its initial volume. At the end of heating, by the slow cooling that follows, a porous structure specific to glass foam is formed [3, 4].

The experimental equipment on which the tests were performed at Daily Sourcing & Research was a 0.8 kW-microwave oven of the type used in the household for food preparation, adapted for operation at high temperature (up to 1200 °C). The

powder mixture previously pressed into a metal mold and then released was freely deposited on a metal plate on a thermal insulating bed composed of several ceramic fiber mattresses. A cylindrical ceramic tube made of a high microwave susceptible material (SiC and Si<sub>3</sub>N<sub>4</sub> in the 80/20 weight ratio) with an outer diameter of 1200 mm, a height of 100 mm and a wall thickness of 2.5 mm was placed between the pressed material and the microwave emission source. The upper opening of the tube was covered with a ceramic lid of the same material provided with a 30 mm hole for visualizing with a radiation pyrometer the surface temperature of the heated material. To avoid the heat loss of the heated material as well as of the ceramic tube and lid outside the system, the tube and lid were covered with ceramic fiber mattresses. It should be mentioned that the method of direct microwave heating is completely different compared to the conventional methods. The energy of the microwave field that comes in direct contact with the material is converted into heat, the heating being initiated in its core. The heat propagation takes place volumetrically throughout the material mass from the inside to the peripheral areas [14]. The heating process is fast. Also, the direct microwave heating is selective. Only the microwave susceptible material absorbs the electromagnetic waves. The other components of the oven (walls, vault, etc.) are not heated. This heating mode ensures a very good energy efficiency of the process [11]. The process temperature control was performed with a radiation pyrometer mounted above the oven at about 400 mm. To visualizing the material, the upper metal wall of the oven was provided with a 30 mm hole on the same vertical axis as the ceramic lid hole of the tube that includes the heated material. The experimental microwave equipment described above is shown in Figure 1.

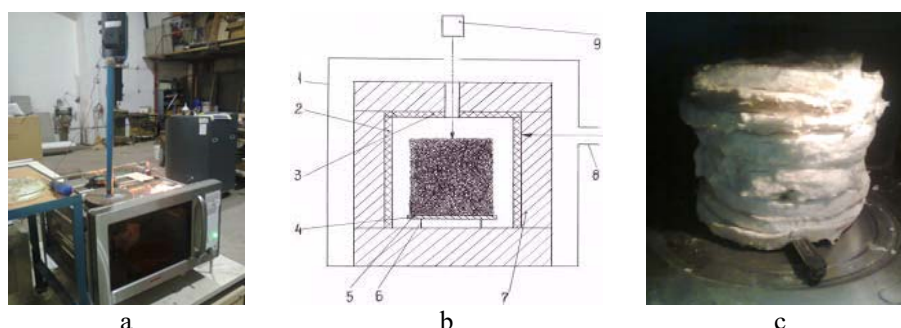
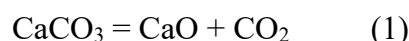


Fig. 1. Experimental microwave equipment

a – overall image of the experimental equipment; b – constructive scheme of the equipment: 1 – microwave oven; 2 – ceramic tube; 3 – ceramic lid; 4 – metal plate; 5 – pressed powder material; 6 – metal support; 7 – ceramic fiber mattress; 8 – waveguide; 9 – radiation pyrometer; c – thermal insulation protection.

The foaming agent adopted for manufacturing glass foam in this experiment was calcium carbonate (CaCO<sub>3</sub>). The decomposition reaction of CaCO<sub>3</sub> occurs at temperatures above 750 °C [15, 16] with the formation of calcium oxide (CaO) and carbon dioxide (CO<sub>2</sub>) according to reaction (1).



Metodă eficientă de încălzire cu microunde pentru fabricarea spumei de sticlă din deșeu de sticlă

CaO is treated in the molten glass, while CO<sub>2</sub> is released into the viscous mass of the glass.

In principle, the foaming process of a common commercial glass using CaCO<sub>3</sub> as a foaming agent takes place between 800-900 °C being mainly influenced by the weight ratio, quality and fineness of the glass granulation and the weight ratio of the foaming agent [3].

As a fluxing agent, borax (sodium borate) was used in the starting mixture. Due to the boron content of over 13 wt.% [17], borax contributes to the increase of mechanical strength of glass foam.

The post-consumer container glass waste is the most widespread waste type in the world. In the current experiments, this type was used, being selected only the colorless glass waste. The chemical composition of colorless commercial glass according to the previous determinations [13] is shown in Table 1.

Table 1

Chemical composition (wt.%) of colorless commercial glass						
SiO <sub>2</sub>	Al <sub>2</sub> O <sub>3</sub>	CaO	Fe <sub>2</sub> O <sub>3</sub>	MgO	Na <sub>2</sub> O	Cr <sub>2</sub> O <sub>3</sub>
71.7	1.9	12.0	0.05	1.0	13.3	0.05

The glass waste was processed before using in experiments in Bilmetal Industries Company in Popești Leordeni-Ilfov (Romania) including its selection by color, breaking, grinding in a ball mill and sieving at a granulation of less than 100 μm.

CaCO<sub>3</sub> purchased from the market at a fine grain size (below 40 μm) was used in experiments without other mechanical processing.

Borax was purchased from the market at a grain size below 400 μm, being ground in a laboratory electric device and sieved for a granulation of less than 130 μm.

The experimental variants composition was adopted taking into account the usual range of CaCO<sub>3</sub> proportions as a foaming agent in the glass foam manufacture (0.7-2.5 wt.%). The weight ratio of borax was adopted at 1.5 wt.% being kept constant for all variants. A water addition as a binder (9.0 wt.%) to facilitate the cold pressing of the powder mixture was also adopted. The composition of experimental variants is presented in Table 2.

Table 2

Composition of experimental variants				
Variant	Colorless glass waste (wt.%)	Calcium carbonate (wt.%)	Borax (wt.%)	Water addition (wt.%)
1	96.0	2.5	1.5	9.0
2	96.6	1.9	1.5	9.0
3	97.4	1.1	1.5	9.0
4	97.8	0.7	1.5	9.0

Usual techniques have been applied in the process of characterizing experimentally manufactured glass foam samples. The gravimetric method [18] was used to measure the apparent density and the comparison method between the apparent density and the density in compact state (true density) of the same material [19] was used to determine the porosity. The use of a TA.XTplus Texture Analyzer allowed to measure the compressive strength and for determining the thermal conductivity the guarded-comparative-longitudinal heat flow (ASTM E1225-04) was applied. The water immersion method (ASTM D570) was used to determine the water absorption of the samples. Using an ASONA 100X Zoom Smartphone Digital Microscope the glass foam microstructures were examined.

### 3. Results and discussion

The functional parameters of the experimental process of manufacturing glass foam by predominantly direct microwave heating are shown in Table 3.

Table 3

**Main functional parameters of the experimental process**

Variant	Dry raw material amount (g)	Process temperature (°C)	Process time (min)	Average rate (°C/min)		Glass foam amount (g)	Specific energy consumption (kWh/kg)
				Heating	Cooling		
1	500	826	29	27.8	5.0	486	0.62
2	500	824	29	27.7	5.3	485	0.62
3	500	825	31	26.0	5.1	487	0.66
4	500	827	33	24.5	5.3	487	0.71

According to the data in Table 3, the amount of dry raw material was kept constant at 500 g. The energy efficiency of the microwave heating process was remarkable, the heating rate having values between 24.5-27.8 °C/min. Given that the temperature of the sintering/foaming process was between 824-827 °C, the duration of the process was very low (29-33 min). The specific energy consumption decreased to very low values (up to 0.62 kWh/kg) corresponding to variants 1 and 2 with CaCO<sub>3</sub> weight ratio of 2.5 and 1.9 wt.%, respectively. The literature provides insufficient data on the specific consumption of industrial processes for the manufacture of glass foam by conventional heating techniques. The market study [4] mentions an average energy consumption in Misapor Company of 100 kWh/m<sup>3</sup>, i.e. about 0.66-0.75 kWh/kg and the bibliographic source [20] indicates an average consumption of Energocell Company of 140 kWh/m<sup>3</sup>, i.e. about 0.8 kWh/kg. Thus, the energy efficiency of the application of predominantly direct microwave heating technique was superior to conventional techniques, especially since it is known that the working conditions of an experimental process are disadvantageous in energy terms compared to an industrial scale process [5].

Metodă eficientă de încălzire cu microunde pentru fabricarea spumei de sticlă din deșeu de sticlă

Pictures of the cross section of the four glass foam samples are shown in Figure 2.

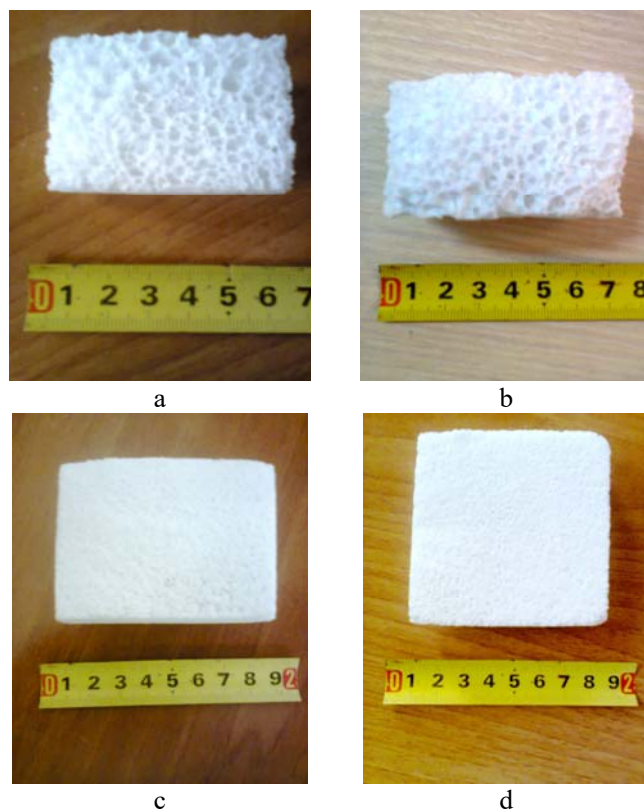


Fig. 2. Cross section of the glass foam samples  
a – sample 1 heated at 826 °C; b – sample 2 heated at 824 °C;  
c – sample 3 heated at 825 °C; d – sample 4 heated at 827 °C.

According to Figure 2, the appearance of the glass foam samples section differs clearly depending on the weight ratio of  $\text{CaCO}_3$ . The maximum ratio of 2.5 wt.% (sample 1) favored the formation of a higher pore size structure, while by reduction the  $\text{CaCO}_3$  proportion up to 0.7 wt.% (sample 4) the pore size obviously decreased. The examination with the digital microscope of the microstructural configuration (Figure 3) allowed the pore size determination and their homogeneity distribution identification.

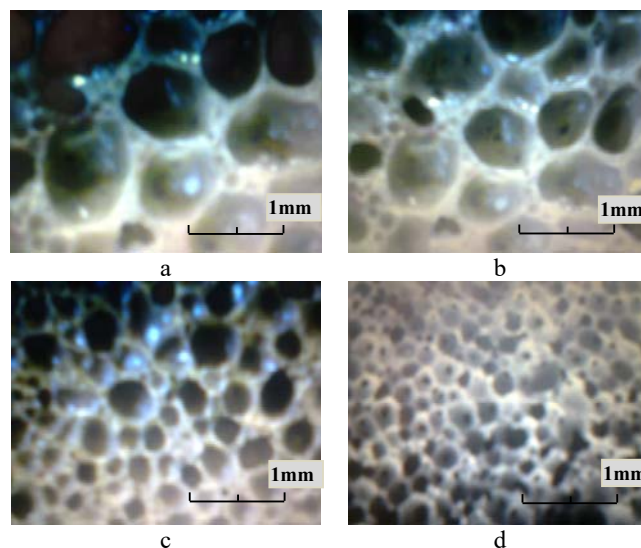


Fig. 3. Microstructural configuration of the glass foam samples  
a – sample 1; b – sample 2; c – sample 3; d – sample 4.

The physical, thermal, mechanical and microstructural characteristics of the glass foam samples are presented in Table 4.

Table 4

**Main physical, thermal, mechanical and microstructural characteristics of glass foam samples**

Variant	Apparent density (g/cm <sup>3</sup> )	Porosity (%)	Thermal conductivity (W/m·K)	Compressive strength (MPa)	Water absorption (vol.%)	Pore size (mm)
1	0.17	91.8	0.049	1.32	0.93	0.60-1.00
2	0.19	90.9	0.053	1.51	1.25	0.50-0.80
3	0.22	89.4	0.060	1.83	1.16	0.20-0.50
4	0.23	88.9	0.063	2.02	1.84	0.10-0.25

According to the data in Table 4, the main characteristics of glass foam samples show excellent thermal insulating properties. The apparent density values are very low between 0.17-0.23 g/cm<sup>3</sup> and the thermal conductivity is also very low (0.049-0.063 W/m·K) determining the thermal insulating properties. The porosity values are high, the range being between 88.9-91.8 %. The glass foam samples are waterproof materials, the water absorption being below 1.84 vol.%. According to the pictures in Figure 3, the pore size is between 0.60-1.00 mm for sample 1 and between 0.10-0.25 mm for sample 4. Compared to the glass foams industrially manufactured by conventional heating techniques, the characteristics of the experimental glass foams produced by the unconventional technique of microwave heating are similar being suitable for using as thermal insulating building material.

The compressive strength of glass foam (1.32-2.02 MPa) was significantly improved by the addition of borax in the composition of the raw material mixture.

Generally, a foamed material prepared with only  $\text{CaCO}_3$  as a foaming agent has a compressive strength less than 1.3 MPa [13]. By decreasing the  $\text{CaCO}_3$ /borax ratio from 1.67 (variant 1) to 0.47 (variant 4) the compressive strength value increased by 1.5 time.

Analyzing the glass foam characteristics it is found that all four experimental variants correspond in terms of quality and energy to the requirements of an adequate thermal insulation material. However, the authors adopted as the optimal variant, variant 3 produced with 1.1 wt.%  $\text{CaCO}_3$  and 1.5 wt.% borax mixed with 97.4 wt.% colorless glass waste and a water addition of 9 wt.% as a binder. Its apparent density was  $0.22 \text{ g/cm}^3$  and the thermal conductivity had the value of  $0.060 \text{ W/m}\cdot\text{K}$  ensuring very good thermal insulation properties. The compressive strength of 1.83 MPa is high enough for the material to have excellent mechanical strength. The specific energy consumption was very low ( $0.66 \text{ kWh/kg}$ ).

#### 4. Conclusion

The paper aimed to improve in terms of energy the process of manufacturing glass foam from glass waste by applying an unconventional technique of predominantly direct microwave heating, unlike the conventional techniques industrially used in the world. The heating method is original, being tested by authors in various variants in the last four years. The experimentally manufactured glass foam with  $\text{CaCO}_3$  as a foaming agent and borax as a fluxing agent has characteristics similar to those industrially produced by conventional techniques (apparent density of  $0.22 \text{ g/cm}^3$ , thermal conductivity of  $0.060 \text{ W/m}\cdot\text{K}$  and compressive strength of 1.83 MPa). The specific energy consumption of the experimental process was very low ( $0.66 \text{ kWh/kg}$ ) below the level of energy consumptions of industrial producers.

#### References

- [1] \*\*\* Glass: Material-Specific Data, Environmental Protection Agency of the United States, November 2020. <https://www.epa.gov/facts-and-figures-about-materials-waste-and-recycling/glass-material-specific-data>
- [2] C. Bina, „World Oil and Crisis of Globalization” in A Prelude to the Foundation of Political Economy, New York, 2013, pp. 17-43. [https://doi.org/10.1057/9781137106971\\_2](https://doi.org/10.1057/9781137106971_2)
- [3] G. Scarinci, G. Brusatin, E. Bernardo, „Glass Foams” in Cellular Ceramics: Structure, Manufacturing, Properties and Applications, Wiley-VCH GmbH & KgaA, M. Scheffler, P. Colombo eds., Weinheim, Germania, 2005, pp. 158-176.
- [4] J. Hurley, “Glass-Research and Development”, Final Report, A UK market survey for foam glass, The Waste and Resources Action Programme Publication, Banbury-Oxon, Great Britain, 2003.
- [5] Oxana Kharissova, B.I. Kharissov, J.J. Ruiz Valdés, “Review: The Use of Microwave Irradiation in the Processing of Glasses and their Composites”, Industrial & Engineering Chemistry Research, vol. **49**, no. 4, 2010, pp. 1457-1466.
- [6] M. Knox, G. Copley, “Use the Microwave Radiation for the Processing of Glass”, Glass Technology, vol. **38**, no. 3, 1997, pp. 91-96.



- [7] R.R. Menezes, P.M. Souto, R.H.G.A. Kiminami, "Microwave Fast Sintering of Ceramic Materials" in *Sintering of Ceramics-New Emerging Techniques*, 2012. <https://www.doi.org/10.5772/34181>
- [8] M.N. Rahaman, "Sintering of ceramics, CRC Press, Taylor & Francis Group, Boca Raton, London, New York, 2007. <https://books.google.ro>
- [9] U. Kolberg, M. Roemer, "Reacting of Glass", *Ceramic Transaction*, vol. **111**, 2001, pp. 517-523.
- [10] L. Paunescu, B.T. Grigoras, M.F. Dragoescu, S.M. Axinte, A. Fiti, "Foam Glass Produced by Microwave Heating Technique", *Bulletin of Romanian Chemical Engineering Society*, vol. **4**, no. 1, 2017, pp. 98-108.
- [11] D.A. Jones, T.P. Lelyveld, S.D. Mavrofidis, S.W. Kingman, N.J. Miles, "Microwave Heating Applications in Environmental Engineering-A Review", *Resources, Conservation and Recycling*, vol. **34**, no. 2, 2002, pp. 75-90.
- [12] L. Paunescu, S.M. Axinte, B.T. Grigoras, M.F. Dragoescu, A. Fiti, "Testing the Use of Microwave Energy to Produce Foam Glass", *European Journal of Engineering and Technology*, vol. **5**, no. 4, 2017, pp. 8-17.
- [13] S.M. Axinte, L. Paunescu, M.F. Dragoescu, Ana C. Sebe, "Manufacture of Glass Foam by Predominantly Direct Microwave Heating of Recycled Glass Waste", *Transactions on Networks and Communications*, vol. **7**, no. 4, 2019, pp. 37-45. <https://doi.org/10.14738/tnc.74.7214>
- [14] Helen J. Kitchen, S.R. Vallance, Jennifer L. Kennedy, Nuria Tapia-Ruiz, Lucia Carassiti, "Modern Microwave Methods in Solid-State Inorganic Materials Chemistry: From Fundamentals to Manufacturing", *Chemical Reviews*, vol. **114**, no. 2, 2014, pp. 1170-1206.
- [15] K.S.P. Karunadasa, C.H. Manoratne, H.M.T.G.A. Pitawala, R.M.G. Rappakse, "Thermal Decomposition of Calcium Carbonate (Calcite Polymorph) as Examined by In-Situ High-Temperature X-Ray Powder Diffraction", *Journal of Physics and Chemistry of Solids*, vol. **134**, 2019, pp. 21-28.
- [16] T. Koizumi, K. Kido, T. Nakamura, "Foaming Agent for Powder Metallurgy Production of Aluminum Foam", *Materials Transactions*, vol. **52**, no. 4, 2011, pp. 728-733. <https://www.doi.org/10.2320/MATERTRANS.M2010401>
- [17] H.F. Miller, "Borax, Borates and Other Boron-Carrying Compounds", *Agronomy Notes*, no. 16, University of Kentucky, 1964.
- [18] \*\*\* "Manual of Weighing Applications", Part 1, Density, 1999. [http://www.docplayer.net/21731890-Manual-of-weighing-applications-part-1-density\\_html](http://www.docplayer.net/21731890-Manual-of-weighing-applications-part-1-density_html)
- [19] L.M. Anovitz, D.R. Cole, "Characterization and Analysis of Porosity and Pore Structures", *Reviews in Mineralogy and Geochemistry*, vol. **80**, 2005, pp. 61-164.
- [20] \*\*\* Foam Glass Manufacturing, Energocell Foam Glass, Debrecin, Hungary, 2014. <https://www.energocell.hu/en/foamglass-manufacturing/>

## Expansion of glass waste by the double effect of liquid and solid foaming agents for manufacturing the cellular glass gravel (CGG) in a 10 kW-microwave oven

Expandarea deșeurilor de sticlă prin dublul efect al agenților de spumare lichid și solid pentru fabricarea pietrișului din spumă de sticlă (CGG) într-un cuptor cu microunde de 10 kW

Lucian Păunescu<sup>1</sup>, Sorin Mircea Axinte<sup>2</sup>, Marius Florin Drăgoescu<sup>3</sup>, Bogdan Valentin Păunescu<sup>4</sup>

<sup>1</sup>Daily Sourcing & Research SRL

95-97 Calea Grivitei street, sector 1, Bucharest 010705, Romania

E-mail: [lucianpaunescu16@gmail.com](mailto:lucianpaunescu16@gmail.com)

<sup>2</sup>Department of Applied Chemistry and Materials Science, University „Politehnica” of Bucharest

1-7 Gh. Polizu street, sector 1, Bucharest 011061, Romania

E-mail: [sorinaxinte@yahoo.com](mailto:sorinaxinte@yahoo.com)

<sup>3</sup>Department of Applied Chemistry and Materials Science, University „Politehnica” of Bucharest

1-7 Gh. Polizu street, sector 1, Bucharest 011061, Romania

E-mail: [mar\\_dmf@yahoo.com](mailto:mar_dmf@yahoo.com)

<sup>4</sup>Consitrans SA

56 Polona street, sector 1, Bucharest 010504, Romania

E-mail: [pnsbogdan@yahoo.com](mailto:pnsbogdan@yahoo.com)

DOI: 10.37789/rjce.2021.12.4.10

**Rezumat.** *O rețetă de fabricare industrială a pietrișului din spumă de sticlă (CGG) din deșeu de sticlă printr-o tehnică originală neconvențională utilizând simultan un agent de spumare lichid și solid (glicerină și carbonat de calciu) a fost testată într-un cuptor cu microunde de 10 kW. Utilizând un creuzet ceramic de mari dimensiuni din carbura de siliciu, în interiorul căruia a fost introdusă o matriță metalică conținând amestecul de materie primă fin măcinată și presată, a fost produsă o cantitate mult mai mare de produs spumat. Caracteristicile probelor de CGG au fost densitatea în vrac de 0,20-0,25 g/cm<sup>3</sup>, conductivitatea termică de 0,062-0,070 W/m·K și rezistența la compresiune de 7,1-7,4 MPa.*

**Cuvinte cheie:** pietriș din spumă de sticlă, încălzire cu microunde, deșeu de sticlă, glicerină, carbonat de calciu.

**Abstract.** *An industrially manufacturing recipe of cellular glass gravel (CGG) from glass waste by an original unconventional heating technique using simultaneously a*

*liquid and solid foaming agent (glycerol and calcium carbonate) was tested on a 10 kW-microwave oven. Using a large silicon carbide ceramic crucible, inside which a metal mold containing the finely ground pressed raw material mixture was inserted, a much higher amount of foamed product was produced. The characteristics of CGG samples were bulk density of 0.20-0.25 g/cm<sup>3</sup>, thermal conductivity of 0.062-0.070 W/m·K and compressive strength of 7.1-7.4 MPa.*

**Key words:** foam glass gravel; microwave heating; glass waste; glycerol; calcium carbonate.

## 1. Introduction

In the last decades several major global problems have affected our planet, beginning with the onset of the energy crisis in the 1970s and continuing with the overheating danger due to the destruction of the ozone layer by extensive and uncontrolled emissions of greenhouse gas (mainly carbon dioxide). The rational energy management [1] has led to the waste recycling (plastic, metal, glass, paper, etc.) and its reuse as a raw material in the manufacturing processes that have its generated. The need for greening the environment by removing large areas of land occupied by the storage of materials considered unusable has led to the tendency to study the possibilities of turning this waste into new created value materials for other application fields, especially in building and road construction.

The industrial glass manufacturing processes characterized by high consumptions of primary energy uses recycled glass waste as a raw material for energy reasons. According to the literature [2], the manufacture of 1 kg of new glass requires 4500 kJ (1.25 kWh), while manufacturing the same amount using recycled glass waste requires only 500 kJ (0.139 kWh). However, glass waste processing operations such as its selection by color (and implicitly, its chemical composition) are expensive. Given the very large quantities of glass waste in the world and the increasing rate of its generation (especially post-consumer packaging glass representing about 56 % of the total glass amount produced in the EU [3], new domains of using this waste have been found through expansion techniques at temperatures between 800-1100 °C by addition of a foaming agent [4]. The obtained products (cellular glass) uniquely combine physical, thermal and mechanical characteristics (light weight, low thermal conductivity and high compressive strength) as well as resistance to fire, water, frost and other external agents such as bacteria, acids, insects, rodents, easy handling, low transportation costs, etc. [4], being used in applications in various fields of constructions.

This combination of the properties mentioned above makes cellular glass practically irreplaceable in both construction (interior and exterior insulation of walls, floors and ceilings of buildings, insulation in the perimeter of buildings, drainage, road and railway construction, sports fields, insulation of underground pipes for energy fluids and underground storage tanks, bridge abutments, etc.) as well as in

many other areas such as filters, absorbers, gas sensors, heat exchangers, etc. [4-6], being able to compete with commercially available traditional building materials.

The most used traditional insulation materials [7] are: expanded or extruded polystyrene and phenolic foam (as boards), glass mineral wool (as rolls), hempcrete (as blocks or made in-situ), etc. The mechanical strength and resistance to various external agents of cellular glass are higher compared to all the materials mentioned above. In addition, the energy consumption (about 1500 kWh/m<sup>3</sup>) required to manufacture expanded polystyrene, a commonly used thermal insulation material, is ten times higher than the consumption required for manufacturing the cellular glass [8].

The most recently manufactured type of cellular glass (in the last decade of the 20<sup>th</sup> century) is the so-called cellular glass gravel or foam glass gravel (CGG) available in the form of lumps with dimensions between 10-75 mm. It has excellent thermal and load bearing properties. It is manufactured from 100% recycled glass waste being lightweight (bulk density between 0.12-0.25 g/cm<sup>3</sup>), sustainable (over 50 years) and easy to handle [5, 9]. The CGG is inert to the freeze-thaw cycle effectively protecting against the impact of frost. Also, it has excellent water drainage properties. Furthermore, the CGG has high values of compressive strength (that can reach 5-6 MPa). Generally, all technical books, prospectuses and brochures including CGG characteristics avoid to declare the maximum values of compressive strength, indicating only the minimum values (0.7-2 MPa) [9-12]. The thermal conductivities varies between 0.052-0.12 W/m·K with average values around 0.08 W/m·K.

According to [9], over 600,000 m<sup>3</sup> of CGG are annually manufactured in Europe (Germany, Switzerland, Austria and the Nordic countries). The main manufacturers [13] are: Geocell Schaumglas (Austria), Misapor Switzerland (Switzerland), Glapor Werk Mitterteich (Germany), Veriso (Germany), Technopor Handels (Austria), Hasopor (Sweden), Glasopor (Norway), Foamit (Finland), Vetropor (Switzerland). In the Nordic countries, road construction is the main market of CGG due to the special harsh climate conditions, which favor freeze-thaw cycles. In order to avoid the negative effect of these cycles on the structural integrity of the road, the thermal insulation of the asphalt layer against the frozen ground, the fast drainage, the absence of capillary action and the structural stability of materials are necessary [13]. Recently, the Misapor Company which produced a wide range of cellular glass announced the decision to focus its production activity only on insulation products of the perimeter of buildings [14].

The manufacturing technique of CGG differs from that of the production of cellular glass for the thermal protection of building walls, floors or ceilings [15], the mixture containing glass waste, foaming agent and other mineral additives being loaded directly on the metal conveyor belt of a tunnel oven. Sintering/foaming of the raw material takes place in the oven heated by conventional methods [10]. After reaching the foaming temperature, the material is freely cooled in the oven and then forced cooled by blowing air to create some internal stresses that facilitate the easy breaking of the sintered mass into relatively low lumps (maximum 75-80 mm) at the

end of the conveyor belt. The basic raw material used in the industrial manufacturing processes of CGG is glass waste containing either entirely post-consumer packaging glass, or a mixture composed of this waste type and windows glass waste [13]. The manufacturing recipes of the main producers differ by the nature of the foaming agent and additives. Except for Geocell Company, which does not specify the type of foaming agent, Misapor uses gypsum ( $\text{CaSO}_4$ ), limestone ( $\text{CaCO}_3$ ) or silicon carbide ( $\text{SiC}$ ) in a weight ratio of 2 %. Glapor Werk Mitterteich Company has a manufacturing recipe in which the foaming agent is liquid (glycerol) being used together with sodium silicate (also called "water glass"). Glamaco Company, a very important supplier of industrial equipment for the manufacture of CGG, recommends a recipe with 95 % glass waste, 5 % glycerol,  $\text{CaCO}_3$  as foaming agents and sodium silicate ("water glass") as an enveloping agent as well as water addition and very low ratio of kaolin powder [16].

As mentioned above, the industrially used heating methods are exclusively conventional (electric resistances or gaseous fuel burning). Unlike these methods, the team of authors has adopted in recent years the unconventional technique of microwave heating the raw material. This technique recognized in the literature [17] as fast, "clean" and economical, but applied to a small extent in industrial processes only for drying or heating at low temperature of some solids, has been used experimentally in the manufacture of FGG as a variant of the manufacturing recipe recommended by Glamaco [16] on a 0.8 kW-microwave oven in the Romanian company Daily Sourcing & Research.

The experimental results [18] showed that using a powder mixture composed of 93.1 wt. % colorless glass waste, 1.0 wt. % glycerol, 4.8 wt. % water glass, 0.8 wt. %  $\text{CaCO}_3$ , 0.2 wt. % kaolin and 14.5 wt. % water addition, sintered at 834 °C, a CGG with excellent characteristics can be obtained (apparent density of 0.28 g/cm<sup>3</sup>, thermal conductivity of 0.063 W/m·K, compressive strength of 7.3 MPa, water absorption of 4.3 vol. % and pore size between 0.10-0.35 mm). The specific energy consumption was very low (0.78 kWh/kg).

In the current paper, the authors aimed to test the manufacturing process of CGG by the unconventional microwave heating technique using an available oven with much higher installed power (10 kW) designed for other operation types, which was adapted to meet the requirements of the experiment. Thus, it was tried to create conditions close to those specific to operations on an industrial scale by substantially enlarging the surface of the material layer subjected to microwave irradiation and the predominantly frontal positioning of the magnetrons. The experiment described further is a new stage of research in the field of foaming glass waste carried out in recent years on a 0.8 kW-microwave oven and has an original character.

## 2. Methods and materials

The very easy dispersion of a liquid foaming agent among the finely ground particles of the glass waste determined the choice of glycerol in the experiment. This organic material ( $\text{C}_3\text{H}_8\text{O}_3$ ) decomposes in the oxidizing atmosphere of the oven

releasing several compounds between carbon dioxide ( $\text{CO}_2$ ) and pure carbon as well as hydroxyl compounds [19]. The decomposition process begins at low temperature (about 190 °C) and continues in several stages up to about 850 °C [20]. Generally, a carbonic foaming agent such as glycerol has a high affinity for oxygen, having oxidizing conditions in the oven for the premature burning of carbon and affecting the foaming process by the loss of  $\text{CO}_2$  and carbon monoxide (CO) which leave the material insufficiently heated. For this reason, a 30% aqueous sodium silicate solution is used to envelope the glass particles. Thus, by heating the decomposition process of glycerol is slowed down and the sintering of the glass is intensified. The addition of water to the starting mixture on the one hand has a role of binder and on the other hand favors the formation of "water gas" containing hydrogen ( $\text{H}_2$ ) and CO resulted after the reaction of water vapor with carbon at about 800 °C. The "water gas" contributes to the intensification of the glass foaming.

The solid foaming agent ( $\text{CaCO}_3$ ) initially mixed with the powder glass waste decomposes into  $\text{CO}_2$  (gas), which forms bubbles in the thermally softened material and calcium oxide (CaO) (solid) which enters in the molten glass composition. The decomposition reaction of  $\text{CaCO}_3$  is initiated at over 750 °C, according to [21].

Due to the increase of the internal pressure of the gas bubbles under the influence of heating, the viscous material increases its initial volume. At the end of the thermal process, by cooling, the bubbles turn into pores generating a typical porous structure [4]. By its nature, the liquid foaming agent usually contributes to the formation of structures with fine porosity.

The experimental equipment used to manufacture CGG in conditions closer to those of industrial scale production was a 10 kW-microwave oven (Figure 1) existing in the company Daily Sourcing & Research, designed and used for other types of thermal processes. The oven having the inner space of parallelepiped shape with the volume of about 0.4 m<sup>3</sup> is equipped with three magnetrons mounted linearly equidistant on each of the two side walls and four magnetrons mounted equidistantly in the flat vault. Because previous experiments have shown that commercial glass (soda-lime glass) which forms the glass waste is not suitable for complete direct microwave heating causing severe destruction of its internal structure at the foaming temperature [22], a ceramic crucible based on silicon carbide with an outer diameter of 300 mm, a height of 450 mm and a wall thickness of 10 mm was placed in a horizontal position inside the oven on an insulating bed made of ceramic fiber mattresses. The outer wall, bottom and opening of the crucible were also intensely thermally protected with ceramic fiber mattresses. The powder mixture was loaded and manually pressed (at about 1-3 MPa) in a metal mold with dimensions of 250x360x50 mm inserted in a horizontal position inside the ceramic crucible. The constructive scheme of the microwave oven is shown in Figure 2. The thermal protection of the ceramic crucible containing the powder mixture is very important in the case of microwave heating. Both the crucible made of silicon carbide (SiC) and the glass-based mixture have in their composition microwave susceptible materials (mainly SiC,  $\text{Na}_2\text{O}$ ,  $\text{K}_2\text{O}$ , water, but also  $\text{Cr}_2\text{O}_3$ ,  $\text{Fe}_2\text{O}_3$ , etc. existing in low ratios), which have the property of

absorbing and converting the microwave energy into heat. The heating initiation takes place in the core of these materials, the heat propagating volumetrically from the inside to the peripheral areas [23], unlike the conventional heating types where the thermal energy is transferred inversely from the energy source to the material and largely includes massive component parts of the oven (vault, walls, hearth). Because the electromagnetic waves are absorbed only by the microwave susceptible materials by selectivity [23, 24], the role of the thermal insulating refractory masonry of the oven is minor.

A thermocouple whose hot welding was fixed on the side wall of the metal mold facilitated controlling the temperature of the process.



Fig. 1

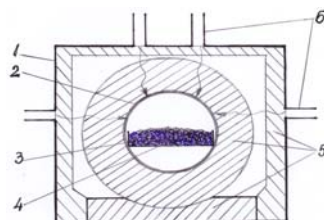


Fig. 2

Fig. 1. Overall image of the 10 kW-microwave oven

Fig. 2. Constructive scheme of the microwave oven:

- 1 – oven wall; 2 – SiC ceramic tube; 3 – pressed powder material; 4 – metal mold;  
5 – ceramic fiber mattress; 6 – waveguide.

The determination of the physical, thermal, mechanical and microstructural features of the CGG lumps was performed by usual methods. The heat-flow meter method (ASTM E1225-04) was used for measuring the thermal conductivity and the compressive strength could be determined by the use of a TA.XTplus Texture Analyzer (ASTM C552-17). The bulk density was measured by the traditional method of weighing a batch of lumps completely loaded into a vessel of known volume and dividing the batch mass by the inner volume of the vessel [25]. The porosity was calculated by the comparing method of the true and bulk density [26]. The volumetric percentage of the water absorption for 24 hours was measured by the water immersion method (ASTM D570). The configuration of the CGG sample microstructures was examined with an ASONA 100X Zoom Smartphone Digital Microscope.

As mentioned, a manufacturing recipe previously applied on the 0.8 kW-microwave oven composed of packaging glass waste as raw material, glycerol and  $\text{CaCO}_3$  as foaming agents (liquid and solid), an aqueous solution of sodium silicate ("water glass") as an enveloping agent, kaolin powder (in a very low ratio) as a thermal protection agent for ceramic materials [27] and water addition as a binder [18], was also tested in conditions closer to those on an industrial scale created by the 10 kW-microwave oven described above.

In this experiment, the glass waste was a mixture composed of colorless glass (50 %), green glass (20 %) and amber glass (30 %) representing approximately the proportion of this waste recycled in Romania. The chemical composition of the three glass types is shown in Table 1.

Table 1

Chemical composition of the glass waste types			
Composition	Glass waste type, wt. %		
	Colorless	Green	Amber
SiO <sub>2</sub>	71.7	71.8	71.1
Al <sub>2</sub> O <sub>3</sub>	1.9	1.9	2.0
CaO	12.0	11.8	12.1
Fe <sub>2</sub> O <sub>3</sub>	-	-	0.2
MgO	1.0	1.2	1.1
Na <sub>2</sub> O	13.3	13.1	13.3
K <sub>2</sub> O	-	0.1	0.1
Cr <sub>2</sub> O <sub>3</sub>	0.05	0.09	-
SO <sub>3</sub>	-	-	0.05
Other oxides	0.05	0.01	0.05

The glass waste processing (selection by color, breaking, coarse grinding, thermal washing at 250 °C, fine grinding and sieving at pore size below 100 µm) was performed in the Romanian company Bilmetal Industries SRL Popesti Leordeni-Ilfov.

CaCO<sub>3</sub> commercially purchased with a granulation below 40 µm was used without a supplementary reduction of the grain size. The commercial kaolin purchased from the market as a very fine powder (below 10 µm) was added in an extremely low proportion to the solid mixture due to the ability of the aqueous suspension of kaolinite (from the composition of kaolin) to provide a thermal protection of the ceramic material. The chemical composition of the kaolin contains: 57.6 % SiO<sub>2</sub>; 37.8 % Al<sub>2</sub>O<sub>3</sub>; 0.35 % CaO; 0.86 % Fe<sub>2</sub>O<sub>3</sub>; 0.6 % MgO; 1.8 % K<sub>2</sub>O; 0.3 % P<sub>2</sub>O<sub>5</sub> and 0.7 % other oxides [28].

The glycerol available in liquid state, together with the aqueous solution of water glass, both purchased from the market, were prepared in a separate vessel in which the water was added as a binder. After mixing with an electrically operated device, the liquid component was poured over the solid powder mixture and the wet material was further mixed for 10-15 min until a homogeneous viscous paste was obtained.

The materials dosage distributed into four experimental variants was influenced by the results previously obtained by the same team of authors when testing the manufacture of a glass foam of CGG type on the 0.8 kW-microwave oven using manufacturing recipes based on the combination of a solid foaming agent (CaCO<sub>3</sub>) and a liquid agent (glycerol) associated with water glass as an enveloping agent [18]. The variants tested in that paper were slightly different, CaCO<sub>3</sub> having values between 0.8-1.1 wt. %, glycerol between 1.0-1.1 wt. % (practically constant) and water glass in the range 3.0-4.8 wt. %. The ratios of kaolin and water addition were kept constant at 0.2 and 14.5 wt. %, respectively. Practically all four tested variants led to excellent results, mentioned above. For this reason, the experimental variants adopted for testing on the 10 kW-microwave oven (Table 2) had values around those successfully experienced on a very small scale.



Table 2

**Material dosage of the experimental variants**

Material (wt. %)	Variant 1	Variant 2	Variant 3	Variant 4
Glass waste	93.5	93.4	93.3	93.2
CaCO <sub>3</sub>	0.8	0.9	1.0	1.1
Kaolin powder	0.2	0.2	0.2	0.2
Glycerol	1.0	1.0	1.0	1.0
Water glass	4.5	4.5	4.5	4.5
Water addition	14.5	14.5	14.5	14.5

The sintering/foaming temperature experimentally determined on the 0.8 kW-microwave oven was in a narrow range of values (834-841 °C), being also adopted in the case of testing on the 10 kW-oven.

Unlike the low amount of the wet starting materials (538 g) used in the experiment performed on the 0.8 kW-microwave oven, the transition to a higher stage of experimentation on a 10 kW-microwave equipment allowed the preparation of a significantly larger amount of materials reaching 4.50 kg (including also the addition of water).

### 3. Results and discussion

The main functional parameters of the experimental manufacture of CGG in the 10 kW-microwave equipment adapted according to the description presented above are shown in Table 3.

Table 3

**Main functional parameters of the experimental process**

Parameter	Variant 1	Variant 2	Variant 3	Variant 4
Wet raw material/CGG amount (kg)	4.50/3.87	4.50/3.85	4.50/3.87	4.50/3.88
Sintering/foaming temperature (°C)	834	836	838	840
Heating time (min)	46.5	48	50	54
Average rate (°C/min)				
-heating	17.5	17.0	16.4	15.2
-cooling	7.3	7.2	7.0	7.0
Index of volume growth	1.45	1.60	1.70	1.95
Specific energy consumption (kWh/kg)	1.57	1.63	1.69	1.82

Under the conditions of pre-establishing temperature values in the optimal range (834-840 °C) experimentally determined on a small scale [18], the other functional parameters of the process shown in Table 3 were modified. The new positioning of the waveguides and their distribution on the walls and vault of the oven, the new type of screen made of microwave susceptible material as well as the large internal volume of the oven and the significant increase of the heated material amount compared to the experimental conditions offered by the 0.8 kW-microwave oven influenced the main functional parameters (process time, average heating rate and specific energy consumption). As expected, the process time increased to 46.5-54 min compared to 34-37.5 min in the reference experiment, the average heating rate

decreased to 15.2-17.5 °C/min compared to 21.9-23.9 °C/min, despite improving the thermal protection of the ceramic crucible and the specific energy consumption increased to 1.57-1.82 kWh/kg compared to 0.78-0.85 kWh/kg, but its values are still considered economical. The authors of the paper [17] believe that a suitable industrial-scale microwave equipment should contribute to increasing the energy efficiency of the heating process by up to 25% compared to a low-power domestic microwave oven (less than 1 kW). The volume growth index of the starting material was between 1.45-1.95 slightly higher compared to the reference experiment (1.30-1.60).

The average cooling rate of CGG was increased to 7.0-7.3 °C/min by fully opening the oven door after completing the heating process and then removing the metal mold containing the foamed material. The effect of this cooling mode was the partial cracking of the CGG, better observable in the case of industrial processes manufactured in conveyor belt ovens by conventional heating techniques.

The appearance of the CGG samples corresponding to the four experimental variants is shown in Figure 3. The materials obtained by heating at lower temperatures are more dense and compact, while those heated at higher temperatures are slightly more porous and less dense.

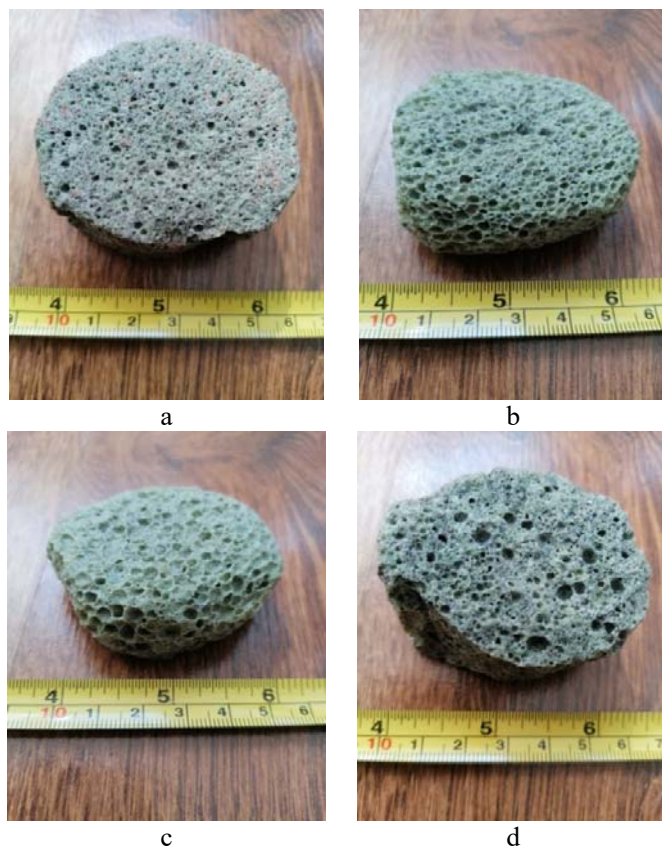


Fig. 3. Appearance pictures of the CGG samples  
a – variant 1; b – variant 2; c – variant 3; d – variant 4.

The main physical, thermal, mechanical and microstructural features of the CGG lump samples are presented in Table 4.

Table 4

**Main physical, thermal, mechanical and microstructural features of the CGG lump samples**

Variant	Bulk density (g/cm <sup>3</sup> )	Porosity (%)	Thermal conductivity (W/m·K)	Compressive strength (MPa)	Water absorption (vol. %)	Pore size (mm)
1	0.25	85.8	0.070	7.4	2.3	0.30 – 0.90
2	0.23	86.7	0.069	7.4	2.4	0.40 – 1.40
3	0.20	88.2	0.060	7.2	2.9	1.00 – 1.80
4	0.21	87.7	0.062	7.1	2.8	1.80 – 3.80

The analysis of the data in Table 4 shows that the CGG lump samples obtained by the unconventional microwave heating method correspond to the requirements of cellular glass gravels usable as thermal insulation materials under mechanical stress conditions. The bulk density (between 0.20-0.25 g/cm<sup>3</sup>) has values located towards the upper limit of this physical characteristic industrially obtained, but it is compensated by the very high level of the compressive strength (7.1-7.4 MPa) above the maximum limit (of about 6 MPa) required for CGG lumps.

The thermal insulation characteristics of CGG samples, influenced by the low thermal conductivity (between 0.062-0.070 W/m·K), low bulk density and high porosity (85.8-88.2 %) indicate a suitable material in terms of quality. In addition, the water absorption has low values (2.3-2.9 vol. %) being at the level required for these insulating material types. The low pore size of CGG lumps characterizes variants 1-2, in which glycerol (1%) was used together with lower proportions of CaCO<sub>3</sub> (0.8-0.9 %), while higher pore sizes were obtained in variants 3-4, in which the CaCO<sub>3</sub> proportions increased slightly to 1.0-1.1%.

The microstructural configuration of the CGG samples is shown in Figure 4.

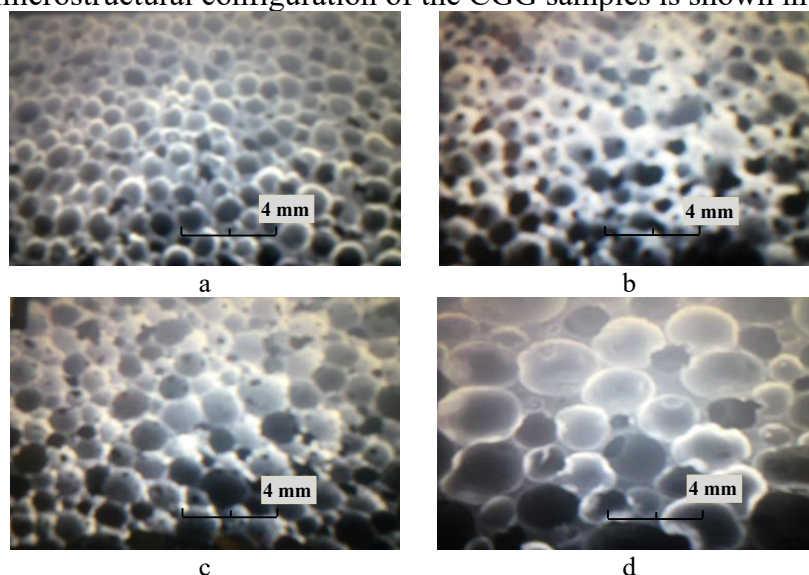


Fig. 4. Microstructural configuration of the CGG samples  
a – variant 1; b – variant 2; c – variant 3; d – variant 4.

#### 4. Conclusion

In the current stage of the research, the authors aimed at the experimental production of CGG corresponding to the market requirement in terms of quality under the conditions of significant increase of processed material amount compared to the previous test on a small-scale microwave oven. The originality of the research presented in the work is the use of an unconventional microwave heating technique unlike the conventional techniques commonly applied by all world industrial manufacturers. The experiment was performed on a 10 kW-microwave oven existing in the Daily Sourcing & Research Company. The authors followed the CGG manufacturing process especially in terms of quality. The main features of the CGG lump samples were: bulk density of 0.20-0.25 g/cm<sup>3</sup>, thermal conductivity of 0.062-0.070 W/m·K, compressive strength of 7.1-7.4 MPa. These features, similar to industrially manufactured products by conventional techniques, are suitable for their use as CGG lumps.

#### References

- [1] S. De Bruyn, C. Jongsma, B. Kampman, B. Görlach, J-E. Thie, „Energy-Intensive Industries- Challenge and Opportunities in Energy Transition”, Policy Department for Economic, Scientific and Quality of Life Policies, European Parliament, Luxembourg, 2020. <http://www.europarl.europa.eu/supporting-analyses>
- [2] G. Scarinci, G. Brusatin, L. Barbieri, A. Corradi, I. Lancellotti, P. Colombo, S. Hreglich, R. Dall’Igna, „Vitrification of industrial and natural wastes with production of glass fibres”, Journal of the European Ceramic Society, vol. **20**, no. 14, 2000, pp. 2485-2490.
- [3] E. Rodriguez Vieitez, P. Eder, A. Villanueva, H. Saveyn, „End-of-waste criteria for glass cullet: Technical proposals”, Publication Office of the European Union, Luxembourg, 2011.
- [4] G. Scarinci, G. Brusatin, E. Bernardo, „Glass Foams” in Cellular Ceramics: Structure, Manufacturing, Properties and Applications, Wiley-VCH, Verlag GmbH Co KGaA, Weinheim, Germany, 2005, pp. 158-176.
- [5] \*\*\* Geocell Foam Glass Gravel-High Performance in Every Aspect, UK Brochure, July 2017. <https://www.mikewye.co.uk/wp-content/uploads/2014/09/GEOCELL-Brochure-UK-Sept-16.pdf>
- [6] \*\*\* Geocell Foam Glass, 2016. <https://www.foamglassgravel.com/en/>
- [7] \*\*\* Insulation materials and their properties, 2017. <http://www.greenspec.co.uk/building-design/insulation-materials-thermal-properties>
- [8] \*\*\* Fabricarea sticlei celulare, Energocell, Debrecen, Hungary, 2019. <http://www.energocell.hu/ro/fabricarea-sticlei-celulare>
- [9] H. Hibbert, „Understanding the production and use of Foam Glass Gravel across Europe and opportunities in the UK”, Final Report, 2016. <http://static1.squarespace.com/static/584175382994caab5d6b2427/t592eb355db29d6b2ff34f305/1496232791849/Foam+Glass+Gravel+Production+in+Europe+and+opportunities+in+the+UK++Mike+Hibbert+July+2016+J+C+Dawes+Report+Final+Version.pdf>
- [10] A. Zegowitz, „Cellular glass aggregates serving as thermal insulation and a drainage layer”, Buildings, vol. **XI**, 2010, pp. 1-8. [https://web.oml.gov>conf-archive>48\\_Zegowitz](https://web.oml.gov>conf-archive>48_Zegowitz)
- [11] \*\*\* Glapor Schaumglasprodukte, 2017. <http://www.glapor.de/en/produkte/cellular-glass-gravel>
- [12] \*\*\* Environmental Product Declaration-Glapor cellular glass, Glapor Werk Mitterteich GmbH, December 2017.

- [https://www.foamrox.no/wp-content/uploads/2020/12/2017-EPD\\_GLAPOR-cellular-glass.pdf](https://www.foamrox.no/wp-content/uploads/2020/12/2017-EPD_GLAPOR-cellular-glass.pdf)
- [13] Felicia Cosmulescu, L. Paunescu, M.F. Dragoescu, S.M. Axinte, „Comparative analysis of the foam glass gravel types experimentally produced by microwave irradiation”, *Journal of Engineering Studies and Research*, vol. **26**, no. 3, 2020, pp. 58-68.
- [14]\*\*\* Misapor, 2019. <http://www.archiexpo.com/soc/misapor-78710.html>
- [15]\*\*\* Foamglas for the Building Envelope-Cellular Glass Insulation Guide, 2016. [https://www.reinish-co.it/fileadmin/user\\_upload/pdfs/Foamglas\\_ENG\\_diverse/FOAMGLAS\\_for\\_the\\_Building\\_Envelope.pdf](https://www.reinish-co.it/fileadmin/user_upload/pdfs/Foamglas_ENG_diverse/FOAMGLAS_for_the_Building_Envelope.pdf)
- [16]\*\*\* Glamaco, Coswig, Germany, 2014. <https://www.Glamaco.com/backend/wp-content/uploads/2014/02/Foam-Glass.pdf>
- [17] Oxana V. Kharissova, B.I. Kharissov, J.J. Ruiz Valdés, „Reviews: The use of microwave irradiation in the processing of glasses and their composites”, *Industrial & Engineering Chemistry Research*, vol. **49**, no. 4, 2010, pp. 1457-1466.
- [18] L. Paunescu, S.M. Axinte, M.F. Dragoescu, F. Cosmulescu, B.V. Paunescu, „Simultaneous use of liquid and solid foaming agents by a nonconventional technique to obtain a high-strength glass foam with fine porosity”, *Nonconventional Technologies Review*, vol. **25**, no. 2, 2021, pp. 3-9.
- [19] Svitlana Karandashova, B.M. Goltsman, E.A. Yatsenko, „Analysis of influence of foaming mixture components on structure and properties of foam glass”, *IOP Conference Series: Materials Science and Engineering*, vol. **262**, 2017, pp. 1-6. <https://www.iopscience.iop.org>article>262>
- [20] B. Dou, V. Dupont, P.T. Williams, H. Chen, Y. Ding, „Thermogravimetric kinetics of crude glycerol”, *Bioresource Technology*, vol. **100**, no. 9, 2008, pp. 2613-2620. <http://dx.doi.org/10.1016/j.biortech.2008.11.037>
- [21] K.S.P. Karunadasa, C.H. Manoratne, H.M.T.G.A. Pitawala, R.M.G. Rappakse, „Thermal decomposition of calcium carbonate (calcite polymorph) as examined by in-situ high-temperature X-ray powder diffraction”, *Journal of Physics and Chemistry of Solids*, vol. **134**, 2019, pp. 21-28.
- [22] L. Paunescu, S.M. Axinte, B.T. Grigoras, M.F. Dragoescu, A. Fiti, „Testing the use of microwave energy to produce foam glass”, *European Journal of Engineering and Technology*, vol. **5**, no. 4, 2007, pp. 8-17.
- [23] Helen J. Kitchen, S.R. Vallance, J.L. Kennedy, N. Tapia-Ruiz, L. Carassiti, A. Harrison, A.G. Whittaker, T.D. Drysdale, S.V. Kingman, D.H. Gregory, „Modern microwave methods in solid-state inorganic materials chemistry: From fundamentals to manufacturing”, *Chemical Reviews*, vol. **114**, no. 2, 2014, pp. 1170-1206.
- [24] D.A. Jones, T.P. Lelyveld, S.D., Mavrofidis, S.W. Kingman, N.J. Miles, „Microwaves heating applications in environmental engineering-a review”, *Resources, Conservation and Recycling*, vol. **34**, no. 2, 2002, pp. 75-90.
- [25] A. Scorgins, „Bulk density of industrial minerals: Reporting in accordance with the 2007 SME Guide”, 2015. <https://www.csa.global.com/wp-content/uploads/2015/07/Bulk-density-of-industrial-minerals-Reporting-in-accordance-with-the-2007-SME-Guide.pdf>
- [26] L.M. Anovitz, D.R. Cole, „Characterization and analysis of porosity and pore structures”, *Reviews in Mineralogy and Geochemistry*, vol. **80**, 2005, pp. 61-164.
- [27] W.B. Jepson, „Kaolins: their properties and uses”, *Philosophical Transactions of the Royal Society A*, vol. **311**, 1984, pp. 411-432. <https://www.jstor.org>stable>
- [28] S. Yahaga, S.S. Jikan, N.A. Badarulzaman, A.D. Adamu, „Chemical composition of particle size analysis of kaolin”, *Traektoriâ Nauki-Path of Science*, vol. **3**, no. 10, 2017. <https://www.doi.org/10.22178/pas.27-1>